The role of p53 and CYLD in mitochondrial death pathways and mechanisms of neuronal necroptosis

Dissertation

zur

Erlangung des Doktorgrades

der Naturwissenschaften

(Dr. rer. nat.)

dem

Fachbereich Pharmazie

der Philipps-Universität Marburg

vorgelegt von

Sebastian Diemert

aus Hamburg

Marburg/Lahn 2011

Vom Fachbereich Pharmazie der Philipps-Universität Marburg als Dissertation am

_____ angenommen.

Erstgutachter: Prof. Dr. Carsten Culmsee

Zweitgutachter: Prof. Dr. Jens Kockskämper

Tag der mündlichen Prüfung am 26.01.2012

Meinen Eltern

ERKLÄRUNG

Ich versichere, daß ich meine Dissertation

„**The role of p53 and CYLD in mitochondrial death pathways and mechanisms of neuronal necroptosis**“

selbständig ohne unerlaubte Hilfe angefertigt und mich dabei keiner anderen als der von mir ausdrücklich bezeichneten Quellen bedient habe.

Die Dissertation wurde in der jetzigen oder einer ähnlichen Form noch bei keiner anderen Hochschule eingereicht und hat noch keinen sonstigen Prüfungszwecken gedient.

Marburg, den 11.11.2011

.....
(Sebastian Diemert)

Table of contents

1. Introduction

Neuronal dysfunction and death are hallmarks of acute and chronic neurodegenerative diseases such as cerebral ischemia, traumatic brain injury and Alzheimer´s disease, respectively. Since afflicted patients suffer from severe and often irreversible disability, the personal and economical burden of these disorders is immense (1). Despite of this huge socio-economic impact, treatment options targeting pathological mechanisms of acute brain injury or progressive neurodegenerative diseases remain poorly evolved.

For instance, the most widely practiced treatment for traumatic brain injury today is still decompressive craniectomy (2; 3). This ancient approach dating back to 4000 BC epitomises the lack of innovative, broadly applicable, and well tolerated treatment options in the field of acute brain injuries (2). Consequently, research on the underlying mechanisms of neuronal cell death is imperative to overcome this shortfall and define reliable and efficient treatment paradigms.

1.1. Apoptosis

According to current classification, neuronal cell death is executed by three major pathways, namely autophagy, apoptosis and necrosis (4-6). The severity and duration as well as the nature of the death stimulus determines which cell death pathway is initiated. The term apoptosis originally has been introduced by Kerr et al. (1972) to describe a morphological phenotype of dying cells, which manifests in rounding-up of the cells, reduction of cellular and nuclear volume (pyknosis), nuclear fragmentation and plasma membrane blebbing (4; 7). Especially the latter characteristic renders apoptosis a favourable form of cell death in development and under physiological conditions, when preservation of surrounding cells is desired. This is the case with apoptosis, since apoptotic cells do not completely disintegrate in the terminal stages of cell death, but rather form apoptotic bodies (remnants of membrane blebbing), which are engulfed by neighbouring cells and thus removed by phagocytosis. The “discrete” removal of apoptotic bodies by the surrounding tissue stands in sharp contrast to effects provoked by cells undergoing necrosis, which literally burst and spill their intracellular content into the interstitial space, causing

severe inflammatory responses and damage to the surrounding tissue (4). Consequently, apoptosis plays an important physiological role in proliferating and developing tissue, as it regulates the replacement of senescent or excessive cells without causing necrosis, subsequent inflammation and scar formation (8). Further, in non-proliferating tissue like the brain, apoptosis has been shown to be of relevance during development by controlling synapses and removing excessive and unneeded neural cells (9).

A more detrimental role of apoptosis in neurons, however, is commonly associated with pathophysiological conditions like e.g. cerebral ischemia or Parkinson´s disease, where apoptotic signaling significantly promotes the progressive and irreversible loss of neuronal cells (10). Consequently, apoptosis is significantly involved in neuronal cell death in numerous neurological diseases.

1.2. Intrinsic and extrinsic apoptosis

Apoptosis can follow two distinct pathways, namely the intrinsic and the extrinsic pathway. These signaling modes, however, share a common final route since both ultimately cause the activation of the major effector-caspases, caspase-3, caspase-6 and caspase-7.

Caspases are cysteine proteases, which are sequestered in the cytosol under physiologic conditions as inactive precursors (11). Activation is effected by (auto)proteolysis mediated by initiating caspases and other proteases. Two families of caspases can be differentiated, the initiator caspases and the executing caspases. The latter group of caspases cleaves various pivotal downstream targets causing e.g. disruption of the nuclear envelope and DNA fragmentation which ultimately leads to cell death (11; 12).

The extrinsic pathway is triggered by death receptor stimulation by e.g. Fas-Ligand (FasL), Tumor Necrosis Factor α (TNF-α) or Tumor Necrosis Factor Related Apoptosis Inducing Ligand (TRAIL) (11; 13). Death receptor stimulation subsequently results in oligomerization and recruitment of adaptor proteins, such as Fas-associated death domain (FADD) and several molecules of caspase-8. This multi-protein complex is commonly referred to as the death-inducing signaling complex (DISC) (12). Autoactivation of caspase-8 at DISC initiates proteolytic activation of downstream caspases like caspase-3, -6 and -7. These activated caspases then

cause destabilization of the cytoskeleton, fragmentation of the nuclear envelope, chromatin condensation and DNA fragmentation. The latter events are mediated by caspase-activated deoxyribunuclease (CAD), which is released from the inhibitory ligand ICAD by the activated caspase-3 (12) (Figure 1). CAD then causes DNA-cleavage, a major hallmark of apoptosis, which often is referred to as the “DNA-ladder”. This term is derived from the fact, that agarose gel electrophoresis of genomic DNA from apoptotic cells shows a “ladder-like” pattern of truncated DNA fragments.

The upstream caspase-8 interconnects the extrinsic and intrinsic pathway, as it activates pro-apoptotic Bcl-2-proteins like Bid, which then set off the cascade of intrinsic apoptosis that is characterized by mitochondrial damage. Therefore, Bcl-2 family proteins have a significant impact on intrinsic apoptosis signaling and cell death in general. Bcl-2 proteins can be divided into three groups depending on their shared Bcl-2 homology domains (BH1-4).
The prosurvival members such as Bcl-2, Bcl-X_L, and Mcl-1 contain BH domains 1–4, whereas BAX and BAK contain BH domains 1–3 and belong to a group of proapoptotic effectors, which cause mitochondrial outer membrane permeabilization (MOMP) during apoptosis. The third group encompasses proapoptotic members, like Bid, Bim and Bad, which contain only the BH3 domain and serve to couple upstream stress stimuli to downstream modulation of the multi-BH domain members (14). The intrinsic route of apoptosis has closely been linked to mitochondria for execution of cell death, relying on the proapoptotic proteins BAK and BAX. In unstressed cells BAX is sequestered in the cytosol, while BAK is integrated into the mitochondrial membrane.
Several BH-3 proteins including tBid, Bim and PUMA (p53 up-regulated modulator of apoptosis) have been shown to induce a translocation of BAX to the mitochondria in response to various stimuli including genomic or metabolic stress (15; 16). Upon mitochondrial translocation, BAX undergoes pronounced conformational changes forming oligomers with additional BAX or BAK molecules. These oligomers then cause the formation of a transmembrane pore in the mitochondrial membrane, which leads to subsequent release of further proapoptotic factors from the mitochondria (14). The antiapoptotic proteins Bcl-X_L and Bcl-2 can sequester BAX and BAK and thereby prevent pore formation (15). Different studies suggested, that Bcl-X_L and Bcl-

2 rather sequester activated proapoptotic BH-3 proteins and thus prevent BAX-BAK dependent pore formation only indirectly (14). Yet another proapoptotic factor, the BH3 only protein BAD has been shown to sequester Bcl-2 and Bcl-X_L and thereby prevent these from exerting their anti-apoptotic function (14).
These mechanisms have given rise to the development of Bcl-X_L and Bcl-2 inhibitors, currently under clinical investigation for the treatment of lymphomas, which sensitize cells to cell death by mimicking the BH3 molecule BAD (17; 18).
Once BAX dependent pore formation occurs at the mitochondria, the proapoptotic factors, cytochrome c (Cytc), apoptosis-inducing factor (AIF), Omi/HtrA2 and second mitochondria-derived activator of caspase (Smac/DIABLO) are released (11; 12). Cytochrome c interacts in the cytosol with APAF-1 to form the apoptosome, a complex, which activates caspase 9 and thereby propagates further caspase activation and subsequent cell death (Figure 1).

Next to the established role of caspase dependent apoptosis, emerging evidence suggests, that AIF release from mitochondria is a detrimental process within programmed cell death. Interestingly, in certain tissues, AIF dependent cell death is far more important than the established caspase dependent apoptosis. This is especially true for neurons and cell death in the adult brain (19; 20). Under physiological conditions the flavoprotein AIF is bound in the intermembrane space of mitochondria, functioning as an important redox-active enzyme (NADH oxidase). AIF release from the mitochondria and AIF mediated induction of cell death has been observed in response to various stimuli including excitotoxicity, ischemia or DNA alkylating agents (21-23).
Upon release from mitochondria, AIF translocates to the nucleus and forms an active nuclease complex with cyclophilin A (CYPA) to promote DNA degradation and cell death (24) (Figure 1). With the discovery of the AIF variant, AIF2, another putative mechanism of AIF isoforms has been found, involving ROS generation at the mitochondria (25).

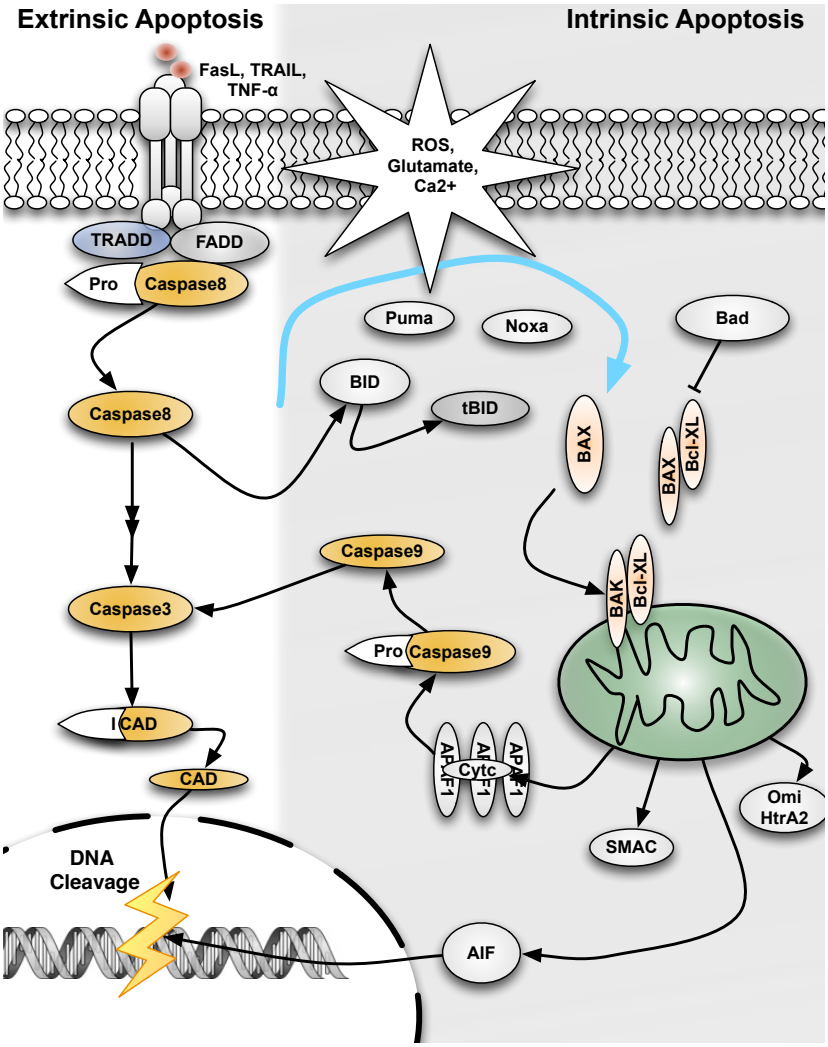

Figure 1: Apoptotic pathways. Extrinsic pathway (left part): Cell death is triggered by activation of death receptors (TNFR1, FasR) inducing the binding of Fas associated death domain (FADD) and/or (TRADD). Pro-caspase-8 is recruited to the complex and (auto)activated, followed by a caspase-8 mediated activation of the effector caspase-3. Caspase-3 in turn cleaves the inhibitor of caspase activated deoxyribonuclease (ICAD) thereby releasing the caspase activated deoxyribonuclease (CAD), which causes DNA cleavage. Alternatively, caspase-8 can cleave the proapoptotic protein Bid, which activates the intrinsic pathway of apoptosis that involves damage to mitochondria (right part). The cleaved Bid protein (tBid), increased calcium-levels or ROS in turn can trigger mitochondrial membrane permeabilization, which causes the release of mitochondrial proteins like cytochrome c (Cytc), Omi/HtrA2, Smac/DIABLO or AIF. Cytochrome c forms a complex with Apaf-1 and pro-caspase-9, called the apoptosome, which enables the auto-activation of caspase 9. The apoptosome then triggers caspase-3 and subsequently CAD. AIF is released from mitochondria and translocates to the nucleus where it induces DNA fragmentation. The mitochondrial proteins Omi/HtrA2 and Smac/DIABLO induce cytotoxicity by sequestering endogenous inhibitors of caspases thus enhancing the caspase response.

1.3. p53 dependent apoptosis

The tumor suppressor p53 plays a central role in assuring genomic stability in mammalian cells. Activation of p53 in response to DNA damage therefore can induce either cell cycle arrest and DNA repair, or apoptosis, depending on the severity of the insult. To evoke both effects, p53 regulates the transcription of a wide set of target genes, ranging from p21 to induce DNA repair and e.g. BAX and BAK for induction of cell death (26-28).

Upregulation and induction of p53 has been reported in response to various stimuli including NMDA receptor mediated excitotoxicity, reactive oxygen species (ROS), alkylating agents, hypoxia, β-Amyloid toxicity and 1-methyl-4-phenyl-1,2,3,6-tetrahydropyridine (MPTP) (28; 29). Despite this vast range of insults, the underlying trigger for p53 stimulation likely lies in the generation of intermediate ROS species such as superoxide anions ($\cdot O2^-$) and hydroxyl radicals ($^{\bullet}OH$) which target the genomic DNA (30).

Such oxidative DNA damage includes chemical lesions like hydroxyl radical-modified bases (8-hydroxyl-20-deoxyguanosine) and DNA strand breaks (28). p53 activation is accompanied by certain modifications of p53 including acetylation, phosphorylation and poly(ADP) ribosylation, which serve to prolong the half life of p53 and/or enhance its DNA-binding affinity. These modifications are mediated by kinases, which function as the actual sensors of DNA damage and transduce the DNA-damage signal to p53 by the aforementioned modifications. Among these kinases are ataxia telangiectasia mutated (ATM), ATM-related protein (ATR) and cell cycle regulating kinases CDK4/6 (28; 31). p53-mediated apoptosis is mostly dependent on transcription, even though alternative transcription-independent functions of p53 have been reported (26; 29).

The major transcriptional targets of p53 for induction of cell death involve the multi-domain Bcl-2 family member BAX and the BH3-only proteins Bid, PUMA and Noxa, among many others. Furthermore, p53 may promote apoptosis by transcriptional repression of anti-apoptotic signaling pathways including CREB (Cyclic AMP response element binding protein) and Nuclear factor-kB (NF-κB) (32). Consequently, p53 activation reduces the expression of antiapoptotic factors under transcriptional control by these pathways, such as Bcl-2, the insulin-like growth factor (IGF) receptor, Manganese superoxide reductase (MnSOD), or X-linked inhibitor of

apoptosis protein (XIAP) (33). The competetive binding of both NF-κB and p53 to p300/CBP (CREB binding protein) has been suggested as the molecular link of this reciprocal inhibition (34-37) since p300/CBP is a crucial co-transcription factor required by both pathways for proper transcriptional function (Figure 2). In summary, p53 possesses a strong apoptotic potential, for which reason inhibition thereof has been established as a promising approach to tackle neuronal cell death.

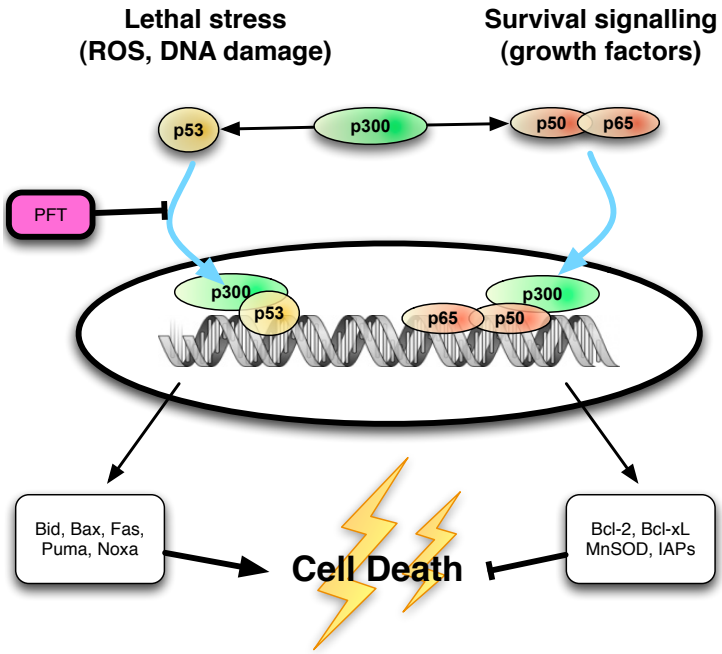

Figure 2: Reciprocal repression of p53 and NF-κB through competitive binding of p300 (modified from Culmsee et al., 2005). When the transcription factor p53 is activated in response to various stress stimuli, it translocates to the nucleus and induces transcription of its various pro-apoptotic target proteins like Bid, BAX or Fas. Activation of NF-κB, in contrast, mediates survival through enhanced transcription of anti-apoptotic proteins such as Bcl-2, Bcl-X_L or MnSOD. For effective binding to the promoter both transcription factors further require co-factors such as p300/CBP. Since, both, p53 and NF-κB compete for the limited pool of p300, blocking p53 by pifithrin-α may indirectly support NF-κB signaling and thereby further enhance neuroprotection.

1.4. The NF-κB pathway and its implication in neurons

As mentioned in the previous section, certain pathways ensure neuronal survival under physiological conditions by antagonizing the various intracellular pro-death effectors. Among these, the NF-κB pathway has been identified as a crucial player in different cell types, including cancer cells and neurons. While the strong anti-apoptotic effect of NF-κB mediates unwanted chemoresistance in cancer cells, this same pathway has been associated with a desirable increase in survival in neurons

(38; 39). The role of NF-κB within the central nervous system, however, is very complex and a matter of ongoing debate. Consequently, NF-κB has not only been linked to increased survival, but also to enhanced neuronal damage (33; 37; 40-42). Even though several possible explanations have been offered, this apparent contradiction has not been resolved completely, yet. Evidence established by some groups working on NF-κB in cerebral ischemia suggests for instance that the duration of ischemia determines the mode of NF-κB response and the final outcome. In this respect, a short duration of ischemia below the threshold of cell death was found to upregulate NF-κB and to protect against a later more severe insult (preconditioning). A strong prolonged ischemia, however, was associated with enhanced NF-κB activity and cell death (43).

Furthermore, a cell-type specific effect of NF-κB is very likely to contribute to the convoluted global effect within the CNS. For instance, activation of NF-κB in microglial cells has been linked to the release of neurotoxins, which overcomes the protection mediated by NF-κB in neurons and thus ultimately promotes cell death (44). The abundance of different NF-κB subunits and possible dimer composition suggests, that NF-κB can evoke different responses depending on the respective dimers. Therefore, the analysis of NF-κB in the CNS requires a detailed investigation of NF-κB taking into account the respective subunit and cell types.

The NF-κB pathway consists of 5 transcription factors, which all share a highly conserved DNA-binding/dimerization domain called the Rel homology domain (RHD). A subset of the NF-κB subunits, namely RelA, RelB and cRel further contains a C-terminal transactivation domain, which enables them to activate transcription. This domain is missing in the p50 and p52 subunits. In order to induce transcription, NF-κB subunits need to dimerize and translocate from their predominant cytosolic location to the nucleus (45).

For successful transcriptional activation, the dimer must contain at least one factor with a transactivation domain; otherwise it can only halt transcription upon DNA binding. An exception to this rule is the binding of the auxiliary NF-κB protein Bcl-3 to p50/p52 dimers, which then can actively initiate transcription, even though Bcl-3 per se does not function as a transcription factor (46).

A huge variety of stimuli has been reported to activate NF-κB-transcription, including proinflammatory cytokines such as TNF-α and interleukin (IL)-1 as well as microbial

pathogens (47). Additionally, in neurons NMDA receptor stimulation as well as stimulation of metabotropic glutamate receptors has been shown to induce NF-κB (48; 49). Further, intracellular stimuli leading to NF-κB activity include oxidative stress, genomic stress by chemotherapeutics and hypoxia.

Activation of NF-κB commonly occurs via two main pathways, the canonical and non-canonical pathway. In their inactive state, RelB, RelA and cRel are sequestered in the cytosol by IκB, while p50 and p52 are retained as precursor proteins p105 and p100 (45).

In the canonical pathway the β subunit of the IκB kinase (IKKβ) is activated which then phosphorylates the IκB-protein. The ubiquitin ligase machinery in turn, recognizes the phosphorylated IκB-proteins and attaches poly-ubiquitin chains, linked via lysine-48. These ubiquitin moieties then are recognized by the proteasome, resulting in IκB degradation (Figure 3).

Consequently, activation of the canonical NF-κB pathway can be evaluated by increased phosphorylation of IκB, a decreased pool of IκB, and a subsequent nuclear translocation of NF-κB dimers (Figure 3 left part).

In the non-canonical pathway, IκB-α kinase (IKKα) causes phosphorylation of either precursor subunit p105 or p100, which then likewise are ubiquitinated and recognized by the proteasome. In this case, however, they are not completely degraded, but processed, liberating p50 from its precursor p100 and p52 from p105 (Figure 3 right part). These subunits now translocate to the nucleus.

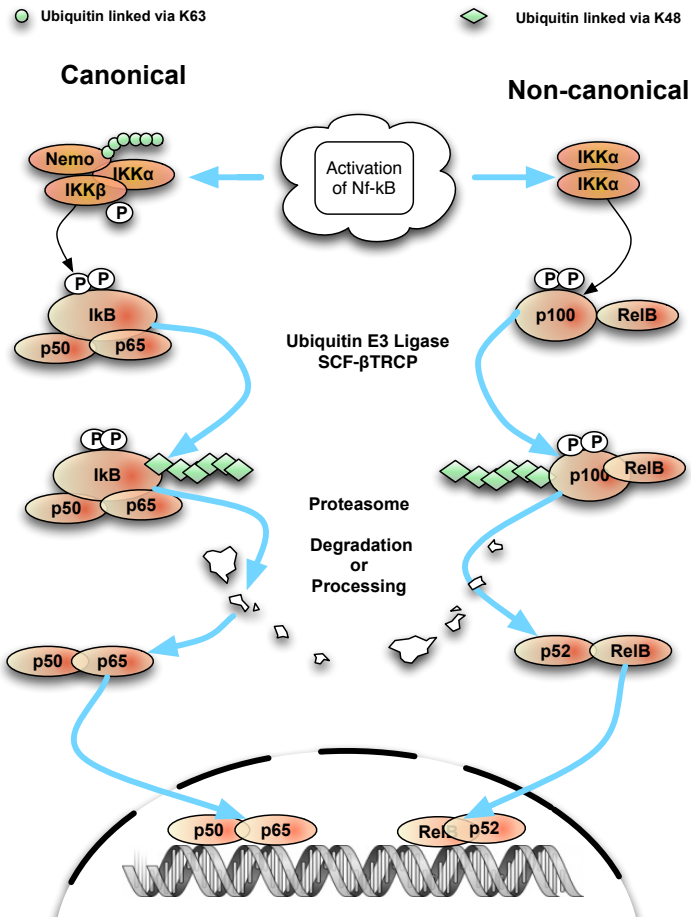

Figure 3: Activation of NF-κB by the canonical and non-canonical pathway. Key elements of the canonical NF-κB pathway include members of the IkB (inhibitor of kB) family and the IkB kinase (IKK) complex that consists of IKKα–IKKβ heterodimers and the regulatory protein IKKγ/NEMO. Several stimuli are known to activate NF-κB, such as the cytokines TNF-α, or an increase in intracellular Ca^{2+} levels, leading to the phosphorylation of the IkB protein. This phosphorylation causes IkB polyubiquitination and its subsequent degradation by the proteasome. The NF-κB proteins are thus liberated from IkB and translocate to the nucleus, where they can alter gene expression upon binding to the promoter within the NF-κB response element. The non-canonical pathway is activated by the IkB kinase-α (IKK-α), which stimulates phosphorylation of p100 to induce its processing to p52. IKKα-induced processing of p100 can stimulate for example the nuclear translocation of the RelB–p52 dimers.

1.5. Regulation of NF-κB - The role of ubiquitination

Regulation of NF-κB occurs at various levels involving acetylation, phosphorylation and ubiquitination of its various signaling proteins. In addition to the aforementioned role of phosphorylation for the initiation of NF-κB by IKK kinases, modifications have also been reported for active NF-κB transcription factors. In this respect, phosphorylation of NF-κB subunits by nuclear kinases, and modification of these subunits by acetylases and phosphatases, can result in transcriptional activation and repression as well as promoter-specific effects (50). The role of ubiquitin in NF-κB

regulation traditionally has been linked to lysine-48 (K48) bound polyubiquitin chains, which are attached to certain substrate proteins, marking them for proteasomal degradation. The most prominent example is the degradation of IκB during activation of the canonical pathway.

More recently, this view on ubiquitination was expanded further, identifying lysine-63 (K63) bound ubiquitin chains as an important mediator of non-degradative processes, such as protein trafficking and signal transduction (51). Further, linear ubiquitin chains, linked via alternative amino-acids have been discovered, although their physiological role has not been fully understood (52; 53). K63 linked ubiquitination has been found on several crucial NF-κB related proteins including Nemo (IKKγ), RIP1 and TNF receptor-associated factor 2 (TRAF2). IKKγ has been described as a crucial regulatory component of the IKK-complex and ubiquitination of IKKγ has been discovered as a prerequisite for proper IKK activation and signal transduction. The K63-linked ubiquitin chains seem to facilitate protein–protein interactions in the assembly of the IKK signaling complex in response to its upstream kinase TGF-β-activated kinase 1 (TAK1) (51).
In addition, TRAF2 and RIP1 are of great importance in TNF-α induced NF-κB activation acting upstream of IKKs and TAK1. Similarly, ubiquitination of these is required to allow effective signal transduction in response to TNF-α (54-56). Furthermore, the auxiliary protein Bcl-3 can be activated upon ubiquitination by the E3 ligase Snail, allowing its nuclear translocation. Transfer of ubiquitin residues to RIP1 and Nemo is mediated by the ubiquitin ligases cIAP1 and cIAP2 (Cellular inhibitor of apoptosis protein-1), while TRAF 2 is ubiquitinated by the ligase Ubc13 (57).
In the light of these manifold ubiquitinations required for signal transduction, deubiquitination of these components emerges as an effective means of negative NF-κB regulation. In line with this notion the deubiquitinating enzymes CYLD and A20 have been identified as major negative regulators of the NF-κB pathway.

1.6. The tumor suppressor cylindromatosis (CYLD)

Cylindromatosis, CYLD, originally was identified in a rare inherited benign tumor of the skin, predominantly affecting the light exposed skin of the face and scalp (58). Patients suffering from this disease, termed cylindromatosis as well, carry heterozygous germ-line mutations in the CYLD gene lacking a catalytically functional deubiquitinating (DUB) domain (59). As mentioned in the previous section, CYLD negatively regulates the NF-κB pathway by removing lysine-63 linked poly-ubiquitin chains from its various target proteins (60). Among these, RIP1, TRAF2, Nemo (IKKγ) and Bcl-3 are the major targets of CYLD.

In 2006 Massoumi et al. established a possible link between tumor formation in CYLD deficient mice and NF-κB activity. In ceratinocytes exposed to UV-light or 12-O-tetra-decanoylphorbol-13 acetate (TPA) they found that in the absence of CYLD, polyubiquitinated Bcl-3 bound to p50/p52 and translocated to the nucleus. As a result, CyclinD1 levels were upregulated thereby promoting cell cycle progression, proliferation and subsequent tumor formation.

A higher susceptibility to tumor formation in CYLD deficient animals has also been found in a model system of colonic inflammation, showing a dramatic increase in the incidence of colitis-associated cancer (61).

A further role of CYLD, that is also likely linked to its role in NF-κB signaling, has been found in the regulation of immune responses to host infections. When exposed to streptococcus pneumoniae and haemophilus influenzae, CYLD KO mice experienced significantly less severe episodes of pneumonia (62).

Apart from its regulatory function in the NF-κB pathway, CYLD also controls the c-Jun kinase (JNK) signaling pathway, a mitogen-activated protein kinase (MAPK) pathway, which is involved in several processes including proliferation, differentiation and apoptosis.

A further pivotal role of CYLD has emerged lately, when CYLD was recognized as a major signaling molecule within a form of necrotic cell death, termed necroptosis (63). This function is described in further detail in the following section.

1.7. Necroptosis – an ordered form of necrotic cell death

As opposed to apoptotic and autophagic cell death, necrosis traditionally was considered as an exclusively unregulated form of cell death happening in a passive manner. Necrosis is characterized by swelling of the endoplasmic reticulum, the mitochondria and the cytosol eventually resulting in plasma membrane rupture (4). With the recent discovery of an intracellular signaling network, mediating necrosis, Hitomi et al. dispensed with the perception of necrosis as an unordered event. In order to emphasize the active nature of the observed cell death, and to distinguish it from accidental necrosis, the term necroptosis was introduced (63). As first molecular entity, RIP1 kinase has been recognized as a prerequisite for necroptotic cell death (64; 65). This finding gave also rise to the development of necrostatins, a class of small molecule inhibitors of RIP1 kinase function, which potently block necroptosis, but leave RIP1 effects on NF-κB and JNK signaling unaffected. Consequently, RIP1 kinase function is considered dispensable for these signaling pathways, while it is essential for necroptosis (66).

Necroptosis was found in response to stimulation by TNF-α (TNF receptor 1, TNFR1), tumor necrosis factor–related apoptosis-inducing ligand (TRAIL), or Fas (also known as CD95) (67; 68). As these receptors also induce apoptosis by the extrinsic pathway, it becomes apparent, that death receptor stimulation can trigger more, than just one signaling pathway.

In line with that notion, TNF-α signaling trifurcates at the site of TNFR1 stimulation leading either to NF-κB activation, apoptosis or necroptosis, depending on intracellular signaling (Figure 4).

Upon TNF-α binding, the cytosolic part of the receptor recruits TNFR-associated death domain (TRADD), RIP1, cIAP1 and cIAP2 and TNFR associated factor 2 and 5 (TRAF2 and 5). This aggregated structure is also referred to as complex 1. The signaling mode of complex 1 is controlled predominantly by regulative ubiquitination. In that respect, cIAP1 and cIAP2 ubiquitinate RIP1, which enables the formation and activation of the TAK1 kinase complex, thus triggering a NF-κB response (Figure 4). Under certain conditions, the membrane bound complex 1 changes to a proapoptotic cytosolic complex II (also termed DISC), that encompasses TRADD, Fas associated death protein (FADD) and caspase-8. Consequently, TNF signaling can be switched from prosurvival NF-κB to cell death signaling, forming complex II/DISC.

A central requirement for transition to complex II/DISC is the deubiquitination of RIP1. This process is mediated by CYLD, thus highlighting the pivotal role of CYLD in complex II formation. Following RIP1 deubiquitination, receptor-interacting protein 3 (RIP3) is recruited to finalize complex II. Complex II has been shown to induce either apoptotic cell death, depending on caspase-8 (as outlined before), or necroptotic cell death, depending on RIP1 and RIP3. Downstream mechanisms of necroptosis have been closely associated with ROS production by various sources including mitochondrial glutamate dehydrogenase 1 (GLUD1), NADPH oxidase, NOX1 or lipoxygenases (69).

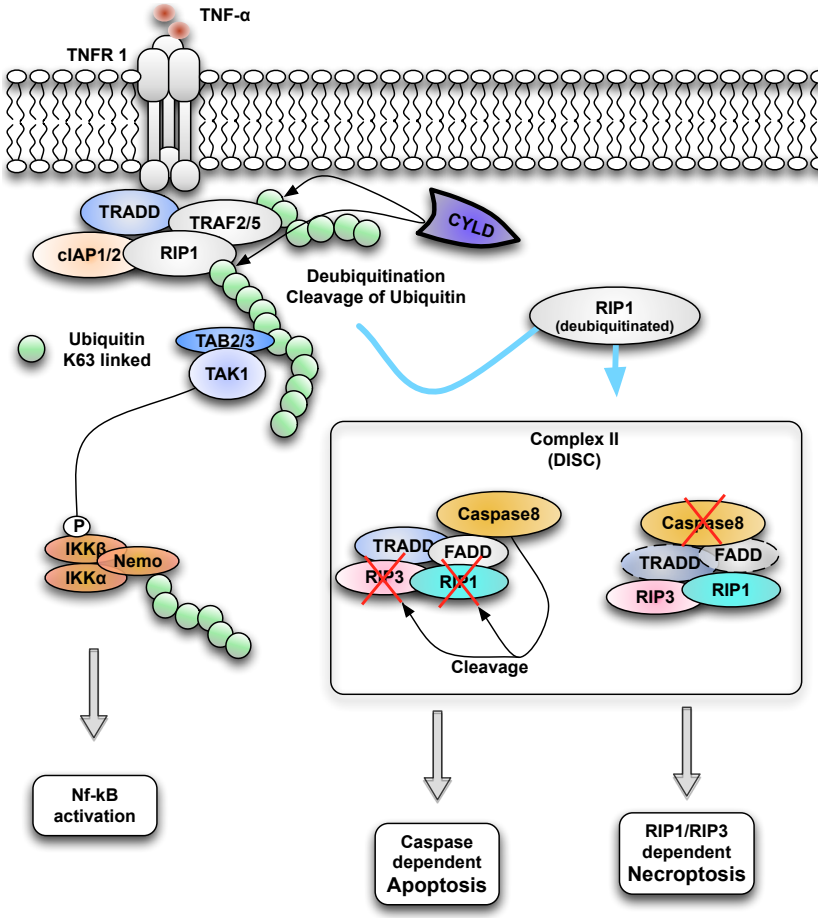

Figure 4: Possible modes of TNF-α receptor mediated signaling: NF-κB activation, apoptosis or necroptosis. (modified from Vandenabeele et al., 2010). Upon tumor necrosis factor (TNF-α) binding, TNF receptor 1 (TNFR1) undergoes a conformational change, allowing for the assembly of complex I, which consists of TNF receptor associated death domain (TRADD), receptor-interacting protein 1 (RIP1), cellular inhibitor of apoptosis proteins (cIAPs), TNF receptor-associated factor 2 (TRAF2) and TRAF5. On cIAP-mediated Lys63-ubiquitynation, RIP1 functions as a scaffold for the recruitment of transforming growth factor-β activated kinase 1 (TAK1), TAK1-binding protein 2 and 3 (TAK2 and 3). This triggers then the canonical activation pathway of NF-κB. In contrast, if RIP1 is deubiquitinated by CYLD, RIP1 promotes cell death by two distinct pathways. When TNFR1 is internalized and undergoes the transition to complex II, its binding partners change to TRADD, FAS-associated protein with a death domain (FADD), caspase-8, RIP1 and RIP3. TRADD and FAS are not consistently found in necrotic complex 2, their role therefore remains elusive. In apoptosis mode, caspase-8 triggers the activation of the classical caspase cascade, while RIP1 and RIP3 are cleaved and thus inactivated. When caspase-8 is inhibited (by a pharmacological inhibitor or genetic intervention) RIP1 and RIP3 initiate the effector mechanisms of necroptosis

1.8. Model system of HT-22 cells – ROS induced neuronal cell death

Intracellular accumulation or uncontrolled release of reactive oxygen species (ROS) is a well accepted trigger of cell death in various neurodegenerative diseases and conditions of acute brain damage (70-72).

The mechanisms underlying ROS mediated cell death include oxidation of membrane proteins, DNA-damage and mitochondrial membrane disruption. Due to the high relevance of ROS in neuronal cell death, this study employed the model system of HT-22 cells that well reflects ROS mediated cell death.

HT-22 cells are derived from immortalized hippocampal neurons, rendering them an easily accessible and relevant system for the investigation of neuronal cell death. In HT-22 cells, cell death is induced by glutamate-exposure (oxytosis), but occurs independently of NMDA receptor stimulation, as these cells do not express glutamate receptors. Instead, glutamate-induced death is mediated through competitive inhibition of the xCT transporter, which leads to impaired import of cysteine, decreased glutathione levels and the subsequent accumulation of reactive oxygen species (ROS) (73; 74).

The xCT-antiporter is a plasma membrane transport-protein, which mediates the import of cystine from the extracellular space and the concomitant export of glutamate. Elevated extracellular glutamate concentration thus causes a competitive blockade of the xCT-transport, leading to cystine and subsequently cysteine depletion in the cell (73-75). The resulting shortage of intracellular cystine/cysteine soon causes a decrease in glutathione-plasma levels. Given the crucial role of glutathione as a redox scavenger, reduced glutathione plasma levels give rise to excessive ROS formation and subsequent cell death. This form of cell death has been termed oxytosis (75).

The induction of oxytosis by glutamate in this model system is therefore clearly different from glutamate dependent cell death in primary neurons, which is characterized by excitotoxic increases in intracellular Ca^{2+}.

As established previously, early initiation of cell death in HT-22 cells is closely linked to a rise in ROS due to an enhanced formation of lipidperoxides by activation of 12/15 lipoxygenases (76). In a recent study in GPx4 knockout mice and murine embryonic fibroblasts, the glutathione peroxidase 4 (Gpx4) has been uncovered as a negative regulator of lipoxygenases, thereby linking decreasing glutathione levels

and reduced Gpx4 activity with enhanced 12/15 LOX activity and AIF dependent cell death (77).

In response to the formation of ROS in HT-22 cells, the BH-3 protein Bid is activated and translocates to the mitochondria causing fragmentation and loss of mitochondrial membrane potential (78; 79). As a late event, AIF is released from the mitochondrial intermembrane space, translocates to the nucleus and induces DNA fragmentation and cell death (Figure 5) (78).

In conclusion, excitotoxicity in primary neurons and oxytosis in HT-22 cells follow different initiating routes. The downstream pathways of neuronal apoptosis, however, are very similar in both models, thus highlighting the general suitability of HT-22 cells for studying neuronal cell death.

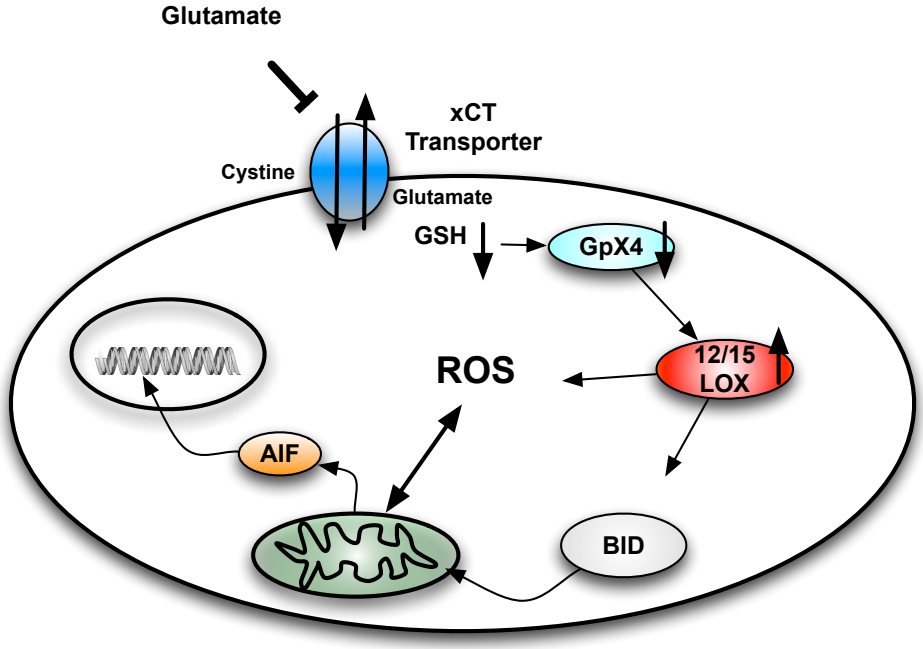

Figure 5: Simplified Model of glutamate toxicity in HT-22 cells (modified from Tobaben, 2011). Exposure to elevated extracellular glutamate concentrations causes a competitive blockade of the xC-Transporter that mediates the import of cystine and the export of glutamate. The resulting decrease in intracellular cystine levels halts glutathione synthesis and causes a fall in Gpx4 activity. In response to these events ROS formation is increased and LOX12/15 is activated, thereby further enhancing the load of intracellular ROS. Downstream activation and mitochondrial translocation of the BH-3 protein Bid causes mitochondrial disintegration and the release of proapoptotic factors, including AIF. AIF in turn translocates to the nucleus leading to DNA cleavage, thereby terminating cell death.

2. Aims of this study

The NF-κB pathway has been recognized as an important transcription factor counteracting pro-apoptotic influences and thereby inducing neuronal survival. Inhibition of the transcription factor p53 by pifithrin-α is an efficient approach to promote neuroprotection, which has been reported to rely at least partially on a mechanism of reciprocal transcriptional repression between NF-κB and p53.

1. It was an aim of this study to investigate the general role of NF-κB in glutamate dependent neuronal cell death and to elicit the subunit-specific profile of the NF-κB response. Further, it should be determined, which transcriptional targets of NF-κB were regulated in glutamate dependent neuronal cell death.

2. It was a second aim to elucidate the subunit-specific response of NF-κB in HT-22 neurons treated with pifithrin-α and to determine how this affects the neuroprotective potential of pifithrin-α.

3. The tumor suppressor CYLD has been implicated in NF-κB signaling, tumor formation and regulated necrotic cell death in various cell types and tissues. The impact of CYLD in neurons, however, has not been addressed so far.
   Therefore, a major aim of this study was to determine the role of CYLD in glutamate dependent neuronal cell death and to evaluate CYLD as a putative target of therapeutic strategies for neuroprotection. Further, it should be determined, which signaling pathways and molecular targets were affected by neuronal CYLD and how this translates into an effect on neuronal survival.

4. The physiological relevance of the findings obtained in model systems of glutamate dependent neuronal cell death should be verified in a model of traumatic brain injury in mice.

3. Materials and Methods

3.1. Cell culture

All standard chemicals were obtained from Sigma-Aldrich (Taufkirchen, Germany) and Carl Roth (Karlsruhe, Germany) if not described otherwise. All buffers and solutions were prepared using demineralized, ultrapure water supplied by the SG Ultra Clear UV plus Reinstwassersystem (VWR, Darmstadt, Germany). Aseptic solutions were prepared using demineralized water, which was sterilized by a steam autoclave (Systec V-40, Systec GmbH, Wettenberg, Germany). Heat sensitive media and solutions intended for use in the cell culture were sterile-filtered using 0.22 µm filter sets (Sarstedt, Nürnbrecht, Germany).

3.1.1. Cell culture material

Cell Culture dishes including 96-, 24- and 6 well plates were acquired from Greiner Bio One (Frickenhausen, Germany). All Falcon-tubes including 50 ml, 15 ml, 2 ml, 1.5 ml and 1 ml tubes were acquired from Sarstedt (Nürnbrecht, Germany). The xCELLigence system and the designated E-plates were obtained from Roche (Penzberg, Germany)

3.1.2. Cell culture medium

HT-22 cells were cultured in Dulbecco's modified eagle medium (DMEM) containing 4.5 mg/l glucose and 110 mg/l sodium pyruvate, which was supplemented further according to table 1. The medium stock and all additional supplements were obtained from PAA (Cölbe, Germany).

Table 1: Dulbeco´s modified eagle medium

DMEM-medium with 4.5mg/l glucose and 110 mg/l sodium pyruvate	440 ml
Heat inactivated fetal calf serum (FCS)	50 ml
L-alanyl-L-glutamine 200 mM	5 ml
Penicillin 10,000 U/ml / Streptomycin 10 mg/ml	5 ml

3.1.3. Culturing HT-22 cells

HT-22 cells were originally generated by Gerald Thiel and David Schubert (Salk Institute, San Diego, USA) and obtained from Gerald Thiel. HT-22 cells have been generated from HT-4 cells, a cell line originating from primary mouse hippocampal neurons. Immortalization has been achieved using a temperature-sensitive SV-40 T antigen (80).

HT-22 stock cultures were kept in 75 cm^2 culture flasks and split twice per week in a ratio 1:10 - 1:20. To this end, growth medium was removed and cells were washed once with warm phosphate buffered saline (PBS, table 3). After removing the washing buffer, 2-3 ml of Trypsin/EDTA solution (Table 4) were added and allowed to incubate for 2-5 minutes. Once the cellular layer has been defeated and cells were largely suspended, trypsination was stopped by adding 10ml of whole DMEM growth medium. Cells were centrifuged at 1000 rpm for 5 minutes, resuspended in 10 ml growth medium and counted using a counting chamber (Neubauer Zählkammer, Brand, Wertheim, Germany). Next, cells were seeded in the appropriate culture dish format, depending on the respective experimental plan. The specific cell densities used in the different formats are given in table 2.

Table 2: HT-22 cells – cell densities

Cell culture format	**Cell density cells/cm^2 (cells/well)**
96 well plate	~ 22,500/ cm^2 (7,000-8,000 cells/well)
24 well plate	~ 180,000/cm^2 (60,000 cells/well)
6 well plate	~ 600,000/cm^2 (200,000 cells/well)
ibidi µ-slide 8-well plates	~ 36,000/cm^2 (10,000-15,000 cells/well)
E-Plate	~ 22,500/ cm^2 - 30,000/ cm^2

Table: 3 Phosphate buffered saline (PBS), pH 7.4

NaCl	9 g
Na_2HPO_4	0.527 g
KH_2PO_4	0.144 g
HCl (0.1M)	q.s. for pH adjustment
Aqua demin.	add to a final volume of 1000 ml

Table 4: Standard Trypsin/EDTA solution

Trypsin (7.500 U/mg)	100 mg
Ethylenediamine-tetra-acetic acid (EDTA)	40 mg
PBS	200 ml

3.1.4. Induction of cell death in HT-22 cells

Cell death in HT-22 cells was induced 24 h after seeding by glutamate addition, typically at a final concentration of 3-5 mM. To this end, growth medium was replaced by culture medium supplemented with glutamate and with additional substances as indicated. Cell death was determined 8-12 h later, with samples taken at the appropriate time points for further analysis by absorption photometry, flow cytometry, epifluorescence microscopy and protein analysis.

3.2. Primary embryonic cortical cultures

3.2.1. Coating of culture dishes

Primary embryonic cortical neurons were cultured in cell culture dishes, coated with 5 % polyethylenimine (PEI, table 6). Coating was performed by incubating culture dishes with 5 % PEI for 2 h at room temperature (the exact composition of PEI-solution is given in table 6). The dishes were then washed three times with aqua demin. and dried while exposed to UV-light for 30 minutes. Cell dishes then were covered with minimum essential medium (MEM+) and incubated overnight (Table 5).

Table 5: Minimum essential medium (MEM+)

MEM (powder)	9.39 g
HEPES	0.238 g
Glucose	10 g
$NaHCO_3$	2.2 g
KCl	112 g
Na-Pyruvate	0.12 g
L-Glutamine	0.176 g
Gentamycin-sulfate (10mg/ml)	1 ml
NaOH (0.1 M)	q.s. for pH adjustment to 7.2
Aqua demin.	add to a final volume of 1000 ml

Table 6: Polyethhylenimin (PEI) coating solution

Boric acid	3.1 mg
Borax	4.75 mg
PEI	1 ml
Aqua demin.	add to a final volume of 1000 ml

3.2.2. Preparation of primary cortical cultures

Primary cortical cultures were prepared as described previously (19). In brief, cortices were removed from embryonic C57black/6 mouse and rat brains (E17-18), trypsinized for 15 min (1 mg/ml) and incubated with DNAse 0.1 mg/ml for one minute (Sigma-Aldrich, Taufkirchen, Germany). Cortices were washed with HBSS, incubated with Trypsin-inhibitor (1 mg/ml, Sigma-Aldrich, Taufkirchen, Germany) and washed again. Afterwards, the cell suspension was triturated and allowed to stand for 2 minutes. Precipitating cellular debris was removed and the cell suspension was subjected to centrifugation.

Cells were resuspended in neurobasal medium (Stock from Invitrogen, Karlsruhe, Germany, final composition given in table 8) and counted using the counting chamber by Neubauer (Brand, Wertheim, Germany). The dissociated neurons were seeded onto polyethyleneimine-coated 6well culture dishes at a density of 400,000-600,000 cells/well. The cultures were grown in neurobasal medium (PAA, Cölbe, Germany) supplemented as described in table 7. On day 5 in culture half of the medium was replaced by fresh media.

Table 7: Hank´s balanced salt solution (HBSS)

10x HBSS stock solution	100 ml
HEPES	2.4 g
Gentamycin-solution (10mg/ml)	1 ml
NaOH (0.1 M)	q.s. for pH adjustment to 7.2
Aqua demin.	add to a final volume of 1000 ml

Primary cortical neurons were cultured in neurobasal medium (Table 8), supplemented with 2% B27 (Invitrogen, Karlsruhe, Germany).

Table 8: Neurobasal medium

Neurobasal medium	490 ml
4-(2-Hydroxyethyl)piperazine- 1-ethanesulfonic acid (HEPES)	575.3 mg
L-Glutamin	88.8 mg
Gentamycin-sulfate (10 mg/ml)	0.5 ml
B-27 supplement	10 ml
NaOH (0.1 M)	q.s. for pH adjustment to 7.2

3.2.3. Induction of excitotoxic cell death in primary cortical neurons

On day six in culture, primary cortical neurons were exposed to glutamate for 1 h at a final concentration of 200-500 µM. To this end growth medium was removed, cells were washed once with warm EBSS and then exposed to glutamate diluted in EBSS (Table 9). If indicated, additional substances such as necrostatins were co-administered. Afterwards, the original growth medium, which had been collected before the treatment, was re-applied to the cells, and supplemented with the respective compounds, as indicated. Cell death was analyzed similarly as for the other damage regime.

Table 9 Earl´s balanced salt solution (EBSS)

10x EBSS stock solution	100 ml
$NaHCO_3$	2.2 g
NaOH (0.1 M)	q.s. for pH adjustment to 7.2
Aqua demin.	add to a final volume of 1000 ml

3.3. Chemicals and reagents

All standard chemicals were obtained from Sigma-Aldrich (Taufkirchen, Germany) and Carl Roth (Karlsruhe, Germany) if not described otherwise. All buffers and solutions were prepared using demineralized, ultrapure water supplied by the SG Ultra Clear UV plus Reinstwassersystem (VWR, Darmstadt, Germany). Demineralized water for aseptic preparation of solutions was sterilized beforehand using a steam autoclave (Systec V-40, Systec GmbH, Wettenberg, Germany). Heat sensitive media and solutions intended for use in the cell culture were sterile-filtered using 0.22 µm filter sets (Sarstedt, Nürnbrecht, Germany).

The following compounds were used for induction or prevention of cell death:

Reagents: soluble, recombinant murine TNF-α, Necrostatin 1, Necrostatin 5, Necrostatin-7 (#ALX-522-009, #AP-309-UU20, #ALX-430-169, #ALX-430-170, all Enzo Life Science, Plymouth Meeting, USA), Geldanamycin (#EI-280-0001, Enzo Life Science, Plymouth Meeting, USA), ABT-737 (#S1002, Selleck Chemicals, Houston, USA), PFT-α (P4359; Sigma-Aldrich, Munich, Germany), L-Glutamic acid (G6642; Sigma-Aldrich, Munich, Germany), SM-164, kind gift from Shamoeng Wang, University of Michigan.

3.3.1. Primary antibodies

All primary antibodies were used at a dilution of 1:1000 for WB and 1:200 for immunocytochemistry (ICC). Antibodies intended for use in western blot applications were diluted in Tris-buffered saline containing 0.05 % Tween 20 and 5 % skim milk powder, if not stated otherwise (Table 10), (Sigma-Aldrich, Munich, Germany). In this study, the following antibodies have been used: anti-CYLD antibody diluted 1:100 (#sc74434 Santa Cruz Biotechnology, Santa Cruz Biotechnology, CA, USA), anti-RIP1 antibody (#610459, BD Biosciences Pharmingen, Heidelberg, Germany) anti-RIP3 (#2283, ProSci, San Diego, USA), anti COX IV (#4844, Cell Signaling Technology, Beverly, USA) anti pan-cIAP (#3400, R&D systems, Minneapolis, USA), anti-IkBα, PIkBα and RelB (#4814, #9246, #4953, Cell Signaling Technology, Beverly, USA), anti neuronal nuclei (#MAB377, Millipore, Billerica, USA), anti p50, p52, p65 (#ab7971, #ab7972, #ab7970, Abcam, Cambridge, UK), anti cRel, anti Bcl-3 (#sc-71, #sc-185, Santa Cruz Biotechnology, CA, USA) anti TNFα (#AB-410-NA, R&D systems, Minneapolis, USA), anti-α-tubulin monoclonal antibody (#T6074 Sigma-Aldrich, Munich, Germany), anti-Aktin (#691001, MP-Biomedicals, Solon, USA).

3.3.2. Secondary antibodies

For Western blot analysis horseradish peroxidase (HRP) labeled secondary antibodies were used (All Vector Labs, Burlingame, California, USA). Secondary antibodies were diluted 1:4000 in Western-blotting buffer consisting of Tris-buffered saline with 0.05 % Tween 20 and 5 % skim milk powder (Sigma-Aldrich, Munich, Germany). For immunocytochemistry, fluorochrome coupled antibodies Alexa488

and DyLight 633 anti-mouse and rabbit antibodies were used (Invitrogen, Karlsruhe, Germany and Thermo Fisher Scientific, Rockford, USA). For ICC, secondary antibodies were diluted 1:200 in phosphate buffered saline (1x PBS) containing 3 % horse serum (Invitrogen, Karlsruhe, Germany.

3.3.3. siRNA sequences

Sequence specific siRNA duplexes for CYLD (5´UGAAAUGACUGAGCGAUAA3´) or 5' CUGCAUUGAUGAUACGAUA3', RIP1 (5'GAAUGAGGCUUACAACAGA3), CyclinD1 (pool of 4, equally)' (ACUAUUUCAUCCCUACCGCtg3'), (5'GCGGUAGGGAUGAAAUAGUtt3') (5'CGAUUUCAUCGAACACUUCtt3'), (5'GAAGUGUUCGAUGAAAUCGtg3') and a nonfunctional mutant (scrambled) siRNA duplex 5' UAAUGUAUUGGAACGCAUATT3' were purchased from MWG (Eurofins MWG Operon, Ebersberg, Germany). The validated smart-pool ON-TARGETplus siRNA for RIP3 (5´UCAAGAUCGUGAACUCGAA´3; 5´CAAGUUCGGCCAAGUAUGA3'; 5´GGUAAAGCAUUAUCUGUCU3'; 5'ACACGGCACUCCUUGGUAU3' and Bcl-3 5'GACCUUUGAUGCCCAUUUA3'; 5' UCGCUGUGGUCCAGAAUAA3'; 5' CGUGAACGCUCAGAUGUAU3'; 5'AAGUAGACGUCCAUAACAA3' were all purchased at Dharmacon (#L-049919-00-0005, #M-045102-00-0005, Dharmacon, Lafayette, USA).

3.3.4. Plasmids

The overexpression vector for murine CYLD was purchased form Open Biosystems (clone-id 3983771, Huntsville, USA). The mitoGFP (mGFP) vector used as a control vector was a gift from Andreas Reichert (Goethe University Frankfurt, Germany). NF-κB reporter plasmid was obtained from BD Bioscience (#6053-1, Clontech, Heidelberg Germany).

All plasmids were amplified using the QIAGEN Plasmid Plus Midi kit (Qiagen, Hilden, Germany). After resuspension, plasmid concentration was determined by UV absorption using a NanoVue Plus Spectrophotometer (Implem, GE Healthcare Europe GmbH, Freiburg, Germany).

3.3.5. PCR-primer

T7-Primers for DICER siRNA generation: CYLD fw 5'GCGTAATACGACTCACTATAGGGAGACTCAGCCTATTTAGAAACAGACT3', rv 5'GCGTAATACGACTCACTATAGGGAGATACACCTCTTGACATAAAGGC3', CYLD primer for mRNA analysis (T7 primers may be used as well) fw 5'CTCAGCCTATTTAGAAACAGACT3', rv 5'ATACACCTCTTGACATAAAGGC3', murine GAPDH fw5`-CGTCTTCACCACCATGGAGAAGGC-3`, rv 5`-AAGGCCATGCCAGTGAGCTTCCC-3. CYLD exon4 fw 5'ACAACATGGATGCCAGGTTG3', rv 5'CCGCTAATAAAGGTCCTCTG3', CYLD LACZ fw 5'GCATCGAGCTGGGTAATAAGCGTTGGCAAT3', rv 5'GACACCAGACCAACTGGTAATGGTAGCGAC3'
All primers were synthesized at MWG (Eurofins MWG Operon, Ebersberg, Germany). Oligo (dt) 15 primers were obtained from Promega (Madison, USA).

3.4. Kits

The following list encompasses the kits used for this study:

Annexin-V-FITC Detection Kit	Promokine, Heidelberg, Germany
Bodipy (581/591 C11)	Invitrogen, Karlsruhe, Germany
JC-1	Invitrogen, Karlsruhe, Germany
RNAiMax	Invitrogen, Karlsruhe, Germany
Pierce BCA Kit	Perbio Science, Bonn, Germany
NucleoSpin RNA II Kit	Machery & Nagel, Düren, Germany
Nucleus extraction kit	Active Motif, Carlsbad, USA
Luciferase assay sytem	Promega, Madison, USA
QIAGEN Plasmid Plus Midi	Qiagen, Hilden, Germany
SuperScript III (One Step RT-PCR)	Invitrogen, Karlsruhe, Germany
M-MLV Reverse Transcriptase	Promega, Madison, USA
Dicer siRNA generation kit	Genlantis, San Diego, USA
DNA tissue extraction kit	Peqlab, Erlangen, Germany

3.5. Transfection methods

3.5.1. siRNA transfections

siRNA was transfected using RNAiMax transfection reagent (Invitrogen, Karlsruhe, Germany) according to the manufacturer´s instructions. The transfection was carried out in a 24 well format using a „reverse-transfection“ protocol. Accordingly, siRNA duplexes were prediluted in OptiMEM medium at a concentration of 120-300 nM. Eleven µl of RNAiMax transfection reagent was added to 1 ml of the premixed siRNA. After repeated inversion of the tubes, 100 µl of the liposomal complexes were transferred into each well of the 24-well plate. Following 20 minutes of incubation, 500-550 µl of cell suspension (60,000 HT-22 cells/ml in DMEM without antibiotics) were added to each well. After gentle shaking of the culture plates, HT-22 cells were returned to the incubator. Samples were taken after 24 h for RNA analysis and after 48-72 h for protein extracts respectively. If a transfer to another cell culture format was necessary, HT-22 cells were reseeded 48 h after transfection.

3.5.2. Plasmid transfection

HT-22 cells were seeded in antibiotic-free medium at a density of 60,000 cells/well in a 24-well format. Twenty-four h later and shortly before transfection, medium was changed to 900 µl/well of antibiotic free and serum free DMEM medium. Polyethylenimin (PEI, was a kind gift from BASF, Germany) particles and DNA-plasmids were diluted in glucose solution (5%) at a concentration of 28.8 µg/ml and 30 µg/ml respectively. Equal amounts were mixed and incubated for 20 minutes to allow the formation of PEI polyplexes. One hundred µl of these polyplexes were added to each well giving rise to a final concentration of 1-1.5µg of PEI/ml and 1-2 µg of plasmid/ml. Following another incubation period of 4 h, medium was replaced by whole DMEM medium.

3.6. Cell viability assays

For detection of cell death by MTT-assay, HT-22 cells were seeded in 96-well plates, or alternatively in 24-well plates. Primary cortical neurons were cultured in 6-well plates and cell death was evaluated by manual counting of pyknotic nuclei. For detection of cell death by Annexin-V and propidium iodide staining, HT-22 cells were seeded in 24-well plates.

3.6.1. MTT assay

The MTT assay relies on the reductive processing of 3-(4,5- dimethylthiazol- 2-yl)-2,5-diphenyltetrazolium bromide (MTT) to formazan by either a lyosomal/endosomal compartment or mitochondria (81). As the MTT turnover primarily reflects metabolic activity, a direct correlation with cell death needs to be established separately using further cell death assays. The reduction of MTT is accompanied by a pronounced change in absorption characteristics, which is easily detected by absorptive spectroscopy.

MTT-reagent (Sigma-Aldrich, Taufkirchen, Germany) is dissolved in PBS at an appropriate concentration of e.g. 1.5 mg/ml. MTT reagent is then added to the culture medium of HT-22 cells at a final concentration of 0.25 – 0.5 mg/ml. Following an incubation of 1h at 37° C, medium was removed and the culture plates were transferred to a -80° C freezer. After at least 1 h at -80° C formazan crystals were dissolved in 100 µl DMSO/per well (Sigma-Aldrich, Taufkirchen, Germany) under continuous shaking at 37° C. Absorption was measured 1h later at 570 nm using a microplate reader (Fluostar OPTIMA, BMG Labtech, Offenburg, Germany). Background was detected at 630nm and substracted accordingly. Cell viability was expressed as absorption level relative to controls. For statistical analysis the experiment was repeated three times.

3.6.2. DAPI staining

Primary cortical neurons from embryonic mice or rat (day 17-18) were cultured in 6 well culture dishes as described before. Following glutamate exposure over the respective time, cells were washed once with PBS and fixed with 4% paraformaldehyde for 20 minutes. Following another washing step with PBS, cells were exposed to 4′,6-diamidin-2-phenylindol (DAPI) at a final concentration of 1

µg/ml in PBS for 5-10 minutes. Replacement of DAPI solution with PBS was performed optionally to reduce background fluorescence, when required. DAPI-stained nuclei were visualized using an epifluorescence-microscope with a 40x magnification and 340 nm for excitation (DMI6000B, Leica, Wetzlar, Germany). Pyknotic cells showing highly condensed or fragmented nuclei were considered apoptotic. Counting and anaylsis of pyknotic nuclei was performed blind to the treatment group. An average of four hundred cells, grown in five different regions, were counted per well. Each experiment was repeated three times.

3.6.3. Annexin-V/propidium iodide staining

The externalisation of phosphatidylserine is a well-recognized event occurring in cells undergoing apoptotic cell death. Binding of fluorescein isothiocyanat (FITC) labeled Annexin-V is commonly used to detect phosphatidylserine residues present on the outer cellular membrane of apoptotic cells. Necrotic cell death in turn can be visualized by propidium iodide, a dye, which upon binding to DNA shows a pronounced shift in absorption characteristics. Under physiological conditions cellular membranes are impermeable for propidium iodide, resulting in no fluorescent staining of nuclei. Membrane leakage, occurring in necrotic cells, however, significantly increases the cellular permeability for propidium iodide, thus staining nuclei of cells prone to undergo necrosis.

For evaluation of cell death using Annexin-V and propidium iodide, HT-22 cells were harvested using 1 x TE, washed once with PBS and incubated in 500 µl binding buffer supplied as a component of the Annexin-V-FITC Detection Kit (PromoKine, Heidelberg, Germany). Five µl of the AnnexinV- and propidium iodide stock solution were added. Apoptotic and necrotic cells were detected using a FACScan (Becton, Dickinson and Company), Annexin-V and propidium iodode fluorescence was exited at a wavelength of 488 nm and emission was detected at 530±40 nm and at 680±30 nm respectively. To avoid detection of cellular debris and clusters, cells were gated accordingly using forward and sideward scatter. For each sample 10,000 cells were analyzed. The experiment was repeated three times.

3.6.4. Detection of the mitochondrial membrane potential - JC-1 assay

Reduction of 5, 5', 6, 6'- tetrachloro-1, 1', 3, 3'-tetraethylbenzimidazolylcarbocyanine iodide (JC-1) was applied to evaluate mitochondrial membrane potential in HT-22 cells. HT-22 cells were stained with JC-1 according to the manufacturer's protocol (Invitrogen, Karlsruhe, Germany) and analyzed by fluorescence-activated cell sorting (FACS). Approximately 10 hours after glutamate treatment, JC-1 was added to each well at a final concentration of 2 µM and incubated for 30 min. As a positive control, carbonyl cyanide m-chlorophenylhydrazone (CCCP) was used, which causes a near complete depletion of the mitochondrial membrane potential following an incubation-period of 15 minutes. Cells were harvested with standard Trypsin/EDTA (Sigma-Aldrich, Taufkrichen, Germany) in 1x PBS. To enhance trypsination, cells were carefully pipetted up and down several times and collected in full DMEM medium. Following centrifugation at 1,000 x g for 5 minutes at room temperature, cells were washed once with 1x PBS, and kept in 0.5 ml 1x PBS on ice. Analysis of JC-1 fluorescence was conducted using a FACScan (BD Bioscience, Heidelberg Germany). JC-1 green fluorescence indicates mitochondrial uptake of the dye, while JC-1 red fluorescence indicates intact mitochondrial membrane. JC-1 green fluorescence was excited at 488 nm and emission was detected using a 530 ± 40 nm band pass filter, JC-1 red fluorescence was excited at 488 nm and emission was detected using a 613 ± 20 nm band pass filter. Cells were gated to exclude cellular debris and cell clusters. At least 10,000 cells were analyzed per sample.

3.6.5. Detection of lipid peroxidation – BODIPY assay

For detection of cellular lipid peroxidation, cells were loaded with 2 µM BODIPY 581/591 C11 (Invitrogen, Karlsruhe, Germany) for 60 min in standard medium. Incubation was carried out at the indicated time points, usually 10 h post-glutamate exposure. Cells were washed once with PBS prior to harvesting them with standard Trypsin/EDTA (1x TE, Sigma-Aldrich, Taufkrichen, Germany) in 1x PBS. To enhance trypsination, cells were carefully pipetted up and down several times and collected in full DMEM medium. Following centrifugation at 1000 x g for 5 min. at room temperature, cells were washed once with 1x PBS, and kept in 0.5 ml 1x PBS on ice. Flow cytometry was performed using 488 nm UV line argon laser for excitation and BODIPY emission was recorded on channels FL1 at 530 nm (green) and FL2 at 585 nm (red). Data was collected for each sample from 10,000 cells. Increased lipid

peroxidation induces a shift from red to green fluorescence that can be detected by flow cytometry (FACScan, BD Bioscience, Heidelberg Germany).

3.7. Detection of cell death by impedance measurement – The xCELLigence system

3.7.1. Measurement of cellular impedance for analysis of cell death

Neuronal cell death follows distinct pathways, including apoptosis, autophagic cell death and necrosis (5). Though progression and execution of these pathways differ significantly, cell death is usually accompanied by clear changes in cellular morphology, allowing also for visual differentiation of living and dead cells. By measuring cellular impedance using e.g. the commercially available xCELLigence system (Roche Diagnostics, Penzberg, Germany), these morphological changes can be tracked indirectly and applied for evaluation of cell death.

The xCELLigence system is a microelectrode biosensor designed for the use with dedicated multi-well plates (E-plates®, Roche Diagnostics, Penzberg, Germany), which feature an integrated network of microelectrodes in each well (Figure 6A). For measuring impedance between these electrodes a low AC excitation voltage level (mV range) and a resulting minor electrical current (µA range) are applied, which have been proven to be without any effect on cellular function. The impedance readout by the xCELLigence system is presented as arbitrary Cell Index values, expressing changes between baseline and each measurement point, according to the following equation CI = (Zi – Z0)/15. In this equation, Zi is the impedance at any given time point and Z0 the background signal.

Usually, impedance measurements in aqueous solution are influenced by the temperature, the shape of the electrodes, the ionic strength and additional insulating material as for instance cell-layers covering the electrodes. Consequently, if the three factors first mentioned are kept even, the impedance readout only depends on the degree of insulation inflicted by cells grown on top of the electrodes. To highlight this dependence, the term cellular impedance is commonly used for describing impedance analyses in cell culture systems. As indicated in figure 6B, changes in cellular impedance occur either, because of increases in cell number (proliferating cells), an increase in the outer cell surface (differentiation) or altered attachment

properties (e.g. cellular detachment during cell death). In conclusion, all these changes in impedance, result from an altered insulating-capacity of the cellular layer. In a previous study, we successfully validated the correlation between cellular impedance readouts and cell death for HT-22 cells, rendering the xCELLigence system a fast and easy approach for confirming viability data gained by ordinary assays (82).

The xCELLigence system, however, adds more to a deeper understanding of cell death processes, as it allows to unravel cell death kinetics and to distinguish between transient or permanent protective effects. This is due to the nature of real time detection, an inherent feature of the xCELLigence system. Nonetheless, certain cell types will prove inadequate for impedance measurements, for which reason suitability needs to be confirmed individually when starting with a new cell type (28).

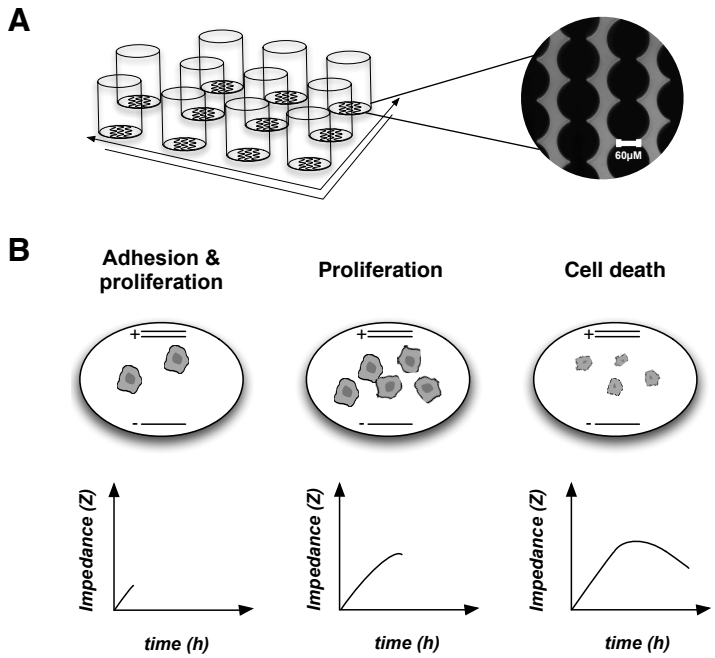

Figure 6: Schematic overview of the measurement principle of cellular impedance. (A) Each well of the culture dish features a bottom with embedded gold-electrodes. The electrode array has a minimal distance of 30 µm between the electrodes. The right picture shows a magnified upright view of the electrode array. (B) Cells were seeded on top of the electrode-covered surface of the culture dish. After attaching to the bottom of the well, the cells partially insulate the electrodes, causing a rise in impedance. With an increasing cell density, the cells have a greater overall insulating capacity, showing in a further increase in impedance. Inflicting cellular damage and cell death causes changes in membrane morphology, cellular shrinkage and detachment, resulting in a decrease in cellular impedance.

3.7.2. The xCELLigence system in HT-22 cells

Using the xCELLigence system for detection of proliferation and cell death in HT-22 cells, an average cell density of 22,500 cells/cm^2 proved most appropriate. Prior to seeding the cells, background impedance was determined using 100 µl of cell culture medium. Next, cell suspension was added to a total of 200 µl/well. Due to the great sensitivity of the system, changes in temperature strongly influence the measurement, for which reason, treatment procedures outside of the incubator were conducted at the utmost speed.

Treatment of HT-22 cells was started as early as 20-24 h after seeding, when the cell index exceeded a value of 1. For any treatment, a mere 100µl were removed and replaced by the corresponding amount containing the respective components of interest. Cell-index values were recorded using RTCA Software 1.2 (Roche Diagnostics, Penzberg, Germany). Each experiment was repeated 3 times.

After concluding each experiment, E-plates were recycled using the following scheme. After removing media and washing the plates twice with demineralised water, standard Trypsin/EDTA (1x TE, Sigma-Aldrich, Taufkirchen, Germany) was added for 15-20 minutes. Afterwards 1xTE was removed, the plates were washed further 3 times and irradiated with UV light for 30 minutes to reassure sterility. Plates handled this way can be reused several times. However, before starting a new experiment structural integrity and functionality of the electrodes should be assessed by evaluating the homogeneity of the impedance profile of the E-plate under control conditions. This can be done easily by choosing the well analysis tab in the RTCA software.

3.8. Immunocytochemistry

3.8.1. Immunocytochemistry of NF-κB subunits, RIP1 and RIP3

Immunocytochemical stainings of HT-22 cells were carried out in ibidi 8-well plates (Ibidi GmbH, Munich, Germany) at a density of 15,000 cells/well. Following the respective treatment regime, cells were washed once with PBS, fixed with 4 % PFA in PBS for 20 minutes and washed again with 1x PBS. Afterwards, the cells were permeabilized by 0.4 % Triton X-100 (Sigma- Aldrich, Taufkirchen, Germany) in 1x

PBS for 5 minutes. Blocking of unspecific binding sites was achieved by incubation with blocking solution containing 3 % horse serum (Invitrogen, Karlsruhe, Germany) in 1x PBS for 30 minutes. Cells were then treated with the primary antibodies listed in the respective section. Antibodies were diluted 1:100 in blocking solution and incubated overnight at 4 °C. After washing with PBS three times, one of the appropriate secondary antibodies enlisted above was incubated in blocking solution for further 90 minutes at room temperature.

After counterstaining the nuclei with DAPI (1 µg/ml), cells were washed again twice. Background fluorescence caused by unspecific binding of secondary antibodies was determined by staining cells only with the secondary antibody. Images were taken using a confocal laser-scanning microscope (Axiovert 200, Carl Zeiss, Jena, Germany) equipped with an UV and an argon laser. Depending on the excitation requirements for the secondary antibody, light was delivered at 488 or 633 nm, DAPI was excited at 364 nm. For digital imaging the software LSM Image software (Carl Zeiss, Jena, Germany) was used.

3.8.2. MitoTracker staining and evaluation of mitochondrial morphology

Mitochondrial morphology in HT-22 cells (grown in ibidi slides, 15,000 cells/well) was visualized using MitoTracker dyes supplied by Invitrogen (Karlsruhe, Germany). MitoTracker DeepRed was dissolved in DMSO at a final stock-concentration of 50 µM and kept protected from light. MitoTracker reagent was then diluted 1:250 in culture medium and added to the cells (final working concentration 200 nM) for 20 minutes before starting the respective treatment. Cells were washed once with warm culture medium after incubation with MitoTracker, to assure complete removal of the dye. After completing the experiment, cells were washed with PBS, fixed with 4% PFA and washed again twice with PBS.

For investigation of mitochondrial localization, subsequent immunocytochemical stainings for RIP1 and RIP3 were performed following the instructions given above. Images were taken using a confocal laser scanning microscope running LSM Image software (Axiovert 200, Carl Zeiss, Jena, Germany). MitoTracker DeepRed fluorescence was excited at a wavelength of 633 nm (band pass filter) and emissions were detected using a 670 nm long pass filter. Evaluation and classification of mitochondrial morphology was performed as described before (79). Following this classification scheme, mitochondria were counted manually and categorized in 3

subgroups, depending on the degree of fragmentation. Accordingly, category 1 reflects the intact tubular network of mitochondria found under control conditions, whereas category 2 and 3 indicate an increasing number of fragmented mitochondria.

As the studies by Grohm et al. revealed, increased mitochondrial fragmentation was accompanied by an apoptotic phenotype, showing e.g. in nuclear condensation and the peri-arrangement of the mitochondrial fragments. For the quantification of mitochondrial morphology, at least two hundred cells per well were counted and experiments were performed at least three times. Counting was performed blinded to the treatment history.

3.9. Protein analysis

3.9.1. Buffers for Western blot analysis

Table 10: Buffers for Western blot analysis

Stacking gel 3.5%

0.5 M Tris HCl solution pH 6.8	2.5 ml
Acrylamid/bisacrylamide (37.5 : 1) 30%	1.2 ml
Sodium dodecyl sulfate solution 10%	0.1 ml
Ammoniumpersulfate solution 10%	0.05 ml
Tetramethylethylenediamine TEMED	0.01 ml
Bidest dH_20	add to a final volume of 10 ml

Collection gel 12.5%

1.5M Tris HCl solution pH 8.8	2.5 ml
Acrylamid/bisacrylamide (37,5:1) 30 %	3.34 (4 ml for 12.5% gels)
Sodium dodecyl sulfate solution 10 %	0.1 ml
Ammoniumpersulfate solution 10 %	0.05 ml
Tetramethylethylenediamine TEMED	0.01 ml
Bidest dH_20	add to a final volume of 10 ml

1 x Electrophoresis-buffer

Tris base	3 g
Glycine	14.4 g
Sodium dodecyl sulfate (SDS)	1 g
Bidest H_2O	add to a final volume of 1000 ml

1x Transferbuffer, pH 8.3

Tris base	3 g
Glycine	14.4 g
Methanol	100 ml
HCl 0.1M	q.s
Bidest dH_20	add to a final volume of 1000 ml

1x TTBS, pH 7.5

Tris Base	2.4 g
NaCl	29.2 g
HCl 0.1M	q.s.
Bidest dH_2O	add to a final volume of 10 ml

1x Blocking buffer

Skim milk powder	25 g
TBST	add to a final volume of 500 ml

Stripping buffer, pH 2

Glycine	15 g
Sodium Dodecyl sulfate (SDS)	1 g
Tween 20	10 ml
HCl conc.	q.s.
Bidest dH_2O	add to a final volume of 1000 ml

5x sample buffer Western blot

1 M Tris-HCl pH 6.8	70 ml
Glycerol	30 ml
D,L-dithiotreitol (DTT)	9.3 g
SDS	10 g
β-Mercaptoethanol	1 ml
Bromophenol blue sodium salt	12 mg

3.9.2. Protein extraction and measurement of protein content

For protein analysis HT-22 cells and primary neurons were seeded in 6-well plates at a density of 200,000 cells/well for HT-22 cells and 400,000 cells/well for primary neurons. To avoid the risk of protein degradation cells were kept on ice during the whole process of extraction. After removing the culture medium, cells were washed

once with PBS. To avoid loss of detached cells, washing buffer was collected and centrifuged.

The remaining pellet was washed again and pooled subsequently with the main extract. Cells were removed from the culture dishes using cell scrapers (Sarstedt, Nümbrecht, Germany) and lysed in protein extraction buffer adjusted to pH 7.8 (0.25 M D-Mannitol 0.05 M Tris-base, 1 mM EDTA, 1 mM EGTA and 1% Triton X-100). The buffer was supplemented with 1 tablet complete mini protease inhibitor cocktail and if required 1 tablet phosphatase inhibitors PhosphoSTOP (both Roche, Mannheim, Germany). For long term storage protein samples were stored at -80° C. Prior to determining protein content, samples were centrifuged at 13,000 U/min at 4° C for 10 min. The supernatant was transferred to a fresh cup and analyzed subsequently for protein content using the Pierce BCA kit according to the manufacturer's instructions (Perbio Science, Bonn, Germany).

The colorimetric reaction of the BCA assay consists of two separate reactions. In a first step, Cu^{2+} is reduced to Cu^{1+} by certain aminoacids including tryptophane and tyrosine. In the second step, Cu^{1+} is chelated by bicinchoninic acid, giving rise to a deeply colored complex, whose concentration is determined by absorptive spectoscropy at 562 nm. Protein content is then determined using a standard curve. Each sample was measured after incubating 2.5 µl of protein lysate with 200 µl of reaction buffer at 60°C for 30 minutes. Samples were cooled on ice to halt the reaction and equal amounts of each sample were transferred to a multi-well plate for spectrophotometric analysis, which was carried out using a microplate reader (Fluostar OPTIMA, BMG Labtech, Offenburg, Germany).

3.9.3. Immunoprecipitation

Immunoprecipitation was performed using DynaBeads coupled with Protein A according to the manufacturer´s protocol (Invitrogen, Karlsruhe, Germany). Briefly, 50 µl of DynaBeads suspension was pulled down and resuspended in 200 µl of PBS, containing 10 µg of the antibody meant for pulldown and 0.05 % of Tween, to prevent clogging of the beads. Following an incubation period of 30 min, the beads were washed with TBST (0.05 % Tween) and crosslinked by 2.5 mM Bis-Sulfosuccinimidyl-substrate for another 30 minutes (BS^3, Thermo Fisher Scientific, Rockford, USA). Crosslinking was terminated by adding 1 M TRIS-buffer (pH 7.5) to a final concentration of 50 mM. The beads were washed again and incubated with

the protein samples for 2-5 h, depending on the affinity at 4°C. Immunoprecipitation was carried out using 1.25 mg of protein.
Importantly, the amount of lysate of the different samples, with which the beads are incubated, needs to be adjusted to the same volume using protein lysis buffer. After thorough washing, elution of immunoprecipitated proteins was performed at 90°C using 70 µl of 2.5x sodium dodecyl sulfate (SDS) -sample buffer. Samples were stored at -80°C for later analysis by Western blot.

3.9.4. Generation of polyacylamide gels for Western Blot analysis

Gels were prepared using BIO-RAD gel casting stand and casting frames. Gels were prepared using a polyacrylamide separation gel with a concentration of 10-12.5 % and a stacking gel with 3.5 %. The specific buffers used for generation of gels and subsequent electrophoresis are given in table 10.

3.9.5. Gel electrophoresis

Sodium dodecyl sulfate polyacrylamide gel electrophoresis (SDS-PAGE) has been used to separate proteins according to their different molecular-mass, thus providing samples for further analysis by Western blot. Prior to electrophoresis, samples were prepared using 20-30 µg of raw protein extract, adjusting the volume to 24 µl with aqua demin. and adding another 6 µl of 5x SDS sample buffer. Samples were heated at 95°C for 5 minutes and loaded onto the gel after reaching room temperature. For comparative evaluation of molecular-mass, 5-10 µl of PageRulerTM Plus Prestained Ladder (Fermentas, St. Leon-Rot, Germany) were loaded next to the samples. Electrophoresis was performed initially at 60 V for approximately 30 min to allow for sample collection and increased later to 120 V. Following electrophoretic separation, proteins were blotted on a polyvinylidenfluorid membrane (PVDF, Bio-Rad, Munich, Germany) according to the recommendations by Bio-Rad at 15 V for 60 minutes.

PVDF-membranes were first activated in methanol for 2 minutes and then incubated for 10 minutes in 1 x transfer buffer before blotting. Meanwhile Whatman-blotting paper and the acrylamide gel were incubated for 10 minutes in transfer buffer. Blotting was carried out, by stacking one layer of Whatman-paper on top of the anodic plate, followed by the second layer the PVDF-membrane, the acrylamide gel as the third, and another final layer of Whatman-paper on top. Blotting was carried

out in a Trans-Blot SD semi-dry transfer cell (Bio-Rad, Munich, Germany) using extra thick Whatman filter paper (Bio-Rad, Munich, Germany) and 1x transfer buffer containing 10 % of methanol.
After blotting for 1h, the PVDF-membranes were transferred directly to 5% Western-blot blocking buffer and incubated for 1 h at room temperature. Then the blots were probed with the primary antibodies (diluted in blocking buffer) overnight at 4°C. The next day, membranes were washed twice with TBST for 5 minutes and probed with the appropriate HRP-conjugated secondary antibody in 5 % blocking solution for one hour. Following 3 washing steps with TBST for 15 minutes each, membranes were incubated with chemiluminescent substrate solution HRP-Juice (PJK GmbH, Kleinblittersdorf, Germany). Chemiluminescent signals were recorded and quantified by densitometric analysis using the semi-automated Chemidoc-XRS Imaging System and the dedicated Quantity One software package (both, Bio-Rad, Munich, Germany).

3.9.6. Subcellular fractionation - Nucleus extraction

Nuclear extracts from HT-22 cells were prepared using the nuclear extraction kit (Active Motif, Carlsbad, USA) according to the manufacturer's protocol. For each nucleus extract cells from three individual 75 cm^2 flasks were pooled, each of them containing 1-2x10^6 cells. Cells were washed once with PBS supplemented with phosphatase inhibitors and then collected in fresh buffer (all components supplied with the kit). Cells were spinned down at 500 rpm for 5 minutes and resuspended in 500 µl hypotonic buffer, to which additional 25 µl of detergent were added. Following disruption of the cytosolic membrane occurring after 15 minutes of incubation, the nuclei were spinned down at 14,000 g for 30 seconds and washed once with hypotonic buffer. The nuclei were then incubated in 60 µl complete lysis buffer for 30 minutes on ice. Samples were vortexed initially and after completing incubation. The remaining membrane fraction was removed afterwards by centrifugation at 14,000 g for 15 minutes. Samples were analyzed by Western blot analysis as described before.

3.9.7. Subcellular fractionation - Mitochondrial extraction

Isolation of mitochondria from HT-22 cells was performed by Julia Grohm as described previously (144). Briefly, $1x10^7$ cells were harvested for each treatment condition and suspended in mito-fractionation buffer (Table 11). Following cellular disruption using a glass douncer, nuclei were separated by centrifugation at 830 g for 10 min. The remaining supernatant was centrifuged again at 16,800 g for 10 minutes to seperate the cytosolic fraction. The supernatant was then transferred to another tube and the remaining pellet, representing the mitochondrial fraction, was resuspended in 50 µl buffer. Mitochondrial extracts were analyzed by Western blot analysis following standard procedures.

Table 11: Mitochondrial fractionation buffer, pH 7.5

Sucrose	4.28 g
HEPES	0.24 g
EDTA	0.06 g
NaOH 0.1M	q.s.
Bidest dH_20	add to a final volume of 50 ml

3.10. PCR

3.10.1. RNA-Extraction

For RNA extraction HT-22 cells were grown in 24 well plates at an average density of 60,000 cells/well. RNA extracts were prepared using the Nucleo Spin II Kit (Macherey und Nagel, Düren, Germany) according to the manufacturer's instructions. Briefly, HT-22 cells were washed with PBS and harvested in cell lysis buffer R1 supplemented with 1 % β-Mercaptoethanol.

For each group, 4-6 wells were pooled to gain appropriate amounts of mRNA. Before continuing with the extraction, all samples were shock-frozen in liquid nitrogen and left to thaw slowly on ice. Next, the raw extracts were filtered through Nucleospin-RNA II columns to remove cellular debris. The supernatant was supplemented with ethanol, mixed carefully and loaded on a NucleoSpin RNA II column to extract nucleic acids by adsorption to the silica matrix of the column.

Excessive electrolytes were removed by washing with MDB buffer (supplied with the kit). Possible contaminations with genomic DNA were removed by adding recombinant DNAse. Further, purification of the column-bound RNA was achieved by subsequent purification, using RA2 and RA3 buffers. RNA was eluted in RNAse free water supplied with the Nucleo Spin Kit II. RNA-concentration was determined by UV-Vis absorption spectroscopy at 260nm. For intermediate storage RNA-extracts were transferred to the -80°C freezer.

3.10.2. RT-PCR

Following RNA purification, mRNA was amplified using the OneStep PCR kit supplied by Invitrogen (Karlsruhe, Germany). Sequence specific primers were used for CYLD and Glyceraldehyde 3-phosphate dehydrogenase (GAPDH) as indicated in section 3.3.5. Each sample was prepared according to the following scheme given in table 12.

Table 12: ONE STEP PCR sample composition CYLD

2x reaction buffer	25 µl
Sample (0.1-1µg)	x µl (0.5 µg)
fw primer (10µM)	1 µl
rv primer (10µM)	1 µl
SuperScript III enzyme	2 µl
Nuclease free water	add to a final volume of 50 ml

Table 13: ONE STEP PCR sample composition GAPDH

2x reaction buffer	12.5 µl
Sample (0.1-1µg)	x µl
fw primer (5µM)	1 µl
rv primer (5µM)	1 µl
SuperScript III enzyme	1 µl
Nuclease free water	add to a final volume of 25 µl

For amplification of CYLD and GAPDH the following cycler programs were used.

Table 14: ONE-Step PCR cycler program – murine GAPDH

60° C	30 min	
95° C	2 min	
95° C	30 sec	
57° C	1 min	25 cycles
70° C	2 min	
70° C	10 min	
4° C	∞	

Table 15: ONE Step PCR cycler program - murine CYLD

60° C	30 min	
95° C	2 min	
95° C	15 sec	
55° C	30 sec	25 cycles
68° C	1 min	
68° C	5 min	
4° C	∞	

3.11. Generation of siRNA using recombinant DICER enzyme

The Dicer siRNA Generation Kit (Genlantis, San Diego, USA) has been used to gain siRNA duplexes for targeting murine CYLD. The kit contains recombinant Dicer enzyme, which cleaves in vitro a pre-transcribed dsRNA into a pool of siRNA fragments that may be used later for gene-repression.

In a first step, mRNA has been extracted as described before, followed by a reverse transcription polymerase chain reaction (rtPCR), transcribing mRNA to cDNA. To this end oligo dt15 primers and Moloney Murine Leukemia Virus Reverse Transcriptase (M-MLVrv) were used (both from Promega, Madison, USA), as well as dNTP and dTT (D,L-dithiotreitol, Sigma-Aldrich, Munich, Germany) according to table 16. In a subsequent reaction the target template was synthesized by transcribing ssDNA into dsDNA (Table 17). To this end, a target region of 750 bp was selected, which did not overlap with the start codon of CYLD. Sequence specific primers had been

synthesized before, featuring a 5´ T-7 overhang necessary for later binding to the T7SuperScript polymerase. PCR products were purified by ethanol/sodium acetate precipitation at -20° C and subsequent re-suspension in 70% ethanol.

After evaporation of the solvent, the DNA pellet was dissolved in nuclease free water. The dsRNA was generated by T7 SuperScript polymerase reaction using the dsDNA template gained in the previous PCR-reaction. Recovery of dsRNA products was achieved, precipitating the PCR products by adding 30 µl of the supplied LiCl- and storage at -20° C for 1h. The precipitate was washed once with cold ethanol (70%) and dissolved again in nuclease free water. The concentration of dsRNA was determined by UV-light absorbance at 260 nm with each A260 unit corresponding to 40 µg/ml. siRNA was generated by subsequent digestion of dsRNA strands using recombinant Dicer enzyme at 37° C for 12 h. siRNA fragments were analyzed and semi-quantitatively assessed by agarose gel electrophoresis and UV-light detection using a dilution series of siRNA.

Table 16: RT-PCR using dt15 Primer (gaining sscDNA)

		Cycler program C°	
5x reaction buffer	10 µl		
Sample (5µg)	x µl	65° C	5 min
Oligo Primer dT15 (100µM)	2.5 µl	37° C	1 h
DTT 0,4mM	2.5 µl	95° C	5 min
dNTPs 10mM	2.5 µl	4° C	∞
Nuclease free water	add to a final volume of 44 µl		
M-MLV rv Transcriptase (50U/µl)	5 µl		
RNAsin (40U/µl)	1 µl		

Table 17: CYLD PCR Dicer - hot start, PCR mix and cycler program (gaining ds cDNA)

10x reaction buffer	5 µl	95° C	2 min	
Sample (mind. 200ng)	x µl	70° C	hold	
fw primer (10µM)	1 µl	addition of polymerase		
rv primer (10µM)	1 µl	95° C	30 sec	} 30 cycles
dNTPs (10mM)	1 µl	58° C	1 min	
$MgCl_2$ (25mM)	3 µl	70° C	2 min	
Nuclease free water	add to a final	70° C	10 min	
	volume of 45 µl	4° C	∞	
Thermoprime Plus (0,2 U/µl)	5µl			

Table 18: T7 reaction (generation of dsRNA)

T7 reaction buffer	2 µl
dNTPs Mix	8 µl
PCR template (ds cDNA) 1µg	x µl
Nuclease free water	ad to 20 µl
T7 enzyme	2 µl

Incubation at 37°C for 2-4h

Tabelle 19: Dicer digestion

DICER reaction buffer	4 µl
1 µl ATP (10mM)	1 µl
$MgCl_2$ (50mM)	0.5 µl
dsRNA (T7 product) 1 µg	x µl
Nuclease free water	2.5 µl - x
DICER enzyme	2 µl

Incubation at 37° C for 12-18h

3.11.1. Genotyping of CYLD$^{-/-}$ mice

CYLD knockout mice were a kind gift from Reinhard Faessler, Max Planck Institute of Biochemistry, Martinsried, Germany. CYLD knockout mice had been generated by inserting a lacZ/neomycin cassette into exon 4, rendering CYLD inactive (Figure 7)

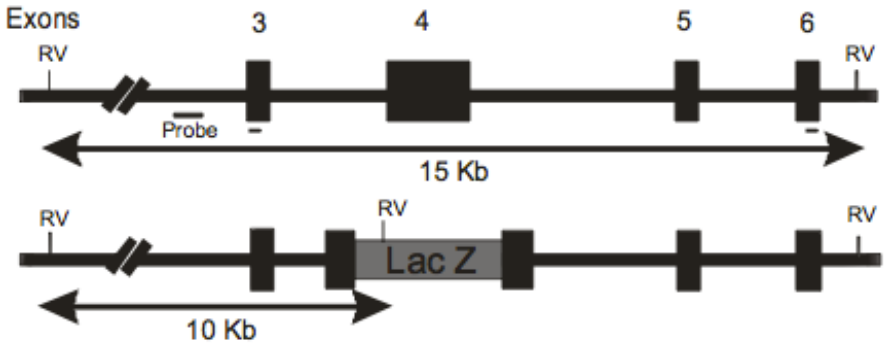

Figure 7: Generation of CYLD $^{-/-}$ mice (Massoumi et al., Cell, 2006)

Genotyping of CYLD mice was performed, running two PCR reactions, covering the lacz insert and the part of the CYLD sequence, into which the lacz cassette is

inserted. DNA was extracted from mouse tails using the tissue DNA extraction kit according to the manufacturer´s protocol (Peqlab, Erlangen, Germany). DNA was amplified by PCR and fragments were analyzed subsequently by agarose gel electrophoresis. Primer sequences (“CYLD exon4” and “lacz”) are provided in 3.3.5. The band pattern returned by the agarose gel electrophoresis shows a positive lacZ band combined with a negative PCR result for CYLD RNA, indicating a homozygous CYLD knockout, and vice versa. If both PCR reactions show detectable bands a heterozygous genotype is present. However, due to unstable PCR results, CYLD knockdown had to be verified by Western blot analysis in primary neuronal cultures.

Table 20: Thermoprime Plus – PCR reaction for CYLD genotyping

Thermoprime Plus (0,2 U/µl)	5 µl
PCR Puffer (10x)	5 µl
MgCl2 (25mM)	3 µl
dNTPs (10mM)	1 µl
Primer (10µM)	1 µl
Primer (10µM)	1 µl
DNA (200ng)	x µl
Nuclease free H_2O	Add to a final volume of 50 µl

Table 21: PCR for lacZ and CYLD (Exon4)

95°C	180 sec	
95°C	60 (45) sec	} 35 cycles
72°C (55°C)	240 (45) sec	
72°C	5 (60) sec	
72°C	600 sec	
4°C	∞	

3.11.2. Agarose gel electrophoresis

PCR products were analyzed by agarose gel electrophoresis and subsequent detection by SYBR Gold (Invitrogen, Karlsruhe, Germany) an intercalating agent that upon DNA binding increases its fluorescent emission. Usually 1.5 g of agarose (Sigma-Aldrich, Taufkirchen, Germany) were suspended in 100 ml of 1x Tris/Borate/EDTA (TBE) buffer (10x stock, Invitrogen, Karlsruhe, Germany) and dissolved by heating up the suspension in a microwave oven. For analysis of siRNA

fragments gels containing 2-3 % of agarose were used. Remaining clumps of agarose were removed by occasional stiring while heating up the suspension. Once the agarose was completely dissolved, 2 µl of SYBR Gold was added, stirred carefully and the solution was transferred to the gel cartridge to allow gel formation. Thereafter, a comb was inserted in the gel, to generate the pockets needed for later sample addition. Samples were loaded using 1 µl of PCR product 5 µl nuclease-free water (Sigma-Aldrich, Taufkirchen, Germany) and 2 µl of BJ-sample buffer. Next to the samples 4 µl of a pre-prepared 100bp reference marker (Fermentas, St. Leon-Roth, Germany) were loaded on the gel. Electrophoresis was conducted at 110 V for 1 h. SYBR Gold stained PCR-products were detected by UV-light excitation and fluorescent emission using the Chemidoc Imaging System (Bio-Rad, Munich, Germany). Pictures were taken and analyzed using Quantitiy One software (Bio-Rad, Munich, Germany).

3.12. Measurement of NF-κB activity

NF-κB activity was determined using a luciferase-reporter vector that encodes for firefly luciferase under the transcriptional control of a NF-κB response element. Thus, upon successful transfection of the reporter plasmid, changes in transcriptional NF-κB activity become accessible through the amount of luciferase protein generated by a certain cell population. Relative changes of luciferase activity are determined by measuring the oxidation of luciferin, a substrate of firefly luciferase. Consequently, luciferase protein, set free by cellular lysis is incubated with luciferin in the presence of ATP-Mg^{2+} as a cosubstrate, and the amount of light, which is generated by this reaction is measured as a readout (83). The reaction is given in figure 8.

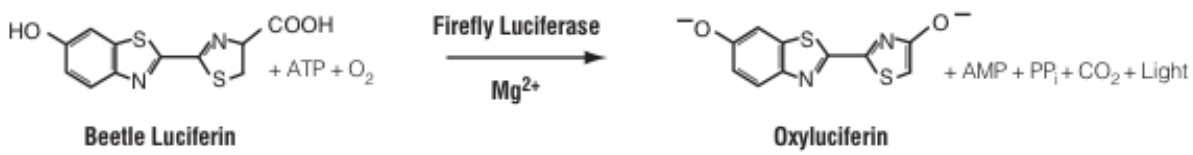

Figure 8: Luciferin oxidation catalyzed by Firefly Luciferase

To assess NF-κB activity in HT-22 cells the reporter plasmid was transfected following the PEI-transfection protocol given in the respective section. If siRNA transfection was required, this was carried out first, as described in section 3.5.1, and then, 24 hours later, the transfection of the reporter plasmid was conducted.

Following further 24 h of incubation cells were transferred to 96-well plates suitable for luminescence-measurement and subjected to the respective treatment regime on the following day. Luciferase activity was determined at the indicated time points using the luciferase assay system (Promega, Madison, USA) according to standard procedures. Briefly, cells were washed with PBS and lysed with passive lysis buffer (Promega, Madison, USA). Addition of luciferin substrate and subsequent measurement of luciferase activity was achieved using the Fluostar OPTIMA plate reader equipped with a luminescense collection lense and an automated injection system (BMG Labtech, Offenburg, Germany).
As an internal control, experiments were repeated in a 24-well layout, to allow for the normalization to protein content (when indicated). For evaluation of luciferase activity equal amounts of extract were transferred to a chemiluminescence plate, with the other half being used for protein determination.

3.13. In vivo model of traumatic brain injury

Traumatic brain injury was simulated using a model system of controlled cortical impact as described previously (37). CYLD knockout mice and wild-type littermates were subjected to controlled cortical impact (CCI) to the surface of the brain (impactor tip diameter: 3 mm, impact velocity: 8 m/s, brain compression: 1 mm for 150 ms). Before CCI animals were craniotomized above the right parietal cortex under Halothane/N_2O anesthesia.
Following the controlled impact, the craniotomy was closed again. Sham-operated animals underwent the same surgical procedure including anesthesia and craniotomy without receiving impact injury. For quantification of brain injury, animals were sacrificed by cervical dislocation in deep halothane anesthesia. Brains were carefully removed, frozen in dry ice and stored at -80°C until further use. Histomorphometric quantification was performed using 10 µm coronal sections that had been collected every 500 µm on a cryostat (CryoStar HM 560, Microm, Walldorf, Germany) and stained with cresyl violet. The contusion area of each section was measured on digitized images with a standard image analysis software (Optimate 6.52, Media Cybernetics, Silver Spring, MD, USA) by an investigator blind to the treatment of the animals. The infarct volume (Vi) was calculated based on the contusion areas (A) obtained from 15 sections by the equation: $V_i = 0.5mm \times (A_1 + A_2 + \ldots + A_{15})$

4. Results

4.1. Glutamate-dependent cell death in HT-22 cells

HT-22 cells are a well established model for studying the mechanisms underlying neuronal cell death induced by oxidative stress (19; 76; 78). Exposing HT-22 cells to millimolar concentrations of glutamate results in ROS-dependent cell death (oxytosis) caused by glutamate mediated inhibition of the xCT transporter (73; 84). Such glutamate-induced cell death occurs in a time dependent manner, usually 8-12 h after onset of glutamate exposure and is easily monitored by standard cytotoxicity assays like the MTT assay (Figure 9A).

Oxytosis in HT-22 cells is accompanied by pronounced changes in cellular morphology (Figure 9B), which correlate well with overall viability (82). The impedance based xCELLigence system has recently been validated as a suitable tool for real time monitoring of cell death, exploiting morphological changes for readout (82).

As depicted in figure 9A and 9C, oxytosis in HT-22 cells follows a characteristic profile, showing no damage over the early hours of treatment and a sudden, fast paced cell death occurring 8-10 hours post glutamate exposure. In line with earlier findings, cell death in HT-22 cells occurs as a two-step process, with early events of continuously increasing cellular stress like e.g. increases in lipid peroxidation and later events such as AIF translocation from mitochondria to the nucleus (76; 78).

Sensitivity to glutamate varies in HT-22 cells with passage number and cell density, for which reason glutamate concentrations were recurrently adapted, using concentrations between 1-5 mM for the induction of cell death in the present study.

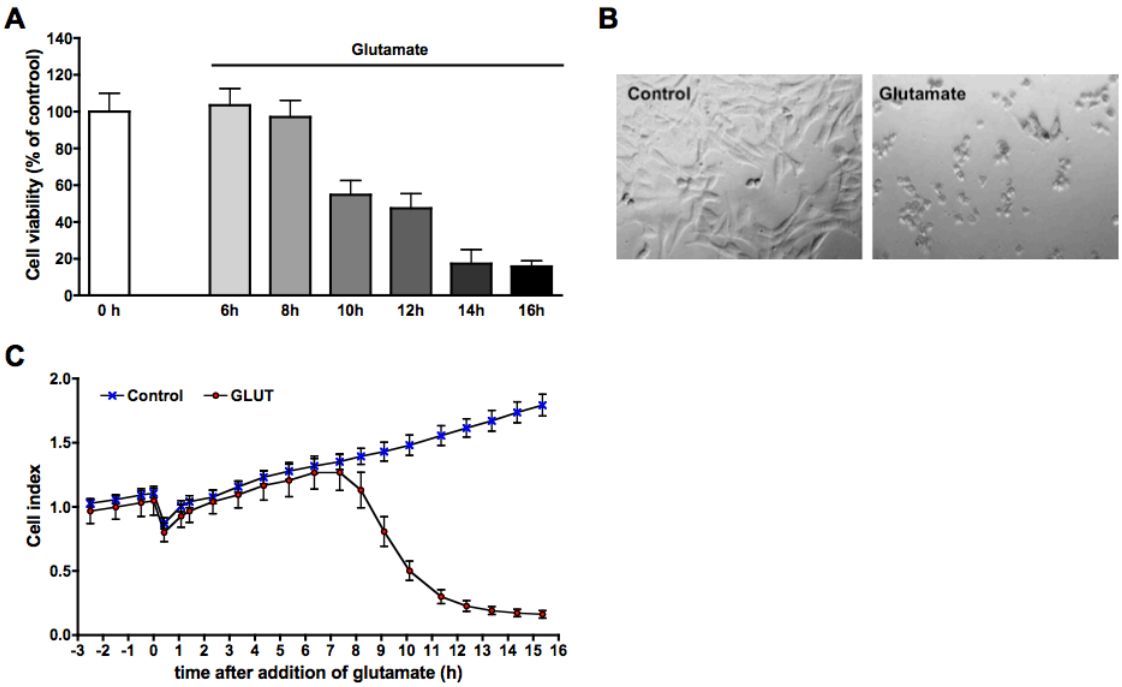

Figure 9: Glutamate induces cell death in HT-22 cells in a time dependent manner. HT-22 cells were seeded at a density of 30,000 cells/cm^2 and treated with glutamate over the indicated period of time. **(A)** Time dependent cell death in HT-22 cells exposed to glutamate over 6-16h as detected by MTT-assay (n=8). **(B)** HT-22 cells undergoing morphological changes in response to glutamate (10x magnification). **(C)** Cellular impedance recording showing HT-22 cells treated with glutamate as recorded by xCELLigence system (n=5). The experiments were repeated three times and the results presented as mean values ± S.D.

4.2. The p53 inhibitor pifithrin-α prevents glutamate-induced oxytosis in HT-22 cells

The tumor suppressor p53 propagates cell death in neurodegenerative diseases, and inhibition of p53 is regarded as a promising approach to prevent neuronal loss (28). For studying the effects of p53 within neuronal cell death, the p53 inhibitor pifithrin-α (PFT) has been established as a valuable and widely applied pharmacological tool (85). PFT prevents nuclear translocation of p53 and transcriptional upregulation of prominent pro-apoptotic p53 target proteins such as e.g. BAX (86). In order to investigate, if p53 was involved in glutamate-induced cell death in HT-22 cells, PFT was applied 1 h prior to glutamate treatment. As shown in figure 10A, glutamate-induced cell death occurs in a concentration dependent manner and could be reduced almost completely by the p53-inhibitor PFT (Figure 10A). Such pronounced

protective effect of PFT suggested a significant contribution of p53 to glutamate-induced oxytosis.

As stated previously, glutamate treatment causes a pronounced increase in reactive oxygen species. To address the general concern that PFT functions as a radical scavenger, PFT was applied in paradigms of oxidative stress caused by incubation with H_2O_2 or glucose oxidase. While H_2O_2 poses an imminent burden of ROS, addition of glucose oxidase provides a milder source of ROS, inducing a permanent but low paced increase in reactive oxygen species. As shown in figure 10B and 10C, PFT does not mitigate cell death in response to any of these stimuli, indicating that PFT does not possess an anti-oxidative potential and, therefore, does not promote neuronal survival by simply acting as a radical scavenger.

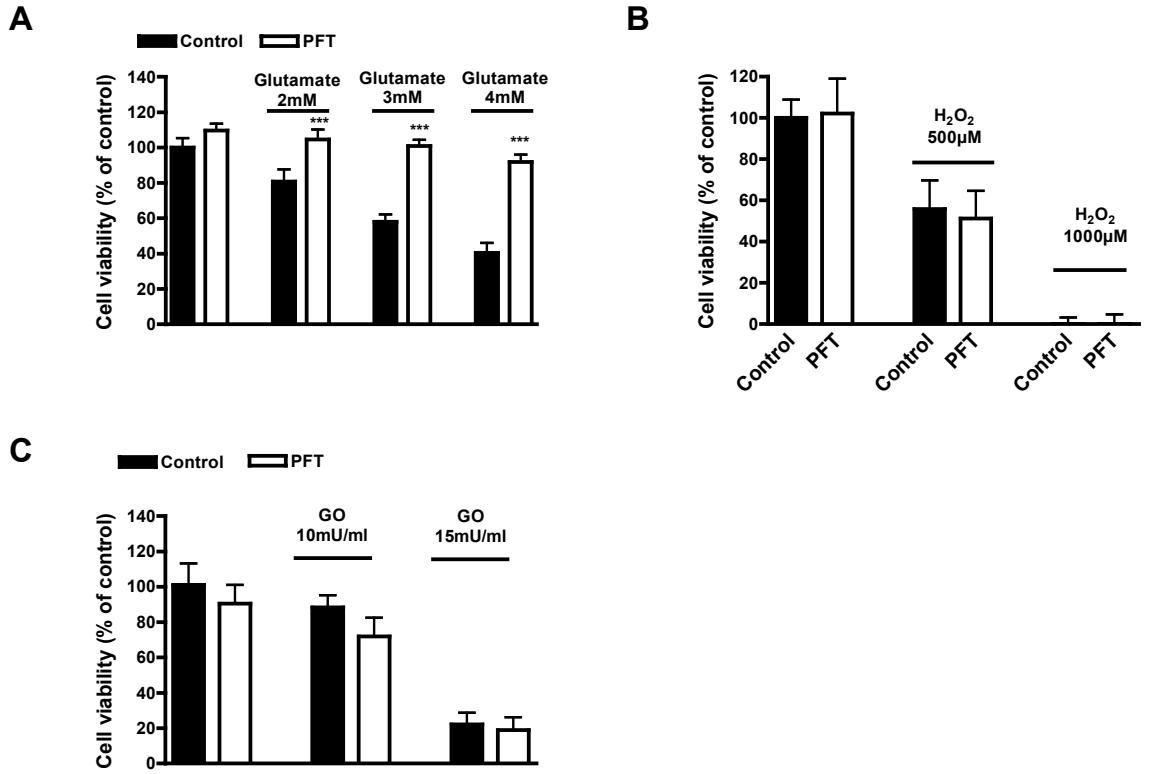

Figure 10: PFT protects HT-22 cells against glutamate-induced cell death, but does not act as a radical scavenger. HT-22 cells were seeded at a density of 20,500 cells/cm^2 in a 96 well plate format. **(A)** HT-22 cells were exposed to glutamate (2-4mM) and cell death was determined by MTT assay. Indicated groups were pretreated with the p53 inhibitor pifithrin-α (10µM) followed by a co-treatment with glutamate (n=8). **(B)** Cells were exposed to H_2O_2 (500µM and 1000µM) over 15h, indicated groups were co-treated with PFT, starting 1h prior to H_2O_2. Cell death was detected using the MTT-assay (n=8). **(C)** Treatment of HT-22 cells with glucose oxidase (GO, 10mU/ml and 15mU/ml) causes significant cell death after 15h, as determined by MTT-assay. Indicated groups were treated with PFT starting 1h prior to GO-treatment (n=8). All experiments were repeated three times and the results presented as mean values ± S.D.

4.3. The NF-κB pathway is not stimulated by glutamate or pifithrin-α

It is commonly accepted, that p53 induced cell death relies to a great extent on the enhanced expression of various pro-apoptotic factors under transcriptional control of p53, like BAX, Bid, PUMA and Noxa (29). In addition, a complementary mechanism has been identified in tumor cells and neuronal cells that involves concomitant repression of NF-κB transcriptional activity by p53 through competitive binding of transcriptional cofactors such as p300 and CREB binding protein (CBP) (36; 50). Consequently, survival signaling by NF-κB is increasingly impaired in the event of cell death, mirrored by decreased levels of anti-apoptotic factors, such as e.g. IAPs and MnSOD (33; 37). Following this concept of reciprocal transcriptional inhibition between p53 and NF-κB, the present study sought to elucidate how neuroprotection induced by inhibition of p53 affected NF-κB activity.

In contrast to previous work, the present investigation relied on HT-22 cells to investigate this question. The HT-22 cells were treated with glutamate and PFT (10μM) over different time intervals. Protein levels of IkB-α and pIkB-α were determined to estimate induction NF-κB activity along the canonical pathway. Activation of this pathway is reflected by initially increased levels of phosphorylated IkB-α, followed by IkB-α degradation and subsequent release of the NF-κB transcription factors from the inhibitory IkB-complex.

As shown in figure 11 whole protein extracts were taken from HT-22 cells at the indicated time points and analyzed by Western blot for IkB-α and pIkB-α levels. Interestingly, neither treatment caused a change in protein levels of IkB-α and pIkB-α, indicating that the canonical NF-κB pathway was not initiated in the present model system.

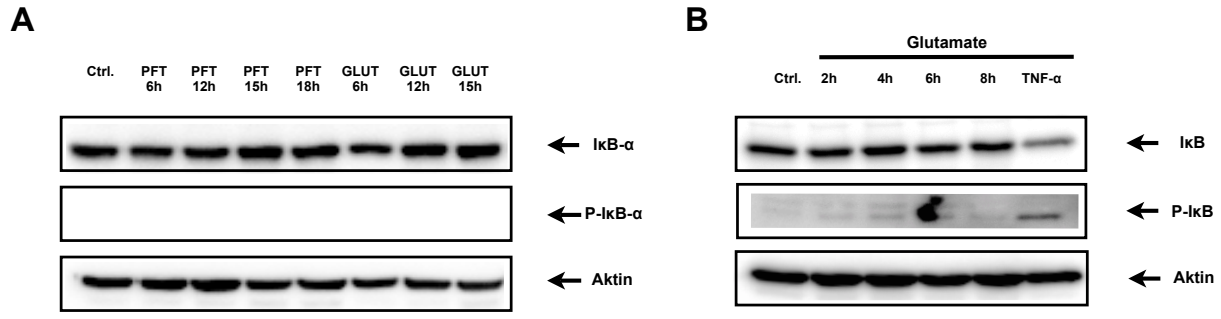

Figure 11: Glutamate treatment and PFT do not stimulate the canonical NF-κB pathway in HT-22 cells. (A, B) HT-22 cells were grown in 6 well plates (21,000 cells/cm^2) treated with PFT (10μM) and glutamate over the indicated time course. Protein extracts were taken and analyzed by Western blot, probing for pIκB-α, IκB-α and Aktin as a loading control. All experiments were repeated three times.

Besides the most prominent canonical activation of NF-κB alternative pathways have been described, which lead to transcriptional activation of NF-κB without affecting pIκB-α and IκB-α levels. To cover these mechanisms as well, a broad approach was applied studying the individual role of all NF-κB subunits in response to PFT and glutamate.

As mentioned previously, the transcriptional response by NF-κB can be mediated by five isoform subunits, which dimerise upon activation, translocate from the cytoplasm to the nucleus and bind to NF-κB response elements for induction of transcription. Consequently, the cytosolic/nuclear distribution of any given subunits is a first approach for estimating the transcriptional activity.

In order to investigate the diverse role of the different NF-κB subunits in HT-22 cells, all transcription factors were stained, applying immunocytochemistry and analyzed by confocal microscopy. Counterstaining of the nuclei with DAPI allowed evaluating nuclear translocation.

HT-22 cells were treated with glutamate and PFT in ibidi-slides and fixed 12 h later using PFA. In HT-22 cells, all NF-κB subunits (p50, p52, p65, cRel and RelB) were found in the cytosol but not in the nucleus under control conditions (Figure 12). Interestingly, no marked translocation of either subunit was detected in the cells when stimulated with glutamate or PFT, showing the same distribution pattern as control cultures.

PFT mediated protection against glutamate toxicity was reflected well by unharmed cell bodies and nuclei as opposed to shrunken cells and pyknotic nuclei in the glutamate-challenged cells. The distribution of NF-κB subunits, however, was unchanged in cells protected by PFT compared to controls. These findings clearly indicated that the p53 inhibitor PFT could not enhance transcriptional activation of NF-κB in HT-22 cells and the associated protective effect was unlikely mediated by NF-κB transcriptional activity.

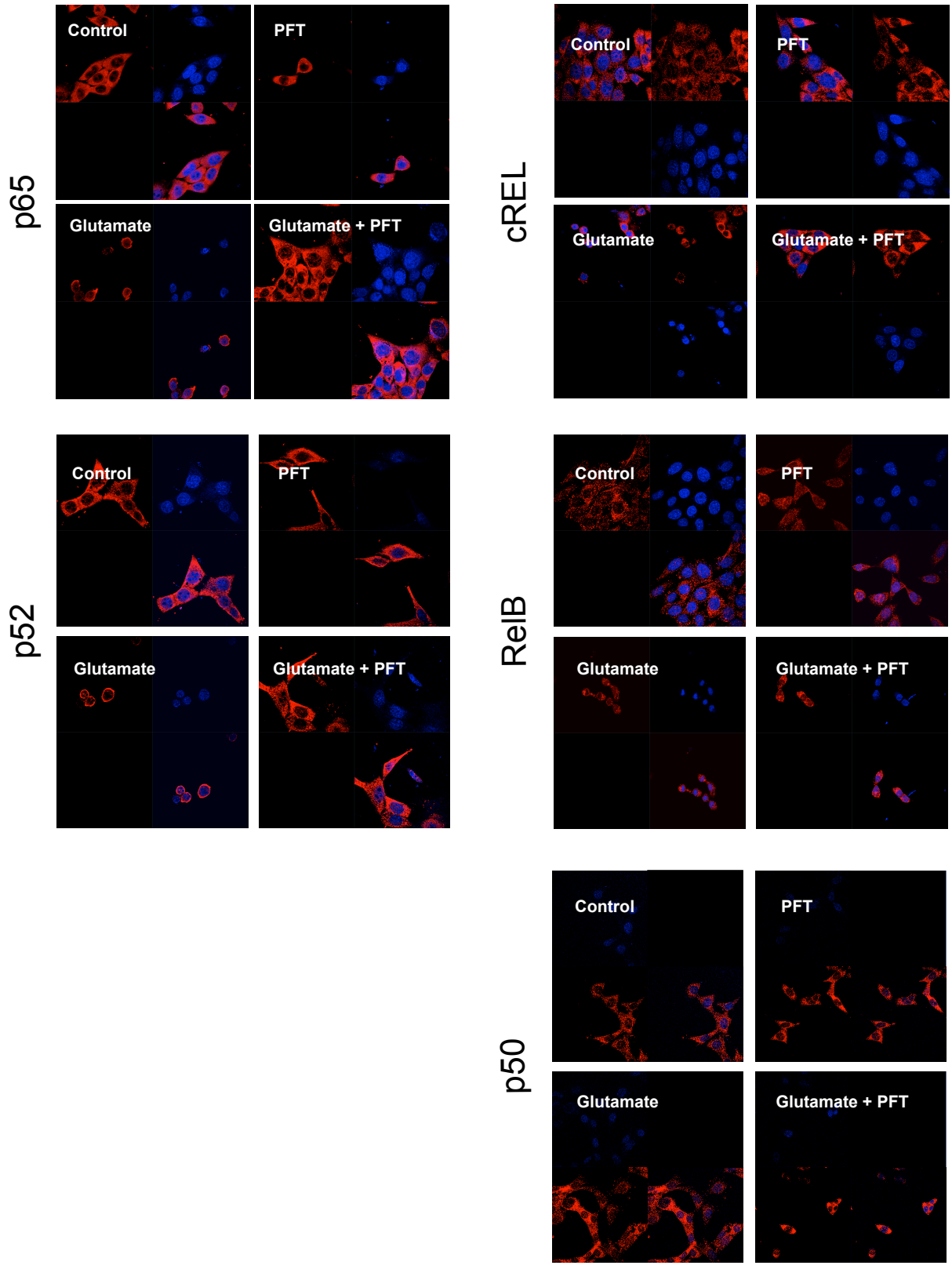

Figure 12: NF-κB subunits do not show any sign of nuclear translocation after treatment with glutamate or PFT in HT-22 cells (ICC analysis). HT-22 cells were treated with PFT (10μM) and glutamate. NF-κB subunits were stained by immunocytochemistry (red) and nuclei were counterstained with DAPI (blue). The cytosolic/nuclear distribution pattern of HT-22 cells was not markedly altered by PFT or glutamate.

To confirm the results gained by immunocytochemistry, the distribution of NF-κB subunits was re-evaluated by nuclear/cytosolic fractionation and subsequent Western blot analysis. In line with previous findings NF-κB subunits show a predominant cytosolic distribution, which was not altered by any treatment, with PFT or without glutamate (Figure 13).

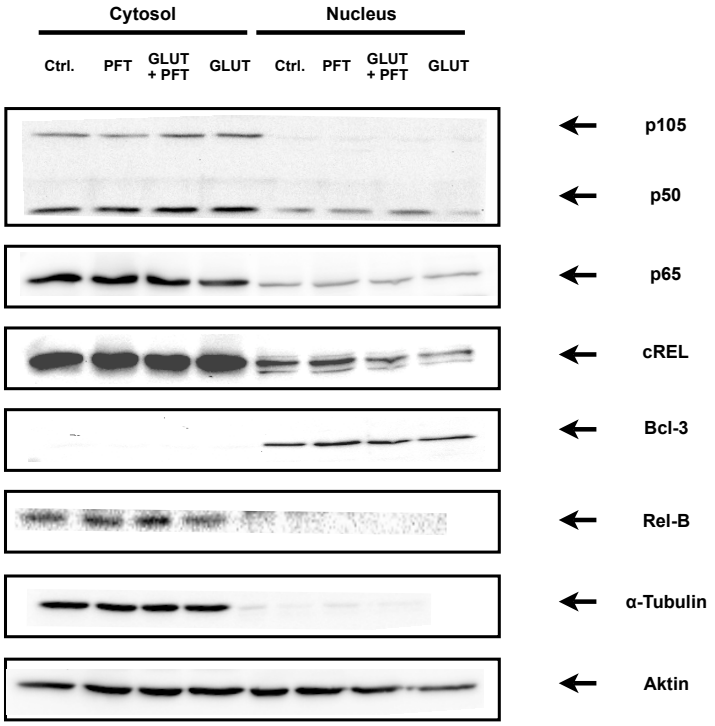

Figure 13: No translocation of NF-κB subunits is detectable in HT-22 cells after glutamate or PFT treatment (WB analysis). HT-22 cells were treated with glutamate, PFT (10μM) or a combination of the two substances. Nuclear and cytosolic fractions were separated and analyzed by Western Blot, probing for NF-κB subunits. Purity of nuclear extracts was confirmed by the absence of α-Tubulin. Equal loading was verified, comparing Actin levels. NF-κB subunits do not show any sign of nuclear translocation in response to PFT or glutamate. The experiment was repeated three times with similar results.

While previous experiments clearly indicated that neither glutamate nor PFT treatment induced translocation of NF-κB subunits to the nucleus, this was insufficient for concluding that transcriptional activity of NF-κB was not affected by either treatment.

For instance, it has been shown previously that posttranslational phosphorylation of the NF-κB subunit p65 enhances transcriptional activity, without the need for a further increase in the nuclear fraction of p65. Given the multitude of possible post-translational modifications, the present study rather sought to study overall transcriptional activity, than screening for individual factors and modifications. To this end, NF-κB activity was determined using a luciferase-reporter vector that encoded

for firefly luciferase under the transcriptional control of a NF-κB response element as indicated in figure 14.

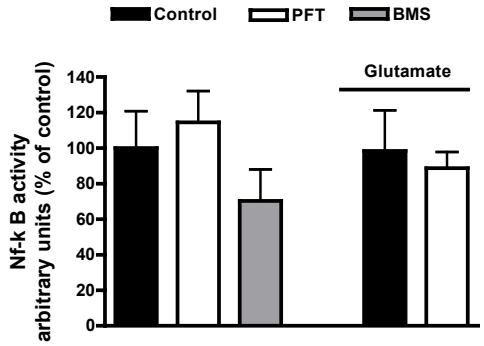

Figure 14: NF-κB activity in HT-22 cells is not altered by PFT or glutamate treatment. HT-22 cells were transfected with a NF-κB reporter plasmid and reseeded in 96-well plates 24h after the transfection. Following 8h of PFT (10μM) and glutamate treatment, NF-κB activity was evaluated by luminometric detection of luciferase activity. The NF-κB inhibitor BMS was used as a negative control. Glutamate and PFT treatment did not affect transcriptional activity.

In summary, these findings suggested that NF-κB did not play a major role in glutamate-induced cell death in HT-22 cells. Moreover, the proposed mechanism of PFT-mediated neuroprotection, involving NF-κB transcription in addition to p53 inhibition was apparently not relevant for this model system.

4.4. Depolarization and fission of mitochondria is prevented by p53 inhibition

Disturbance of mitochondrial integrity and function recently emerged as an important hallmark of neuronal cell death, implicated in various neurodegenerative diseases (87; 88). As established previously, mitochondrial fragmentation and subsequent loss of metabolic activity also precedes cell death in HT-22 cells (76; 79). In line with these findings, glutamate treatment of HT-22 cells was found to cause pronounced mitochondrial fission 8-10 h post glutamate exposure, which coincided well with the beginning of the execution phase of cell death (Figure 9C and figure 15).

The work by Tobaben et al. and Grohm et al. gave rise to the concept of “the point of no return” according to which neuroprotection in HT-22 cells cannot be reached, once mitochondria are damaged. Thus, given the impact of mitochondrial fission on

long-term survival, this study investigated the effect of pifithrin-α on mitochondrial morphology and function.

As shown in figure 15, PFT prevented loss of mitochondrial integrity and glutamate-induced fission in HT-22 cells. A more detailed analysis of mitochondrial morphology was conducted, using the classification scheme introduced by Grohm et al. (2010). Accordingly, cells were categorized in 3 subgroups, depending on the degree of mitochondrial fragmentation.

Category 1 represents cells containing an intact tubular network of mitochondria as usually found under control conditions, whereas categories 2 and 3 indicate an increasing number of fragmented mitochondria. Glutamate toxicity caused a shift towards category 2 and 3, whereas PFT treatment rescued mitochondrial morphology maintaining the tubular structure of mitochondria found under control conditions (Figure 15 A und B).

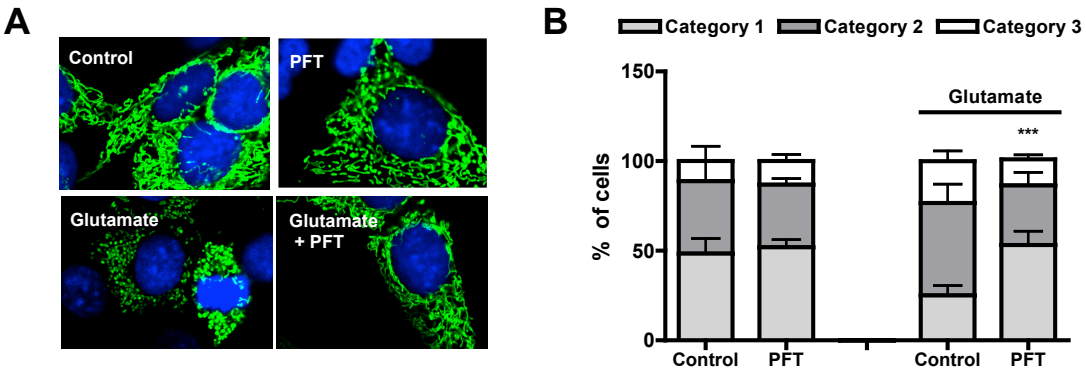

Figure 15: PFT prevents glutamate-induced mitochondrial fragmentation in HT-22 cells. Mitochondria of HT-22 cells were stained with MitoTracker (green) and treated with glutamate and PFT (10µM) for 10-12h. **(A)** Representative pictures of mitochondrial morphology, showing increased fragmentation induced by glutamate. PFT mediated protection preserves mitochondrial morphology, found under control conditions (63x magnification). Nuclei were counterstained with DAPI (blue). **(B)** Cells were counted manually and classified into 3 groups depending on the degree of mitochondrial fragmentation. Category 1: elongated, tubular like mitochondria; Category 2: intermediate size; Category 3: severe mitochondrial fragmentation. 200 cells were counted per condition (n=5), ***p<0.001 Category 1 and category 2 of the glutamate + PFT group, compared to respective control (ANOVA, Scheffé's). All experiments were repeated three times and the results presented as mean values ± S.D.

Mitochondrial membrane potential, as assessed by JC-1 staining, is a further indicator of mitochondrial function, correlating with mitochondrial integrity and overall viability (79). In HT-22 cells glutamate treatment induces a significant loss of JC-1 red fluorescence 10-12 h after glutamate exposure, indicating mitochondrial

depolarization (Figure 16). Treatment with the p53-inhibitor, however, could potently prevent this loss of mitochondrial potential. Moreover, PFT treatment did not only rescue the membrane potential, but also enhanced it beyond original control levels. A direct effect of PFT at the level of mitochondria thus may account for this effect and may contribute to the neuro-protective potential of the p53 inhibitor.

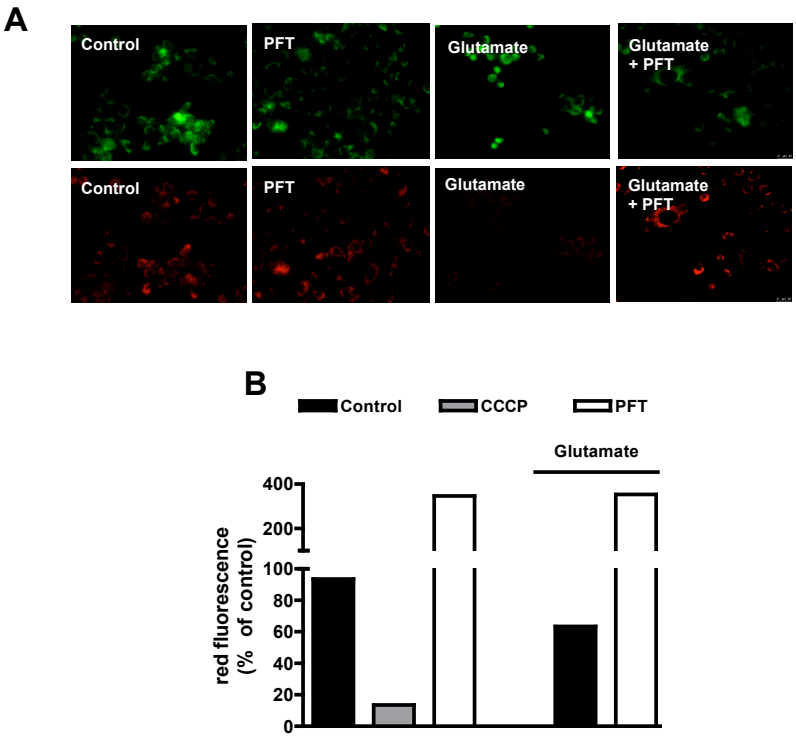

Figure 16: Glutamate-induced depolarization of mitochondria is blocked by pifithrin-α. HT-22 cells were exposed to glutamate and PFT (10 µM) in the indicated groups. After 10-12h cells were incubated with JC-1 (2µM) for analysis of mitochondrial membrane potential. **(A)** Representative fluorescent pictures (40x magnification) showing glutamate-induced loss of red fluorescence (lower panel), which indicates mitochondrial depolarization. PFT treatment protects the mitochondrial potential shown by the preserved red fluorescence. Comparable cellular uptake of the dye was confirmed by evaluation of the green fluorescence. **(B)** Quantitative FACS analysis of 10,000 cells/group. The ionophor CCCP was applied to induce a full decrease in red fluorescence thereby functioning as a positive control for mitochondrial depolarization. The decrease evoked by glutamate was smaller than the effect observed with CCCP. PFT caused a pronounced increase in mitochondrial membrane potential in control cells and in cells exposed to glutamate.

4.5. Inhibition of Bcl-2 and Bcl-X_L does not attenuate pifithrin-α mediated neuroprotection

Bcl-2 and Bcl-X_L are well known members of the Bcl-2 protein family with important antiapoptotic functions (12). Bcl-X_L and Bcl-2 have been shown to prevent cell death by antagonizing the effects of BAX, a further member of the Bcl-2 family with a strong

pro-apoptotic function. In response to apoptotic stimuli, BAX induces the formation of pores within the outer mitochondrial membrane causing the subsequent release of apoptotic factors and cell death (89). By forming heterodimers with BAX, both, Bcl-X_L and Bcl-2 can sequester BAX and thus prevent cell death.

Since PFT may exert its neuroprotection partially at the level of the mitochondria and Bcl-2 and Bcl-X_L are the most prominent anti-apoptotic effectors with a mitochondria related mode of action, this study investigated if PFT mediated effects are related to Bcl-2 proteins (Figure 15 and 16). To this end, the Bcl-2 inhibitor HA-141 (90) and ABT-737, an inhibitor of Bcl-2 and Bcl-X_L with a preferential binding for Bcl-X_L, were used (18).

HT-22 cells were treated with glutamate for 10 h and PFT (10 µM) was applied as described previously. As shown in figure 17A, co-administration of HA-141 (20 µM) did not result in any endogenous toxicity, nor did it enhance glutamate-dependent cell death. Moreover, PFT mediated protection was not altered by HA-141, indicating, that Bcl-2 did not contribute to protection by PFT. Similar results were obtained with ABT-737 (10 µM), suggesting that Bcl-X_L was dispensable for PFT mediated protection (Figure 17 B).

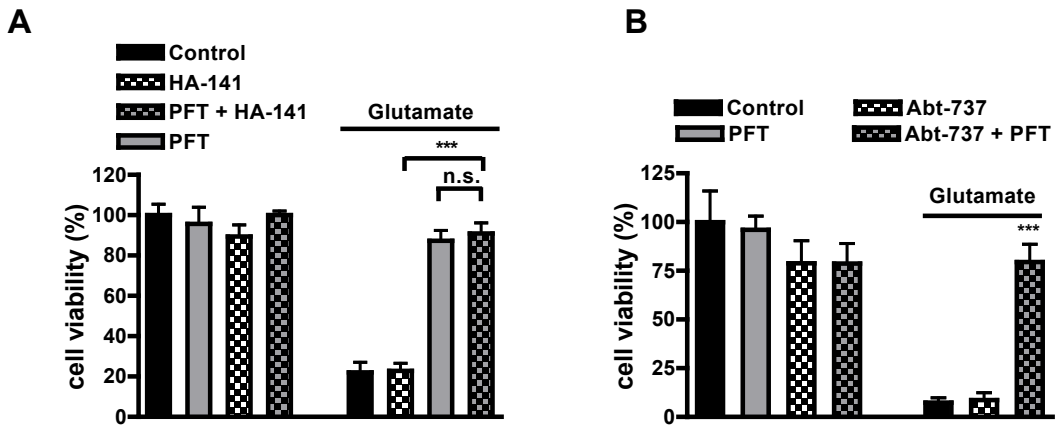

Figure 17: PFT mediated protection is independent of Bcl-2 and Bcl-X_L. (A) HT-22 cells (22,500 cells/cm^2) were treated with glutamate, PFT (10µM) and HA141 (20µM) over 15h. Cell viability was assessed by MTT assay (n=8). ***p<0.001 (ANOVA, Scheffé's-test). **(B)** HT-22 cells (22,500 cells/cm^2) were treated with glutamate, PFT (10µM) and ABT-737 (10µM) over 15h. Cell viability was assessed by MTT assay (n=8). ***p<0.001 compared to glutamate and HA-141 treated cells (n=8) (ANOVA, Scheffé's-test). The experiments were repeated three times and the results presented as mean ± S.D.

4.6. Silencing the deubiquitinase CYLD promotes neuroprotection against glutamate toxicity

The tumour suppressor CYLD has been recognized as a major regulative factor within the NF-κB pathway (91). As a deubiquitinating enzyme, CYLD affects ubiquitination of its various substrates including Nemo, RIP1, TRAF or Bcl-3 (44; 91; 92; 93; 94-96). Deubiquitination of these components, in turn, has been associated with a decrease in NF-κB activity, while loss of CYLD results in increased ubiquitination and enhanced transcriptional activity of NF-κB (51).

Since neuronal cell death can be mitigated by enhancing survival signaling by e.g. NF-κB (44; 92; 93), such survival signaling might be obtained by repressing CYLD in neurons. In the present study, siRNA mediated gene silencing was applied to elucidate whether CYLD plays a major role in neuronal cell death after glutamate toxicity.

CYLD expression in HT-22 cells was successfully repressed by siRNA treatment, as assessed by semi-quantitative analysis of CYLD mRNA and protein content (Figure 18 A and B). Importantly, silencing CYLD preserved HT-22 cell morphology in response to glutamate and significantly reduced glutamate dependent cell death in HT-22 cells as detected by MTT assay and impedance measurements (Figure 18 C-E).

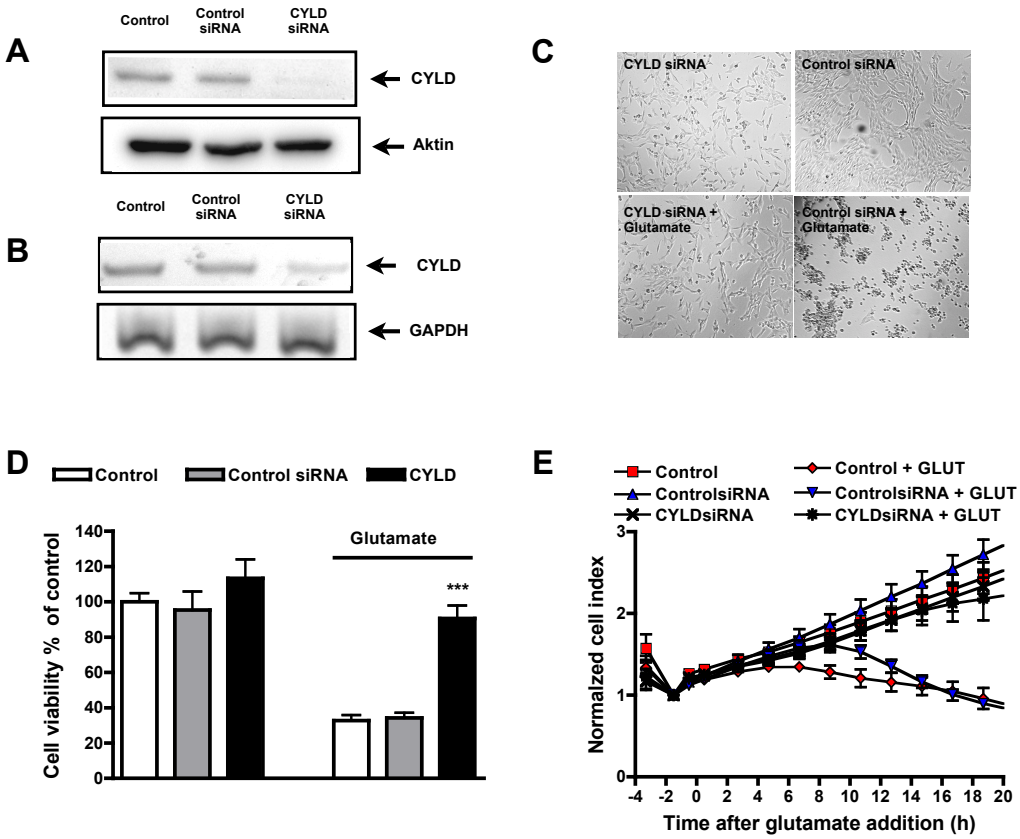

Figure 18: CYLD siRNA attenuates glutamate toxicity in HT-22 cells. HT-22 cells were transfected with CYLD siRNA for 48h and then exposed to glutamate. **(A, B)** Successful knockdown of CYLD was confirmed by Western Blot analysis and RT-PCR. **(C)** Glutamate-induced cell death in HT-22 cells is accompanied by pronounced morphological changes that were prevented by CYLD siRNA treatment. **(D)** Cell viability was assessed by MTT assay 10h after addition of glutamate, showing a pronounced neuroprotective effect of CYLDsiRNA (n=8). ***p< 0.001 compared to glutamate treated control (ANOVA, Scheffé´s) **(E)** Analysis of cellular impedance confirmed the viability data gained by MTT assay. Glutamate causes a drastic drop of the cell index, which was prevented in CYLD depleted cells. All experiments were repeated three times and results are displayed as mean values ± S.D.

Similar results were obtained, when HT-22 cells were transfected with a pool of siRNAs that had been generated using recombinant DICER enzyme.

Even though cellular tolerance towards this siRNA pool was comparably low, this pool of CYLD siRNA offered a significant degree of protection (Figure 19).

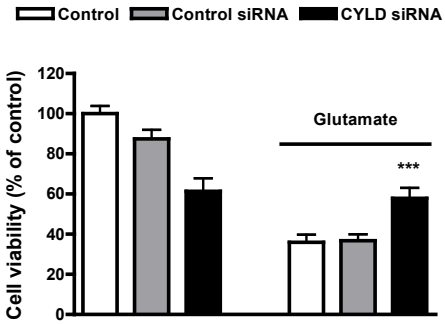

Figure 19: Neuroprotection through silencing of CYLD using a pool of DICER-generated siRNA. HT-22 cells were transfected with siRNA generated by recombinant DICER enzyme and exposed to glutamate. Silencing CYLD offered significant protection against glutamate toxicity. CYLD depletion was confirmed by Western Blot analysis (data not shown). ***p< 0.001 compared to glutamate treated control (ANOVA, Scheffé´s). The experiment was repeated three times and results are displayed as mean values ± S.D.

Detection of propidiumiodide- and Annexin-V stained cells by FACS analysis further confirmed the protective potential inherent with CYLD repression, showing a strong reduction of the late apoptotic and necrotic cell population (Figure 20).

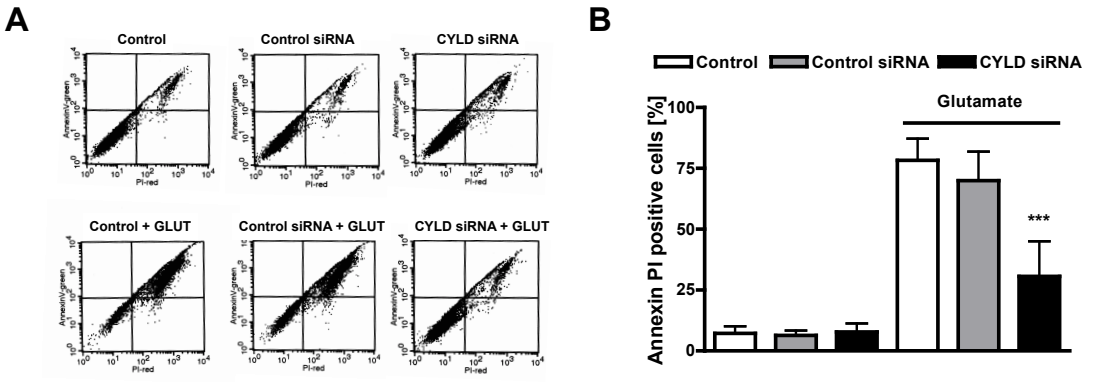

Figure 20: CYLD siRNA attenuates neuronal cell death in HT-22 cells as determined by FACS analysis. (A, B) HT-22 cells were transfected with control-siRNA and CYLD siRNA and exposed to toxic doses of glutamate. Cell death was quantified by FACS analysis of Annexin-V/propidium iodide stained cells. CYLD siRNA treatment exerts a significant neuroprotective effect (n=4, 10,000 cells/sample). ***p< 0.001 compared to glutamate treated control (ANOVA, Scheffé´s).

In summary, all assays indicate, that glutamate toxicity occurred to a similar degree in control siRNA treated cells and untransfected controls, while silencing CYLD by both approaches offered significant protection. These results exposed CYLD as a novel and promising target for neuroprotective strategies.

4.7. Silencing CYLD promotes neuroprotection independent of NF-κB

Massoumi et al. recently reported, that loss of functional CYLD causes an elevated nuclear translocation of Bcl-3 complexes, which subsequently led to a dramatically increased expression of CyclinD1 and enhanced cellproliferation (97).

To investigate if these factors under CYLD regulation, contributed to neuronal survival, sequence specific siRNAs against CyclinD1 and Bcl-3 were applied. As shown in figure 21, both gene silencing approaches caused a downregulation of the respective target proteins. Silencing either protein, however, did not affect glutamate dependent cell death in HT-22 cells (Figure 21 B and C). Consequently, Bcl-3 and CyclinD1 were unlikely to be involved in glutamate-induced oxytosis and did not account for protection against glutamate toxicity observed in CYLD deficient HT-22 cells.

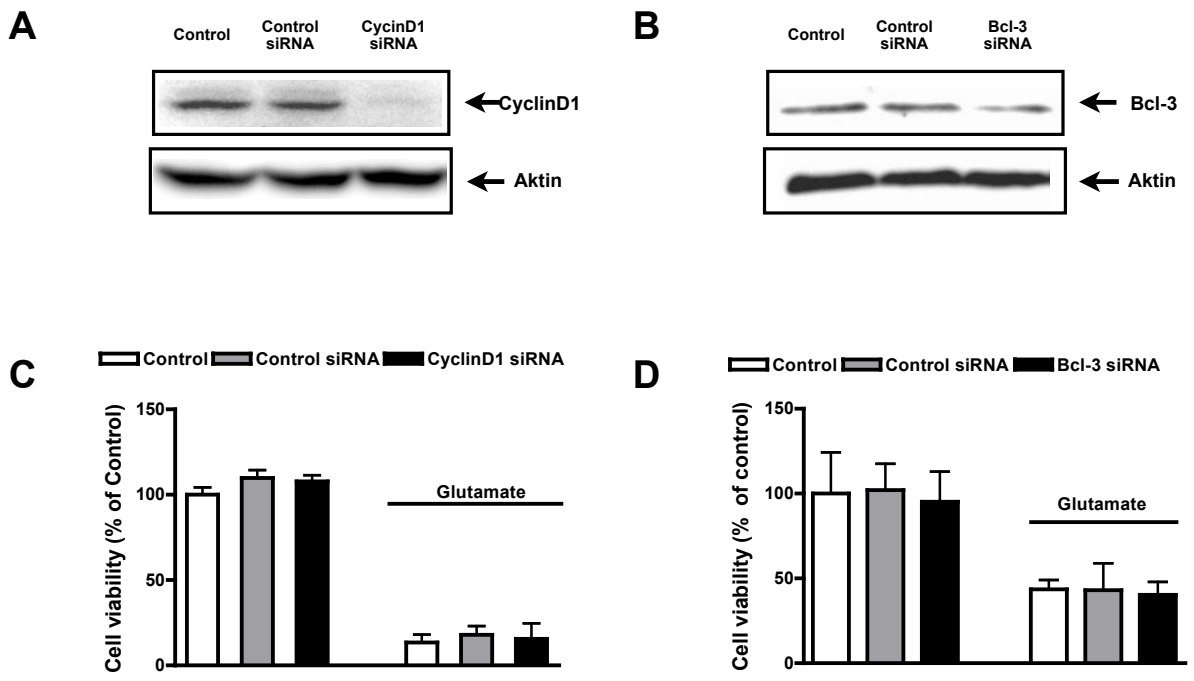

Figure 21: CYLD associated factors CyclinD1 and Bcl-3 are not involved in mediating glutamate dependent cell death in HT-22 cells. (A, B) CyclinD1 and Bcl-3 were silenced using siRNAs and knockdown efficiency was evaluated by Western Blot analysis. **(C, D)** HT-22 cells depleted of either CyclinD1 or Bcl-3 show no protection against glutamate toxicity, as assessed by MTT analysis. All experiments were repeated three times with similar results.

As mentioned before CYLD is a well-established regulative protein of the NF-κB pathway (94). Although previous results suggested that NF-κB was not primarily involved in glutamate dependent cell death in HT-22 cells (Figure 11 and 14), it

remained to be clarified, if silencing CYLD affected NF-κB activity. Consequently, the present study sought to investigate if enhanced survival signaling through NF-κB accounted for the neuroprotection associated with CYLD repression. To this end, protein levels of IkB and pIkB-α were determined by Western Blot analysis, revealing that siRNA mediated silencing of CYLD did not alter levels of either protein compared to control siRNA or non-transfected cells. Treating HT-22 cells with glutamate, likewise, did not cause any detectable effect on protein levels of IkB-α and pIkB-α, neither in CYLD siRNA treated cells nor in respective controls. TNF-α was employed as a positive control stimulating the canonical pathway of NF-κB, as reflected by decreased IkB-α and enhanced pIkB-α levels. Furthermore, transcriptional activity of NF-κB was evaluated using a luciferase reporter plasmid. While TNF-α caused a pronounced increase in transcription, CYLD silencing did not alter NF-κB activity compared to control siRNA. In line with previous results, glutamate treatment did not affect NF-κB transcriptional activity, neither in control siRNA treated cells nor in cells transfected with CYLD siRNA.

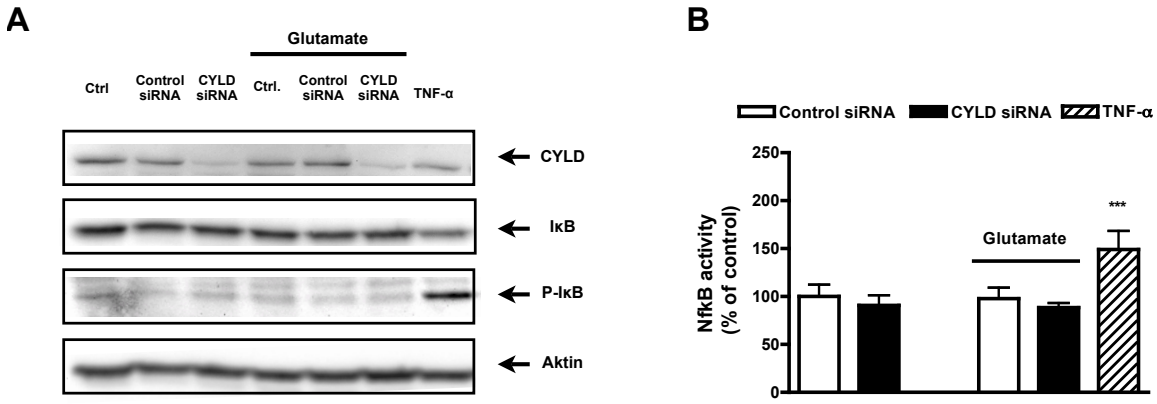

Figure 22: Silencing CYLD does not affect NF-κB transcriptional activity. HT-22 cells were transfected with control- and CYLD siRNA and exposed to glutamate for 8h as indicated **(A)** Western Blot analysis of IkB-α and p-IkB-α levels revealed no change in CYLD depleted cells, compared to controls. TNF-α (100ng/ml, 1h) was applied as a positive control. **(B)** Luciferase driven NF-κB reporter assay showed no increased transcriptional activity in CYLD depleted cells over control. Treatment with TNFα (100ng/ml, 8h) was carried out as a positive control (n=6). *** p< 0.001, compared to untreated control (ANOVA Scheffé´s). The experiments were repeated three times and the results were calculated as mean ± S.D.

In summary, these findings indicate that the observed neuroprotective effects in cells deprived of CYLD were not attributed to survival signaling by NF-κB.

4.8. Glutamate dependent oxytosis in shows features of necroptosis

Glutamate dependent oxytosis in HT-22 cells has been characterized as a form of caspase-independent cell death (19; 78). Recently, another kind of caspase-independent cell death has been discovered in non-neuronal cells upon activation of death receptors by e.g. FASL and TNF-α (63). Interestingly, this form of cell death, also termed necroptosis, depends on CYLD activity as an important regulative component (63).

On the basis of the protective effects obtained with CYLD siRNA, we hypothesized that caspase-independent cell death in HT-22 cells may share signaling components with this newly discovered necrotic cell death pathway. Accordingly, silencing CYLD would promote neuronal survival through inhibition of necroptosis. To test this hypothesis, we first investigated whether glutamate-induced oxytosis showed characteristic features of necrotic cell death. During necroptosis, the kinases RIP1 and RIP3 form a complex, also termed necrosome, which has been identified as an indispensable step for executing necroptotic cell death (98; 99).

In order to investigate the formation of a RIP1/RIP3 necrosome, protein extracts were obtained from HT-22 cells at several time points after onset of glutamate exposure. In these extracts, RIP1 protein was pulled down by immunoprecipitation and analyzed for possible binding partners by Western blot.

These experiments revealed, that glutamate toxicity in HT-22 cells was associated with consecutively increased binding of RIP3 and RIP1 peaking at 12h after the onset of glutamate challenge (Figure 23). As quantified by densitometric analysis, RIP1/RIP3 complex formation increased in a time dependent manner reaching approximately a two-fold increase compared to control levels (Figure 23). Comparable pulldown of RIP1 protein was confirmed in the IP-samples and uniform protein loading of the full lysates was confirmed, probing the blot with β-Actin antibodies. Interestingly, probing the blots with anti-CYLD antibody did not show any binding to the necrosome.

In summary, these findings indicate, that the necroptotic pathway is activated during oxytosis in HT-22 cells and thus may contribute to the progression of cell death in this paradigm of cell death.

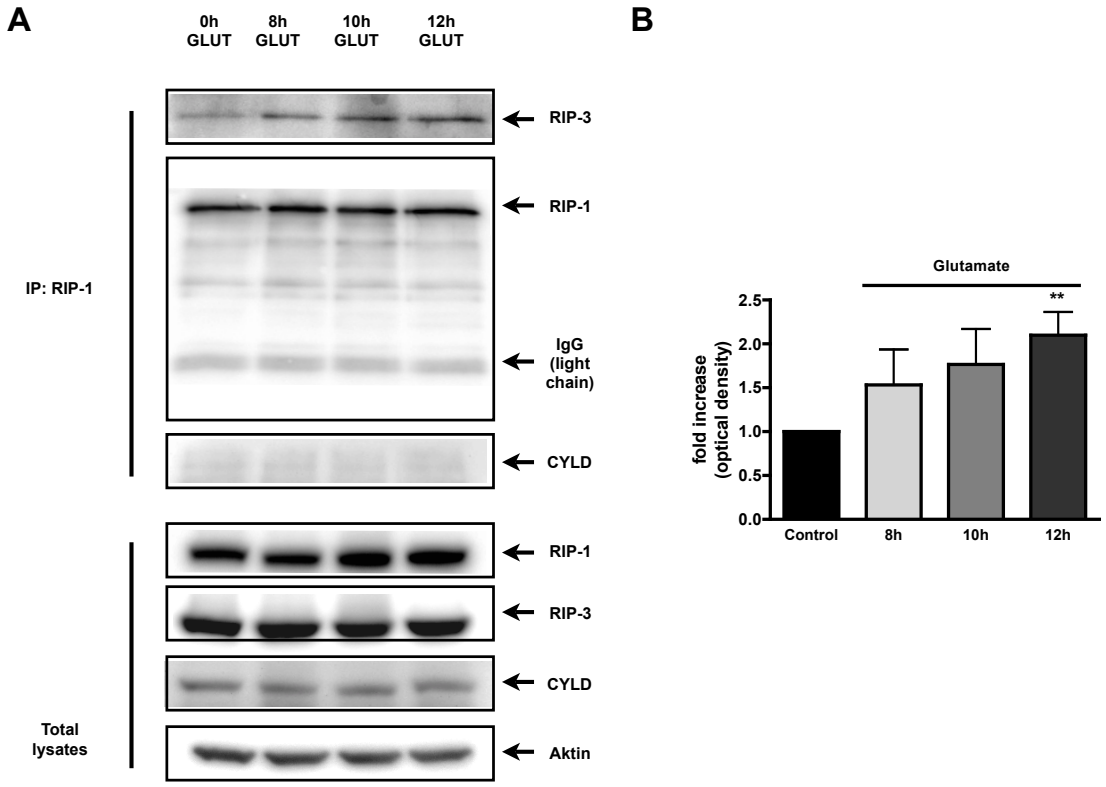

Figure 23: RIP1-RIP3 complex formation in response to glutamate. HT-22 cells were treated with glutamate over the indicated time course. **(A)** Immunoprecipitation of RIP1 from 1.25 mg of whole protein extracts. Subsequent analysis of co-precipitated proteins shows an increased interaction with RIP-3 (uppermost panel). Equal loading was verified by Western blot analysis using whole extracts (lower panels). **(B)** Quantification of the interaction between RIP1 and RIP3 by assessing the ratio of RIP3 to (precipitated) RIP1. The ratio is expressed in relation to control levels. **p<0.01 compared to control (ANOVA Scheffé´s). The experiments were repeated three times and the results were calculated as mean ± S.D.

4.9. Silencing CYLD prevents the necrosome formation in glutamate dependent cell death

Previous results show a complex formation of RIP1 and RIP3 in HT-22 cells exposed to toxic doses of glutamate, thereby implying a contribution of necroptosis to cellular death in this model. Since CYLD was not detected as a part of this complex, it remained to be established if CYLD affected necrosome formation. To address this question, immunoprecipitation-experiments were carried out using protein extracts from control siRNA and CYLD siRNA treated cells, which had been exposed to glutamate. As shown in figure 24 A, glutamate stimulated the formation of the RIP1-RIP3 complex in control siRNA treated cells confirming the previous findings. Quantification of signal intensities revealed an approximate 2-fold increase in RIP1-

RIP3 interaction (Figure 24 B). In contrast, silencing CYLD prevented RIP1-RIP3 interaction in response to glutamate.

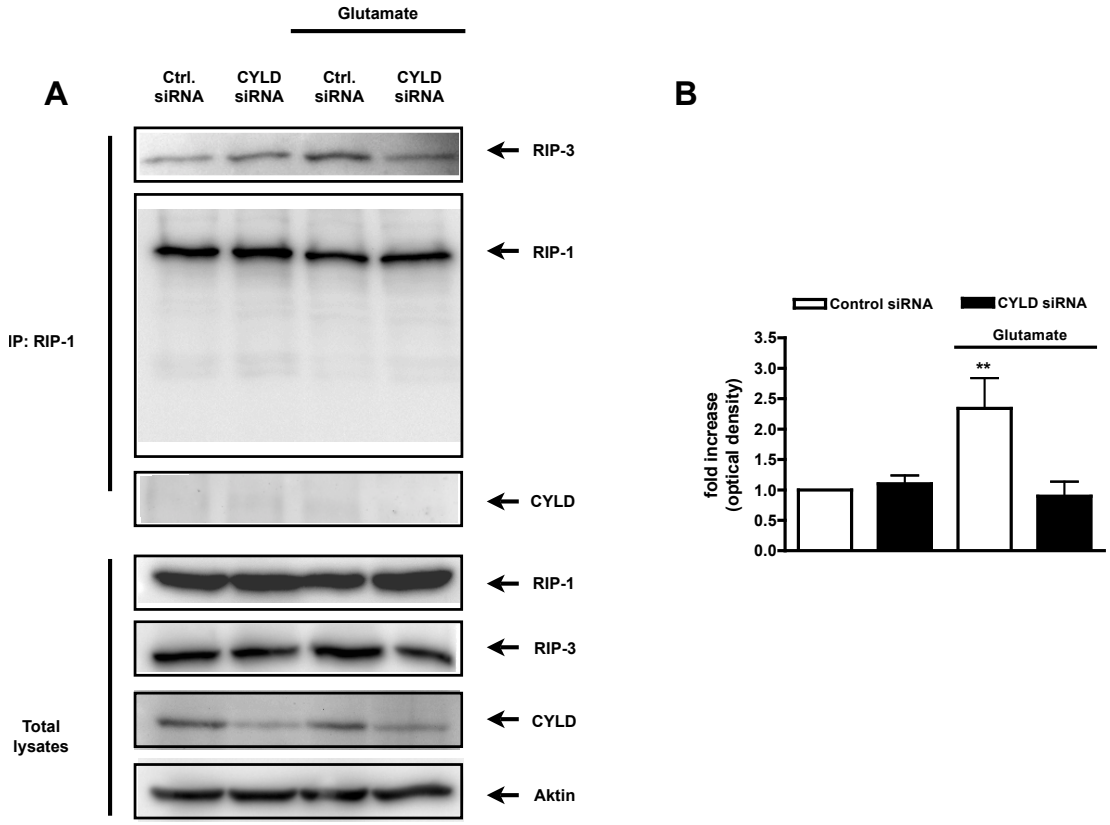

Figure 24: CYLD repression prevents RIP1-RIP3 complex formation in response to glutamate toxicity in HT-22 cells. (A) Immunoprecipitation of RIP1 from 1.25 mg of whole protein extracts obtained from control and CYLD siRNA transfected cells. Glutamate treatment caused an increased co-precipitation of RIP3, as assessed by Western blot analysis (upper panel). Equal loading and CYLD knockdown was verified in the maternal extracts. **(B)** Quantification of the interaction between RIP1 and RIP3, assessing the ratio of RIP3 to (precipitated) RIP1. The ratio is expressed in relation to control. **p<0.01 compared to control (ANOVA Scheffé´s). The experiments were repeated three times and the results were calculated as mean ± S.D.

Overall, these data unveil a role of necroptosis in glutamate-induced cell death in HT-22 cells and further suggest a strong link between the CYLD siRNA mediated protection and the observed inhibition of necrosome formation.

4.10. RIP1 and RIP3 kinases are keyplayers of glutamate dependent cell death

Despite intensive research in the past few years the signaling pathways of necroptosis remain largely unknown (100). With the discovery of the RIP1-RIP3 complex, however, a pronecrotic key-event has been discovered, which propagates necrotic cell death (98; 99). Intact RIP1 kinase function has been reported to be a crucial requirement for the successful formation of the necrosome (98). In this regard, the development of necrostatin-1 (NEC1), a small molecule inhibitor of RIP1 kinase function was a further milestone in the research of necroptosis (66).

Consequently, necrostatin-1 is widely used as a valuable tool for assessing the contribution of necroptosis to cell death in any given system. When co-administered with glutamate, necrostatin-1 was found to attenuate cell death in HT-22 cells, as detected by MTT assay and impedance measurement (Figure 25). Interestingly, protection offered by necrostatin-1 remained stable over several hours, indicating a permanent protection, rather than a transient effect (Figure 25 B). These findings strongly suggest, that necroptosis is an inherent process of glutamate dependent cell death and shed light on a possible future strategy to induce neuroprotection.

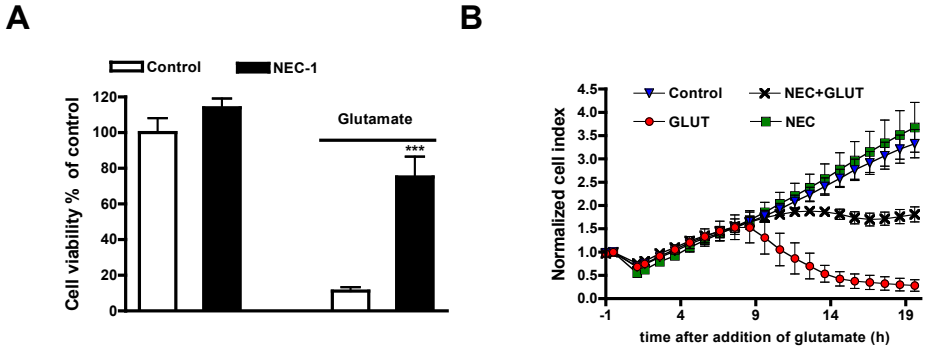

Figure 25: Inhibition of RIP1 kinase by necrostatin-1 attenuates cell death in HT-22 cells. HT-22 cells were treated with glutamate and necrostatin-1 (30µM) over 10h. **(A)** Analysis of cell viability by MTT assay revealed the neuroprotective effect of necrostatin-1 (n=8). ***p<0.001 compared to glutamate treated control (ANOVA Scheffé´s). **(B)** Cellular impedance measurements showed a pronounced decrease in cell index in glutamate treated cells, which was substantially attenuated by necrostatin-1. The experiments were repeated three times and the results are presented as mean values ± S.D.

RIP3 has been suggested, to be of even greater importance for the execution of necroptotic cell death, than RIP-1, partly owing to the fact of its exclusive involvement in this pathway (100). Using siRNA mediated silencing of RIP3 and RIP1, we sought to further elucidate the role of both proteins in glutamate-treated HT-22 cells and tried to confirm the results gained with necrostatin-1. As shown in figure 26 A and B siRNA treatment successfully repressed the respective RIP kinase, compared to vehicle control and control siRNA.

When exposed to glutamate, RIP1 depleted cells were partially resistant to glutamate toxicity, as detected by MTT assay and compared to controls (Figure 26 C). Consequently, a similar degree of protection was achieved by silencing RIP1 as by inhibition of RIP1 kinase function using necrostatins. Using a pool of sequence specific siRNAs for RIP3, a decisive role of RIP3-kinase in glutamate dependent cell death became apparent. As determined by MTT assay, RIP3 siRNA significantly protected against glutamate toxicity compared to control and control siRNA (Figure 26).

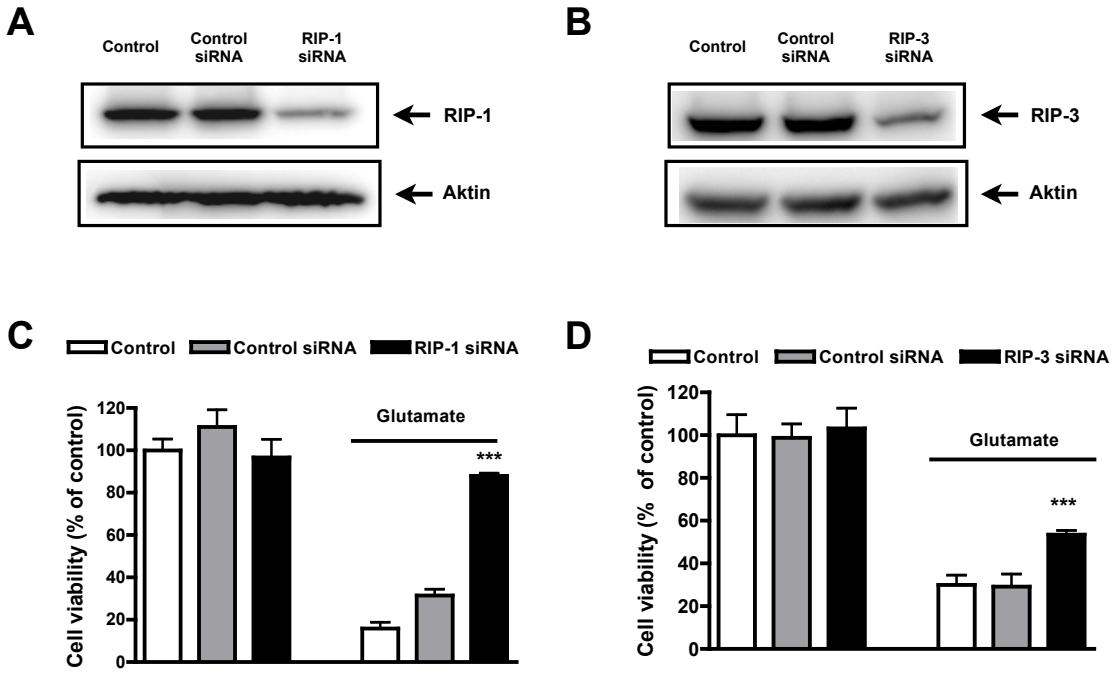

Figure 26: Repressing RIP1 and RIP3 promotes neuronal survival in HT-22 cells. HT 22 cells were transfected with the indicated siRNA targeting RIP1 or RIP3 (40nM) and were treated with glutamate over 10h. **(A, B)** Western Blot analysis revealed a significant decrease in RIP1 and RIP3 protein-levels in response to the respective siRNA. **(C)** Assessing cell viability by MTT assay showed a significant protection of RIP1 depleted cells against glutamate-induced cell death (n=8). **(D)** MTT assay analysis of RIP3 siRNA treated cells revealed a significant protection against glutamate dependent cell death (n=8). ***p<0.001, compared to glutamate treated control siRNA (ANOVA, Scheffé´s).

The effect of RIP1 and RIP3 depletion on cell death was studied in further detail by targeting heat shock protein 90 (HSP90). The heat shock protein 90 has been closely linked to protein stability of RIP1 and RIP3 by functioning as a chaperone protein. In line with this notion, loss of HSP90 function has been associated with a subsequent decrease in RIP proteins.

The antibiotic geldanamycin has frequently been used to reduce the ability of HSP90 to bind its client proteins. Due to inhibition of the ATPase domain of HSP90 by geldanamycin, the scaffold function of HSP90 is inversed, causing HSP90 to present its client proteins to the proteasome. As a consequence, most HSP90-binding proteins are degraded.

In accordance with these reports, geldanamycin (1 µM) was found to cause a pronounced downregulation of RIP1 and RIP3 protein levels when administered to HT-22 cells (Figure 27). Of note, protein levels had already significantly decreased as early as 8 hours after initiation of geldanamycin treatment. This is particularly relevant, as this effect anticipates the execution phase of cell death, which approximately starts 8-10 hours post glutamate exposure (Figure 9). As expected, HT-22 cells, which were co-treated with geldanamycin and glutamate, were almost completely protected against glutamate-induced cell death (Figure 27). These findings thus further strengthen the significance of RIP1 and RIP3 in oxytosis in HT-22 cells.

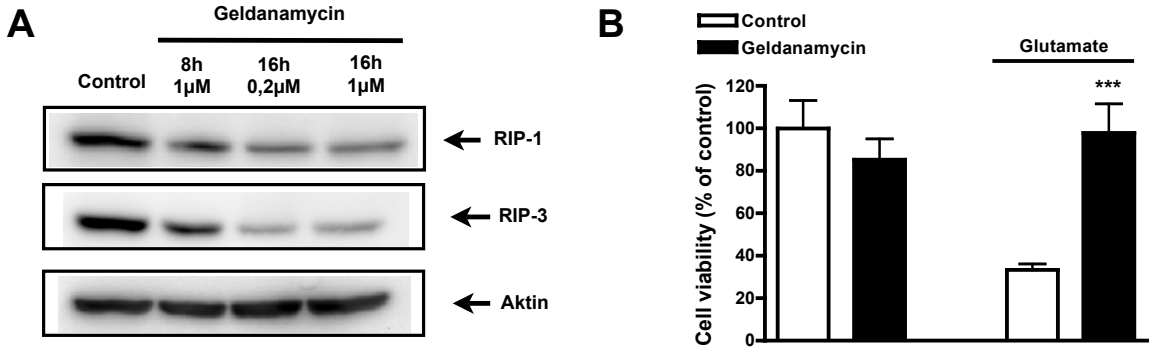

Figure 27: Inhibition of HSP90 mediates neuroprotection by degradation of RIP1 and RIP3. **(A)** HT-22 cells were exposed to geldanamycin (1µM) for the indicated period of time. Protein levels of RIP1 and RIP3 were evaluated by Western Blot analysis, showing a time dependent decrease in both RIP proteins. **(B)** HT-22 cells were treated with geldanamycin (1µM) and co-stimulated with glutamate. As assessed by MTT-assay, geldanamycin treatment abolished glutamate toxicity. ***p< 0.001 compared to control (ANOVA Scheffé´s). The experiments were repeated three times and the results are presented as mean values ± S.D.

4.11. cIAPs are dispensable for CYLD siRNA mediated neuroprotection

In TNF-α dependent necroptosis the ubiquitination-level of RIP1 has been identified as a molecular determinant of cell death (101). While deubiquitinated RIP1 allows progression of necroptosis, the ubiquitinated form has been associated with survival through stimulation of NF-κB (101). As previously mentioned, the deubiquitinating enzyme CYLD propagates necroptosis by specifically removing lysine 63 linked ubiquitin residues from RIP1. In contrast, cIAP proteins have been reported to function as ubiquitin ligases of RIP1 proteins thus opposing the effect of CYLD (99; 102). In a model system of TNF-α induced necroptotic cell death, antagonizing cIAPs has been shown to enhance necroptotic cell death, an effect attributed to diminished RIP1 ubiquitination (102).

In order to investigate if this paradigm holds true for the model of HT-22 cells, the Smac mimetic SM-164 was employed to downregulate cIAP1 and cIAP2 (103). By mimicking the physiological impact of Smac/DIABLO release from mitochondria, SM-164 causes proteasomal degradation of various caspase-inhibiting proteins, including cIAP1 and cIAP2.

Treating HT-22 cells with SM-164 (100nM) resulted in a near complete degradation of both cIAP1 and cIAP2, as determined by Western Blot analysis (Figure 28A). Interestingly, treating HT-22 cells with Smac mimetics, however, did not affect viability under basal conditions and further did not exacerbate glutamate-induced cell death (Figure 28B). To test for the proposed competing effects of cIAPs and CYLD, SM-164 treatment was combined with CYLD siRNA. Intriguingly, SM-164 did not affect neuroprotection induced by repression of CYLD, resulting in a similar degree of protection in the presence or absence of SM-164 (Figure 28C).

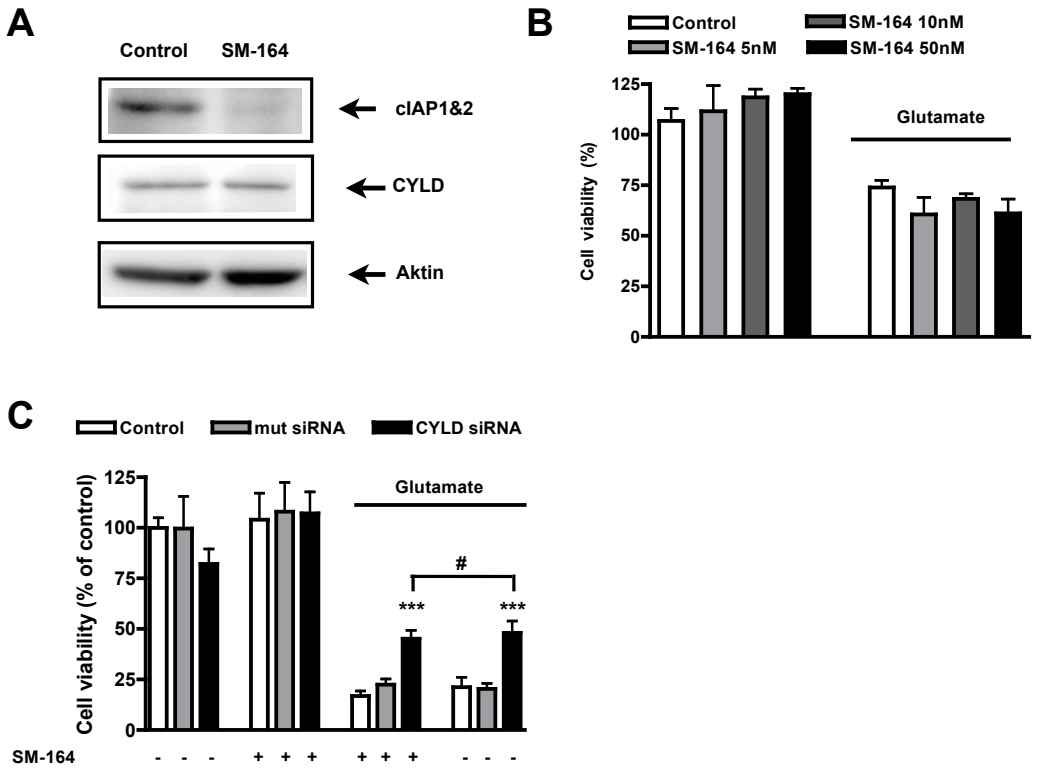

Figure 28: cIAP1 and cIAP2 do not antagonize the neuroprotective potential of CYLD siRNA in HT-22 cells. (A) As evaluated by Western Blot analysis using a pan-cIAP antibody, treatment with the Smac mimetic SM-164 (100nM) causes a near complete degradation of both cIAP1 and cIAP2. **(B)** MTT analysis reveals, that treatment with SM-164 (100nM) did not affect glutamate dependent cell death in HT-22 cells. **(C)** Loss of cIAPs did not influence CYLD siRNA mediated neuroprotection against glutamate toxicity. *** $p < 0.001$, compared to glutamate treated control, # $p > 0.05$ (ANOVA´s Scheffé). All experiments were repeated three times and results are expressed as mean valus ± S.D.

4.12. Overexpressing CYLD does not affect cell viability

Next, this study investigated, whether overexpression of CYLD affected cell viability per se. Even though CYLD levels were strongly increased in HT-22 cells transfected with an overexpression vector, no significant effect on cell viability became evident. This observation was independent of co-stimulation with glutamate (Figure 29). These findings further question the relevance of the ubiquitination level of RIP1, which can be expected to be vastly decreased by the abundantly available deubiquitinase CYLD.

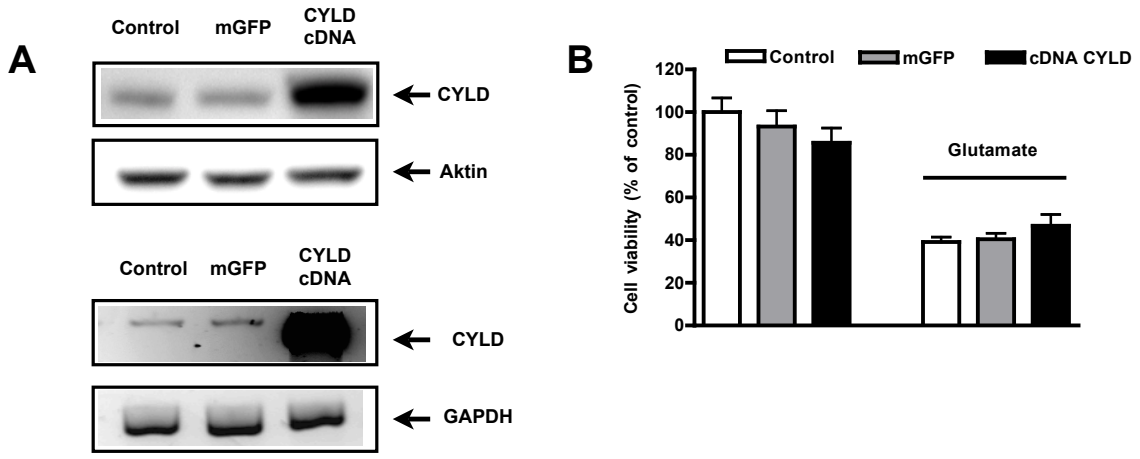

Figure 29: Overexpressing CYLD does not enhance glutamate toxicity or induce cell death. HT-22 cells were transfected with a CYLD overexpression vector. **(A)** mRNA and protein levels were strongly increased in cells transfected with the overexpression vector. **(B)** Overexpression of CYLD did not aggravate glutamate toxicity in HT-22 cells. All experiments were repeated three times and results are presented as mean values ± S.D.

4.13. RIP-1 and CYLD are involved in oxytosis, functioning upstream of mitochondrial damage

Glutamate-dependent cell death in HT-22 cells has been closely linked to the formation of ROS and lipidperoxides, both originating in great parts from mitochondrial dysfunction. Since ROS and lipidperoxides further propagate mitochondrial damage, while mitochondrial rupture simultaneously boosts either one of them, the cytosolic generation of ROS/lipidperoxides and mitochondrial damage forms a self-sustaining loop with a devastating outcome on cell survival. (76; 78; 79).

Similar to oxytosis in HT-22 cells, TNF-α dependent necrosis had been shown to involve ROS formation and the generation of lipidperoxides, with both processes bearing a link towards mitochondrial dysfunction (104-106).

In line with previous findings, HT-22 cells showed a pronounced formation of lipidperoxides following glutamate stimulation, as detected by BODIPY-assay (Figure 30 A and B). Inhibiting RIP-1 kinase activity using necrostatin-1 attenuated this glutamate-induced increase in lipidperoxidation (Figure 30 A). Further, repressing CYLD by siRNA mediated knockdown provided a similar finding, strongly reducing the levels of lipidperoxides (Figure 30B). In summary, these data suggest that protection exerted by both approaches occurred upstream of the massive increase in lipidperoxides, which preceded cellular death.

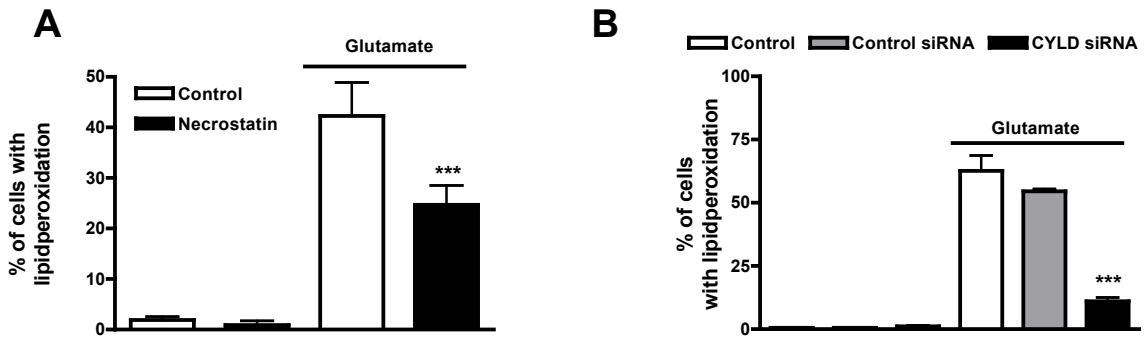

Figure 30: Inhibition of RIP1 and CYLD attenuated lipidperoxidation in HT-22 cells exposed to glutamate. Lipidperoxidation was determined in HT-22 cells following 10 h of glutamate exposure using BODIPY staining and subsequent FACS analysis. **(A)** Treating HT-22 cells with necrostatin1 (30 µM) prevented the glutamate-induced increase in lipidperoxide-levels (n=4, 10,000 cells/sample). **(B)** Silencing CYLD likewise attenuated the formation of lipidperoxides (n=4, 10,000 cells/sample). ***<0.001 compared to glutamate treated control (ANOVA Scheffé´s).

The pivotal role of mitochondrial integrity for neuronal survival has been reported before (76; 78; 79). As extensively studied by Grohm et al. changes in mitochondrial morphology occurring e.g. in response to toxic ROS levels, closely correlated with loss of mitochondrial ATP-production, membrane depolarization and subsequent cellular death (79). Likewise, a role of mitochondria and mitochondrial ROS has been implied in TNF-dependent necroptosis. Consequently, the present study investigated the influence of CYLD and RIP1 inhibition on mitochondria.

To this end, fusion and fission processes were quantified using the classification scheme introduced by Grohm et al. and described in chapter 4.4. In line with earlier findings these investigations confirmed a glutamate dependent increase in mitochondrial fragmentation, reflected by a shift of mitochondrial morphology towards category 3 (Figure 31).

Importantly, necrostatin-1 and CYLD siRNA significantly prevented mitochondrial fission and preserved the tubular mitochondrial network as found under control conditions (Figure 31). These findings indicate, that RIP-1 and CYLD function upstream of mitochondria and further suggest, that the attenuated lipidperoxidation observed previously, can be attributed at least partially to this effect.

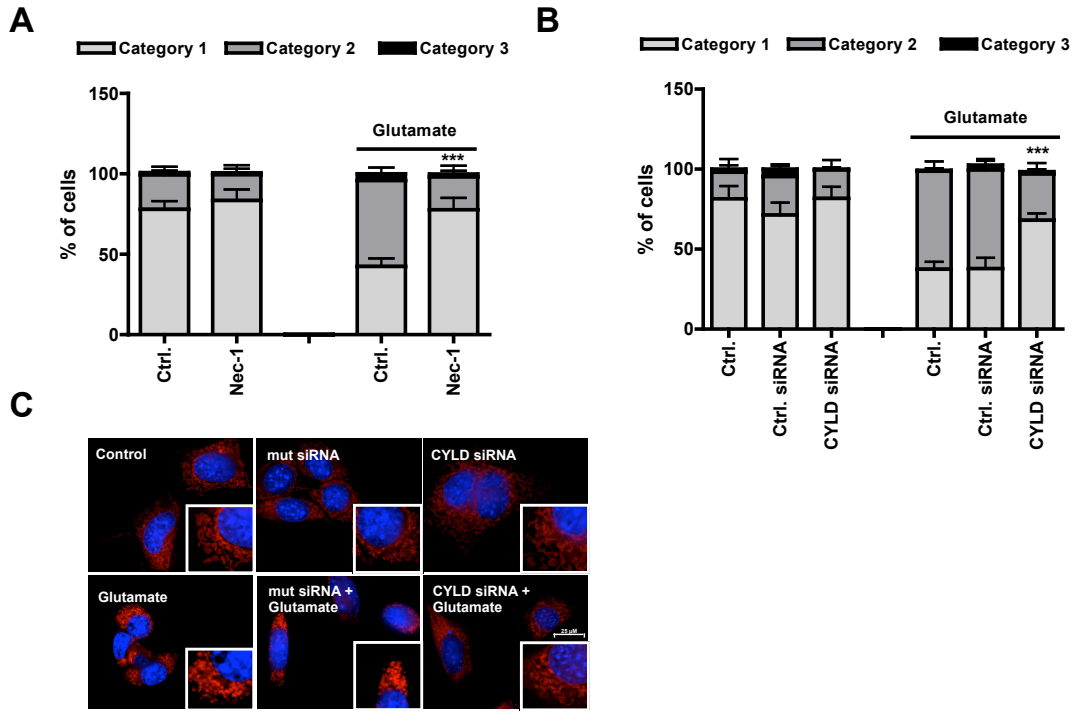

Figure 31: Inhibition of RIP1 and CYLD preserves mitochondrial morphology. Mitochondria were visualized using the mitochondrial dye MitoTracker-red. Morphological changes in response to glutamate were assessed and quantified manually using a classification scheme, which subsumes fragmented mitochondria in categories 2 and 3, reflecting increasing fission events. Elongated tubular mitochondria as found under control conditions were assigned to category 1. **(A)** Glutamate toxicity causes mitochondrial fragmentation (shift towards category 3), which could be prevented by necrostatin1 treatment (n=4, 200 cells/sample). **(B)** CYLD siRNA also protected mitochondrial morphology, maintaining a distribution pattern of mitochondrial categories similar to control conditions (n=4, 200 cells/sample). **(C)** Representative pictures of mitochondrial morphology, showing fragmented, dot-like mitochondria in glutamate treated groups and tubular mitochondria in cells pre-treated with CYLD siRNA. ***p<0.001 compared to glutamate treated control (ANOVA, Scheffé´s).

4.14. RIP1 and RIP3 do not directly interact with mitochondria

As mentioned previously, accumulation of mitochondrial ROS has been suggested as a major trigger of TNF-α dependent necroptosis. Some reports described a direct interaction of RIP kinases with mitochondrial enzymes involved in energy metabolism and deduced from this a causal role of RIP1 and RIP3 in ROS-dependent necroptosis (107; 108). Therefore, another aim of this study was to elucidate whether the RIP kinases also promote mitochondrial dysfunction through a physical interaction. Immunocytochemical stainings of HT-22 cells treated with and without glutamate were carried out, staining the respective RIP-proteins and counterstaining mitochondria. In contrast to the findings reported by Temkin et al., confocal

microscopy revealed no mitochondrial translocation of RIP1-protein in response to glutamate toxicity (Figure 32).

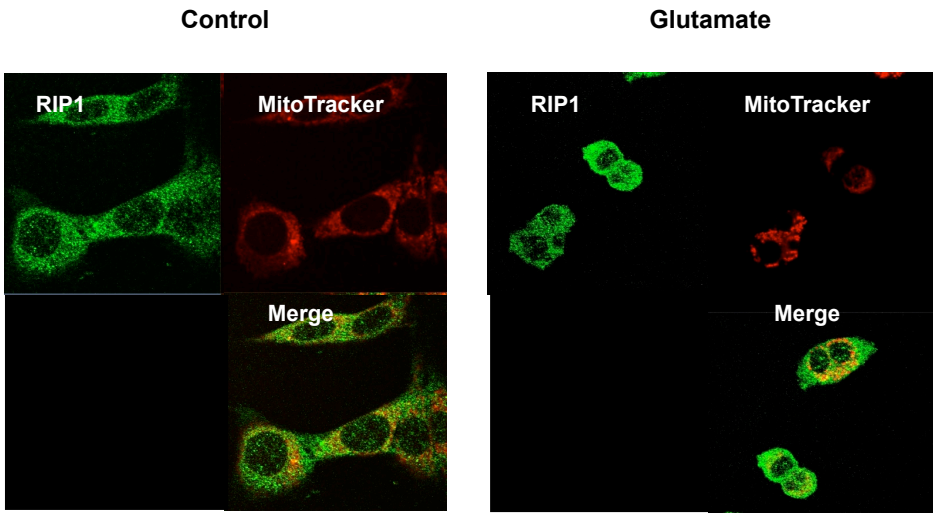

Figure 32: Mitochondrial disintegration in response to glutamate is not caused by a direct interaction with RIP1. Cellular distribution of RIP1 in HT-22 cells as detected by immunocytochemical analysis. RIP1 (green) is localized in the cytosolic compartment under control conditions (left panel). Glutamate toxicity (right panel) does not cause a discernible translocation of RIP1 to the mitochondria (red).

Similar findings were obtained for RIP3, which likewise did not translocate to the mitochondria upon glutamate addition (Figure 33).

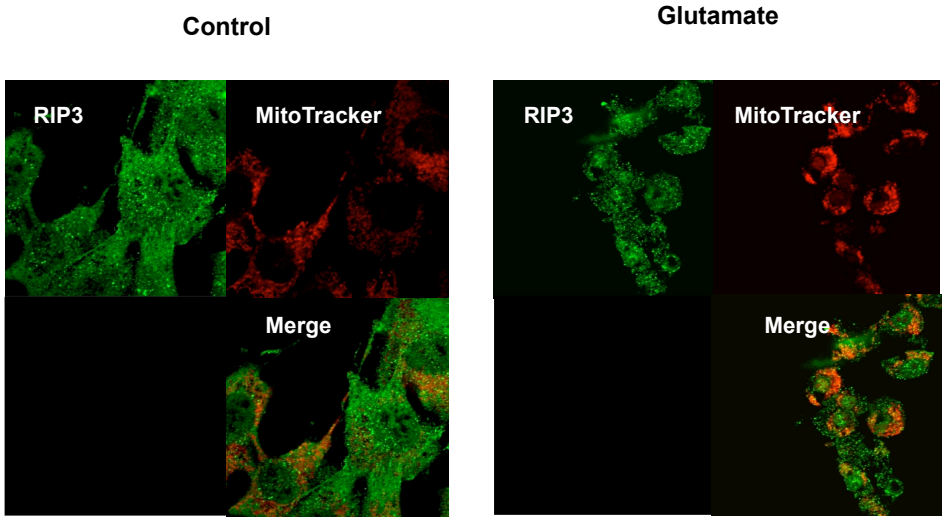

Figure 33: Mitochondrial disintegration is not mediated by a direct interaction of RIP3. Cellular distribution of RIP3 in HT-22 cells as detected by immunocytochemical analysis. RIP3 (green) shows a predominant cytosolic distribution with a fair degree of nuclear staining under control conditions (left panel). Glutamate treatment does not change the distribution pattern of RIP3, no translocation of RIP3 to the mitochondria (red) can be detected (right panel).

To confirm these data, mitochondrial extracts were obtained from protein lysates originating from HT-22 cells treated with or without glutamate. Subsequent detection of RIP kinases was performed by gel electrophoresis and Western Blot analysis. Mitochondrial extracts were equally loaded as confirmed by COXIV levels. The absence of tubulin in mitochondrial extracts was indicative of a high degree of purity (Figure 34). In line with the findings obtained from ICC-stainings and subsequent confocal microscopy, glutamate treatment did not cause any increase in RIP1 or RIP3 kinases in the mitochondrial fraction. A translocation of either RIP protein to the mitochondria thus was not detected in the present model of oxytosis.

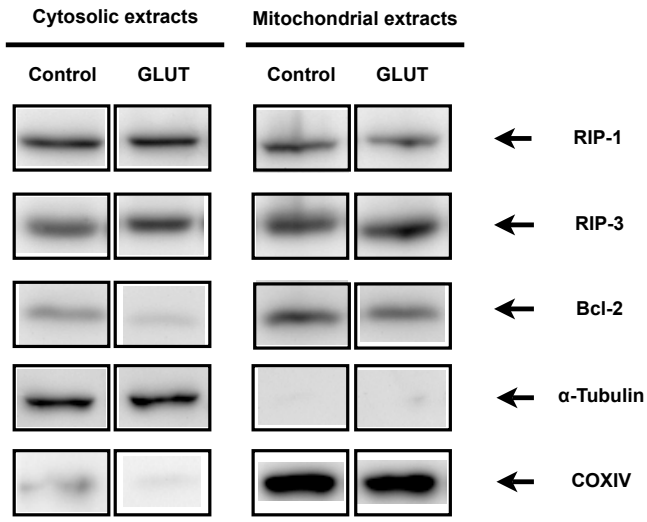

Figure 34: RIP1 and RIP3 do not accumulate in mitochondrial extracts from HT-22 cells exposed to glutamate. Mitochondrial and cytosolic fractions were obtained from whole protein extracts of HT-22 cells treated with or without glutamate, by sucrose gradient centrifugation. Purity and loading of extracts was evaluated by α-Tubulin and COXIV levels. RIP1 and RIP3 levels were not increased in mitochondrial fractions after glutamate addition.

4.15. Necroptotic cell death signaling occurs independent of TNF-receptor stimulation and caspase activity

Recent reports and comments gave rise to the concern that necroptosis, occurring in response to chemically induced cellular stress, may after all result from an endogenous secretion of TNF-α by the dying cells. Consequently, TNF-α had to be considered a potential underlying source of necroptosis in the present model system (68; 109). To investigate the effect of TNF-α stimulation on cell viability in HT-22 cells, TNF-α was administered to the cells in concentrations ranging from 100-1000

ng/ml. As shown in figure 35 A, however, TNF-α did not cause any cytotoxicity. A TNF-α sequestering antibody then was used to determine if autocrine secretion of TNF-α contributed to glutamate toxicity in HT-22 cells. Importantly, this antibody did not affect glutamate-induced cell death in HT-22 cells (Figure 35 B), indicating that autocrine secretion of TNF-α was not involved here.

We next investigated, if TNF-α modulates glutamate-induced necroptosis in HT-22 cells. To this end, the cytokine was combined with glutamate. This experiment showed no additional toxicity in cells co-treated with both compounds. Interestingly, TNF-α was found to reduce glutamate dependent cell death, rather than enhancing it, which may be attributed to NF-κB activation (Figure 35 C and Figure 22). In conclusion, these data strongly suggest, that TNF-α did not contribute to glutamate toxicity in HT-22 cells and thus cannot be considered as the trigger of the necroptotic response.

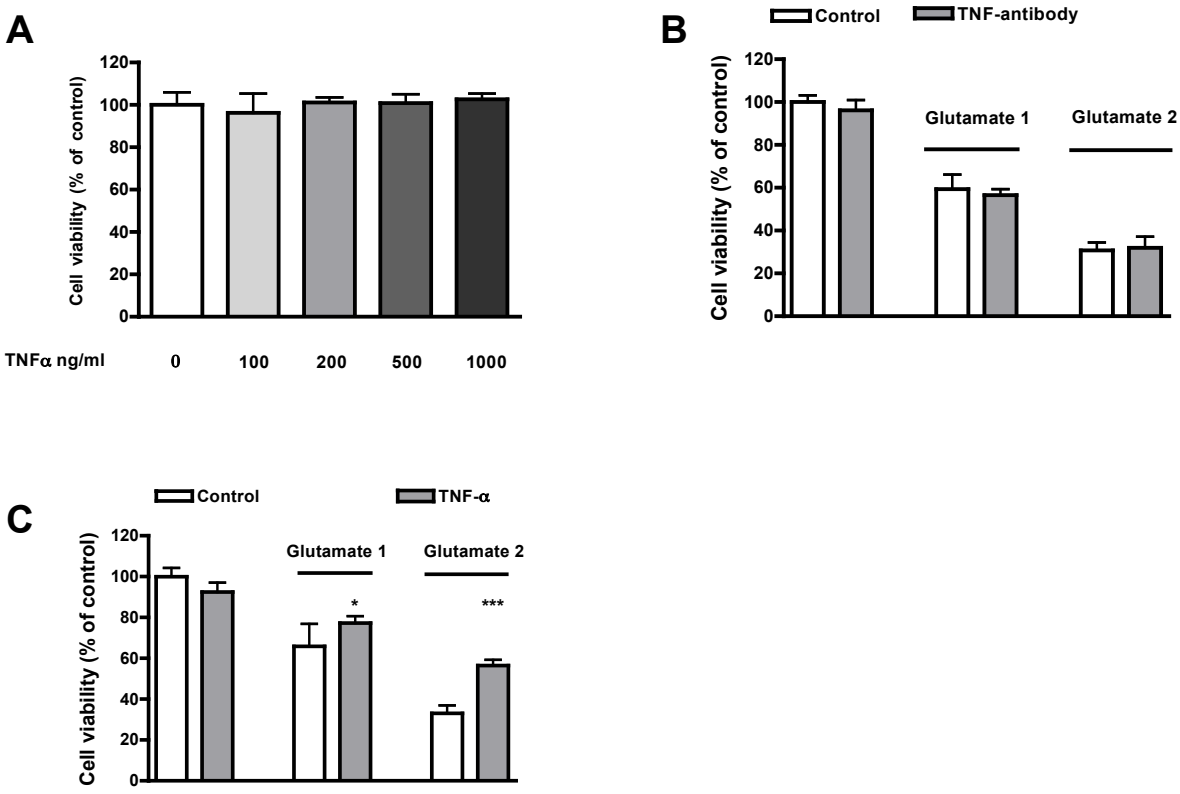

Figure 35: Necroptotic cell death in HT-22 cells does not rely on an autocrine secretion of TNF-α. (A) HT-22 cells were treated with TNF-α at the indicated concentration for 12h. Cell viability was assessed by MTT-assay. TNF-α did not exert cytotoxicity. **(B)** A TNF-α sequestering antibody was added to HT-22 cells at a concentration, capable of neutralizing 500 ng/ml of TNF-α. Following glutamate exposure for 10h, cell viability was determined by MTT assay (n=8). Autocrine secretion of TNF-α is not contributing to glutamate dependent cell death. **(C)** Exogenous addition of TNF-α did not enhance glutamate toxicity in HT-22 cells (n=8). *p<0.05, ***p<0.001 as compared to glutamate treated control (ANOVA Scheffé´s). All experiments were repeated three times and results are given as mean values ± S.D.

A common characteristic of TNF-α dependent necroptosis and glutamate dependent cell death is the caspase independent progression and execution of cell death (78; 98). To confirm this in HT-22 cells, zVAD-fmk a pan-caspase-8 inhibitor was added together with glutamate to the cells.

In line with earlier results this experiment confirmed that cell death in response to glutamate progressed unaltered in the presence of the caspase inhibitors, indicating that caspases were dispensable for oxytosis in HT-22 cells (Figure 36). This is particularly interesting, as the effective inhibition of caspase-8 is a prerequisite for necroptosis in various model systems. Consequently, glutamate dependent cell death seemingly exhibits this characteristic as a naturally occurring trait.

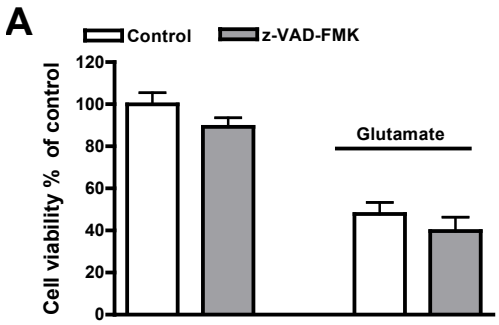

Figure 36: Glutamate dependent cell death in HT-22 cells is independent of caspase-8. Addition of the pan-caspase inhibitor zVAD-fmk (50μM) did not affect glutamate-toxicity as determined by MTT-assay. The experiment has been repeated three times with similar results. Results are presented as mean ± S.D.

4.16. RIP1 but not CYLD mediates glutamate dependent excitotoxic cell death in primary neurons

So far, the effect of neuroprotection through silencing of CYLD has been shown only in immortalized HT-22 cells, in which glutamate causes detrimental glutathione depletion and subsequent accumulation of ROS. This mechanism of cell death, however, reflects only partially the physiological situation, disregarding NMDA receptor mediated excitotoxicity as a major pathway of neuronal cell death in paradigms of acute brain damage (110; 111). To address this issue and expand the understanding of CYLD in cell death mediated by excitotoxicity, in vitro experiments were conducted using cultured primary cortical neurons obtained from $CYLD^{-/-}$ and wild-type mice. It has been shown previously that cell death induced by NMDA receptor stimulation can occur via different pathways (112). While apoptosis was

reported as the predominating type of cell death in response to low concentrations of NMDA-receptor agonists, high concentrations of glutamate or NMDA induced necrotic cell death (112).

Since CYLD has been characterized as a key player in mediating necroptotic cell death (a type of necrosis), this study focused on excitotoxic stimuli, likely to induce this form of cell death. Consequently, cultured cortical neurons from $CYLD^{-/-}$ and wild-type mice were exposed to glutamate concentrations of 200 µM in EBSS for 1 h, followed by media change to neurobasal medium. Additionally, QVD, a broad range caspase inhibitor was used to evaluate the contribution of apoptotic cell death in response to glutamate. QVD addition should help to clarify, if CYLD depletion could add to neuroprotection induced by caspase inhibition.

Following glutamate addition cell death was evaluated 20 h later by assessing pyknotic nuclei stained with DAPI. As shown in figure 37, glutamate treated cells showed a pronounced degree of 75 % of cell death after 20h, which was attenuated when co-treated with QVD. CYLD deficient cells however, were not protected against glutamate-mediated excitotoxicity and neither showed increased survival, when co-treated with QVD, as compared to the respective control (Figure 37). Loss of CYLD was confirmed by Western blot analysis (Figure 37 B).

Investigating the impact of RIP1 on excitotoxicity, primary cortical rat neurons were treated with necrostatin-1 (50 µM) and exposed to glutamate (500 µM, 1 h). Following 1 h of glutamate exposure, medium was changed to preconditioned Neurobasal medium. In line with earlier reports (113), necrostatin-1 proved protective against excitotoxic cell death in primary neurons, maintaining neuronal survival at almost control level (Figure 37 C). Representative pictures of pyknotic nuclei are shown in figure 37 D.

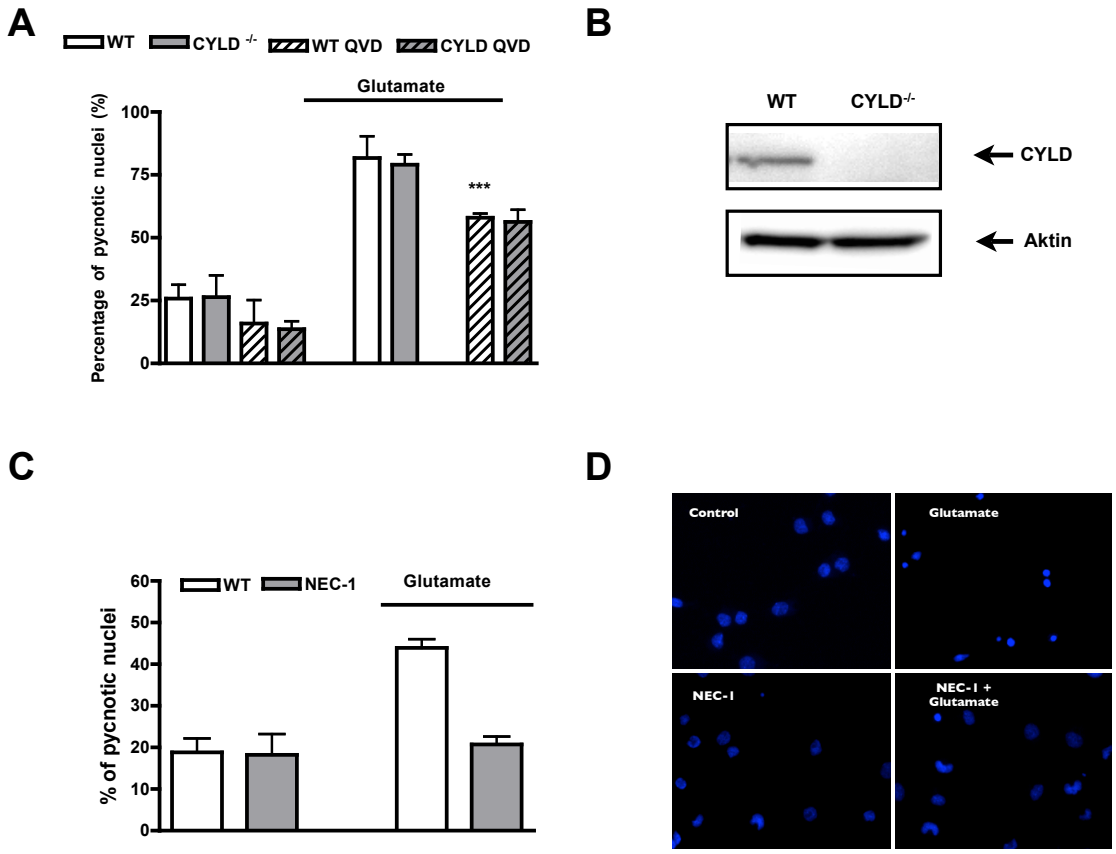

Figure 37: Inhibition of RIP1, but not CYLD protects primary neurons against excitotoxicity. (A) Cortical cultures obtained from CYLD$^{-/-}$ mice were not protected against glutamate damage (200µM 20h) compared to wild-type neurons. Addition of QVD attenuated cell death irrespective of CYLD expression. ***p< 0.001 compared to glutamate treated wild-type (ANOVA, Scheffé´s) **(B)** Loss of CYLD was confirmed in CYLD -/- neurons by Western blot analysis. **(C)** Cultured primary cortical neurons were treated with necrostatin1 (50µM) and exposed to glutamate (500µM). Cell death was quantified by manual counting of apoptotic nuclei stained with DAPI (blue), necrostatin1 mitigated neuronal death (n=4). **(D)** Representative pictures of pyknotic nuclei of cultured cortical neurons treated with necrostatin-1 (50µM) and glutamate (500µM). The nuclei were stained with DAPI.

4.17. Loss of CYLD protects against traumatic brain injury in vivo

Given the limitations inherent with in vitro studies and the promising data on CYLD in the model of HT-22 neurons, this study further investigated the protective potential of CYLD depletion in an in vivo model of traumatic brain injury. This series of in vivo experiments using CYLD$^{-/-}$ mice and wild-type littermates was performed by the collaborating group of Nikolaus Plesnila.

CYLD knockout mice and wild-type littermates were craniotomized above the right parietal cortex under Halothane/N_2O anesthesia and subjected to controlled cortical impact to the surface of the brain. Following the controlled cortical impact, the

craniotomy was closed again. CYLD deficient mice showed a significantly reduced contusion volume 24 h after controlled cortical impact compared to wild-type mice 24h post trauma (Figure 38 A). Formation of brain edema, as determined by the dry-wet weight method was attenuated in $CYLD^{-/-}$ mice compared to wild-type littermates (Figure 38 B). Similarly, CYLD knockout mice experienced a lower intracranial pressure than their wild-type controls (Figure 38 C).

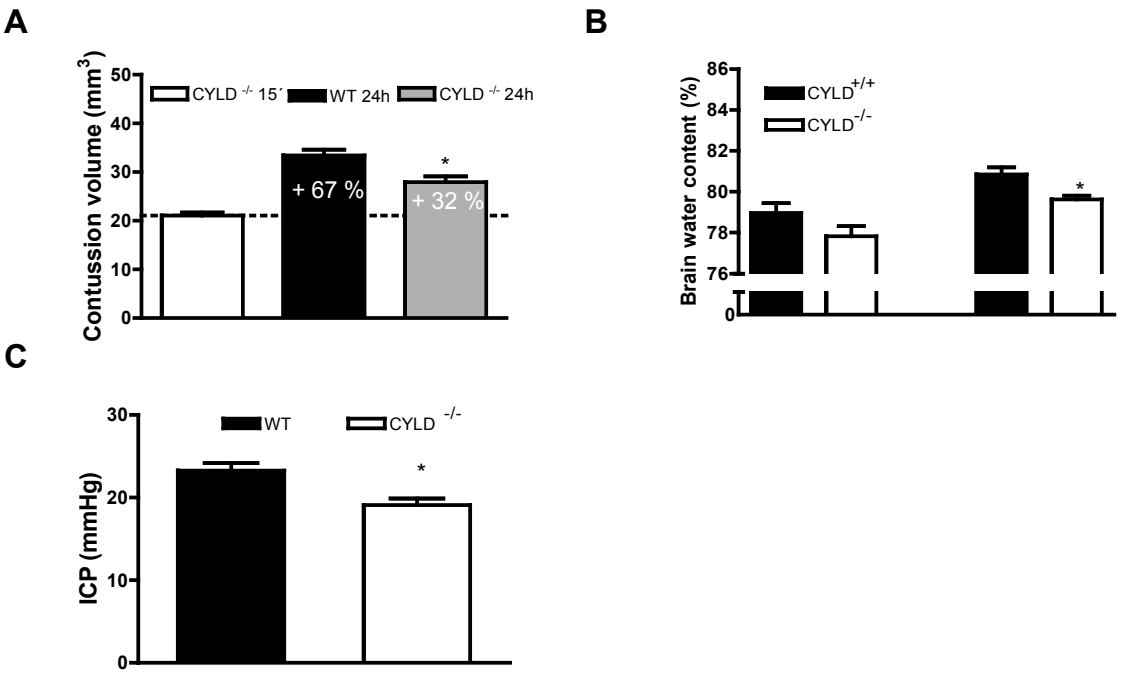

Figure 38 CYLD deficiency preserved brain tissue following traumatic brain injury. (A) CYLD knockout mice and wild-type littermates were subjected to controlled cortical impact to the surface of the brain. The contusion area was determined on the basis of digitized images taken from coronal sections stained for cresyl violet. CYLD deficient mice showed a significantly reduced contusion volume 24h after controlled cortical impact compared to wild-type mice at 24h. $p< 0.01$ (ANOVA, Scheffé´s). **(B)** Formation of brain edema was determined using the dry-wet weight method 24h after traumatic brain injury. CYLD deficient mice demonstrated a significant reduction in brain edema formation. *$p< 0.05$; (Mann-Whitney-U-test**) (C)** CYLD knockout mice showed a lower intracranial pressure compared to wild-type litter-mates. *$p< 0.05$; (Mann-Whitney-U-test).

5. Discussion

The major aim of this study was to explore the roles of p53 and CYLD in neuronal cell death and to connect their function herein with the neuronal NF-κB pathway. This issue was addressed in immortalized mouse hippocampal HT-22 neurons and in primary neuronal cultures exposed to toxic glutamate concentrations. Furthermore, an in vivo model system of traumatic brain injury was employed using wild-type and $CYLD^{-/-}$ mice.

The first part of this study revealed a strong neuroprotective effect of p53 inhibition by the p53-inhibitor pifithrin-α in HT-22 cells. The obtained data show that the disturbance of mitochondrial morphology and mitochondrial membrane potential in neuronal cell death was prevented by the p53 inhibitor pifithrin-α. Surprisingly, however, the results indicated that neuroprotection induced by pifithrin-α did not involve NF-κB activity. Further, NF-κB expression and transcriptional activity were not significantly altered in HT-22 neurons that were exposed to glutamate. Based on these data, it is concluded that the NF-κB pathway was not significantly involved in glutamate-induced oxytosis in this model system.

In the second part, this study investigated the role of CYLD in neuronal cell death in vitro, using HT-22 neurons and primary cortical neurons, as well as in vivo using C57bl6 mice.

CYLD function was studied using sequence specific siRNA, revealing a pronounced degree of protection in CYLD depleted HT-22 cells. Despite of the established role of CYLD as a negative regulator of NF-κB, neuroprotection induced by silencing of CYLD was completely independent of NF-κB. These findings are in line with the results obtained in the first part of the study, highlighting a minor role of NF-κB in this model system.

Investigating the underlying cause of neuroprotection associated with CYLD depletion, this study unveiled that oxytosis in HT-22 cells occurs through mechanisms of necroptosis. This conclusion is based on the finding, that complex formation of RIP1-RIP3, the so-called necrosome, a hallmark of necroptotic cell death, has been found in HT-22 neurons and silencing of either RIP-kinase provided strong neuroprotection. In turn, repressing CYLD prevented the formation of the necrosome, suggesting that inhibition of necroptosis was the underlying mechanism

by which CYLD depletion promoted neuroprotection. The role of necroptosis in excitotoxic cell death in primary cortical neurons, as established in this study, remains to be clarified. Even though inhibition of RIP1 kinase by necrostatin-1 could significantly enhance neuronal survival, CYLD depletion had no effect on cell death in this model of excitotoxicity in primary neurons. The physiologically highly relevant in vivo model of traumatic brain injury, however, exposed a strong neuroprotection in $CYLD^{-/-}$ mice compared to wild-type littermates, rendering CYLD a key player in acute neuronal cell death.

In summary, these data highlight a yet unknown role of CYLD in neuronal cell death and unravel the inhibition of necroptosis as a putative therapeutic approach for acute and chronic neurodegenerative diseases.

5.1. Neuroprotection by pifithrin-α – no crosstalk between p53 and NF-κB in HT-22 cells

The transcription factor p53 is a prominent tumor suppressor with manifold functions in DNA repair, cell cycle arrest and cell death. As p53 is activated upon DNA-damage, it mediates the following cellular response leading either to DNA repair or controlled cell death. For this reason p53 is also referred to as the “guardian of the genome” (114). DNA stability, however, is not only of utter importance for tumor suppression, it similarly has a great impact on neuronal survival.

Consequently, activation of neuronal p53 and subsequent cell death has been described in response to genotoxic stress, ROS and excitotoxicity in vitro and in cerebral ischemia and traumatic brain injury in vivo. These results were confirmed in HT-22 neurons, demonstrating a strong neuroprotective effect of the p53 inhibitor pifithrin-α in glutamate dependent cell death.

In the past, complementary mechanisms had been suggested to contribute to neuroprotection by pifithrin-α, extending beyond the inhibition of the transcriptional upregulation of the pro-apoptotic p53 target proteins like e.g. BAX, PUMA or Noxa (36; 37; 115). In line with this notion, p300 had been identified as a crucial co-transcription factor, inter-connecting the p53 and the NF-κB pathway in primary neurons and in vivo (36). It became evident, that both transcriptional pathways compete for the same intracellular pool of p300 to induce effective transcription. Consequently, p53 inhibition by pifithrin-α was found to increase the pool of freely

available p300, thereby enhancing concomitantly the pro-survival pathway NF-κB. In HT-22 neurons, however, the present study could not detect an enhanced NF-κB response, when p53 was inhibited with pifithrin-α. Thus, a complementary mechanism of pifithrin-α that might involve NF-κB seems irrelevant for protective effects observed in HT-22 cells.

A possible explanation for the differing results may lie in the model system employed here. Earlier results were obtained in cultured primary hippocampal neurons, which undergo excitotoxic cell death in response to glutamate receptor stimulation. Furthermore, it has been shown previously that glutamate stimulation can also initiate the NF-κB pathway per se in primary neurons (116).

This stands in sharp contrast to the model system of HT-22 cells employed in this study. In HT-22 cells, cell death depends on glutathione depletion but is completely independent of ionotropic glutamate receptors (73; 84) and further does not elicit any sign of NF-κB response. Taken together, these differences in basal NF-κB response and cell death mechanism likely account for the deviating findings on the connection between NF-κB and pifithrin-α mediated protection in HT-22 cells, as compared to primary cells.

5.2. Mitochondrial p53 is involved in pifithrin-α mediated neuroprotection

As discussed before, this study could not substantiate the reported link between p53 inhibition and enhanced survival signaling via NF-κB in HT-22 cells. Nonetheless, the present study could establish a preliminary line of evidence of a transcription-independent mechanism, by which inhibition of p53 promoted neuronal survival. In particular, data gained on the effect of the p53 inhibitor pifithrin-α at the level of mitochondria hint at a direct mechanism occurring at this organelle, which may be independent of the nuclear action of p53.

In this respect, inhibition of p53 by pifithrin-α was found to preserve mitochondrial disintegration and inhibit mitochondrial depolarization in response to glutamate toxicity in HT-22 cells. Arguably, both observations can also be explained by the subsequent effect of pifithrin-α on the BH3 proteins PUMA and Noxa, both under transcriptional control by p53. This mechanism, however, could not explain the

increase in the mitochondrial membrane potential in response to pifithrin-α, an effect most likely mediated directly at the site of mitochondria.

This notion is further supported by the observation that synaptosomal preparations treated with pifithrin-α were protected against mitochondrial depolarisation induced by Fe^{2+} (117). As synaptosomal preparations naturally contain mitochondria, but no nucleus, this effect must be mediated independently of p53 transcription. As a simple ROS scavenging mode of action of pifithrin-α could be ruled out in this study, a separate effect at the level of mitochondria seems most likely, to account for the observed protection.

Interestingly, a possible role of mitochondrial p53 has been reported recently, suggesting, that p53 after translocation to mitochondria sequesters the antiapoptotic Bcl-2 proteins Bcl-2 and Bcl-X_L and thus promotes cell death (118). Although this report has been discussed controversially in the field, the finding supports the notion of a putative role of mitochondrial p53 in regulating neuronal cell death independently of transcriptional activity.

It is important to note, that neither Bcl-2 nor Bcl-X_L were involved in glutamate dependent cell death in HT-22 cells, nor in pifithrin-α mediated protection, indicating that the role of mitochondrial p53 is different in this model. This conclusion was based on the finding, that inhibition of either Bcl-2 family protein did not affect cellular survival in the present study.

A further hint of a direct mitochondrial mechanism of p53 was very recently provided by Nijboer et al. who showed that μ-PFT, a small molecule, which inhibits the association of p53 with mitochondria without affecting p53 transcriptional activity prevents cell death (119).

In summary, pifithrin-α protected HT-22 neurons by a mechanism, which relied at least partially on a direct mitochondrial effect, but was independent of Bcl-2 proteins.

5.3. CYLD is involved in glutamate-induced oxytosis

In the present study the deubiquitinase CYLD has been characterized as an important mediator of neuronal cell death in experimental paradigms of oxytosis and traumatic brain injury, but not in excitotoxic cell death.

CYLD originally has been identified as an important negative regulator of NF-κB signaling, with loss of CYLD being associated with tumorgenesis and immune

dysfunction (94). Within the central nervous system, the role of NF-κB is very complex and highly controversial, since numerous reports either designated a pro-apoptotic or a pro-survival effect to enhanced NF-κB activity.

The apparent contradiction of these reports has not been completely resolved yet, but emerging evidence suggests, that the diverging findings could be explained with different experimental settings, different cell types as well as by a NF-κB sub-type specific effect (44; 93; 120). In neuronal cultures, NF-κB complexes mostly promote survival, whereas in microglial cells and glial-neuronal co-cultures NF-κB stimulation has been associated with an increased inflammatory response and an overall adverse effect (93).

Given the alleged effect of sustained NF-κB transcription in neurons, the working-hypothesis emerged that by depleting CYLD enhanced NF-κB activity could be obtained, which then promotes neuronal survival.

In the present study it was found, that CYLD repression by siRNA in HT-22 neurons significantly reduced glutamate dependent cell death as determined by numerous detection methods. Surprisingly, however, this study showed that neuroprotection through targeted deletion of CYLD in HT-22 cells was independent of NF-κB activity. This conclusion is based on the finding, that NF-κB activation and transcriptional activity were unaffected by CYLD depletion in HT-22 cells exposed to glutamate (Figure 22*)*. These results are especially interesting, when compared to recent reports from other groups, which confirmed the reportedly strong correlation between NF-κB activity and cellular levels of CYLD (121; 122). In the light of these reports it becomes obvious, that the susceptibility to CYLD depletion must be far less pronounced in HT-22 cells than in other cells.

In conclusion, silencing CYLD in HT-22 cells promotes neuroprotection against glutamate toxicity by a mechanism, which is independent of NF-κB signaling.

5.4. Neuronal cell death in HT-22 cells occurs by necroptosis and can be prevented by CYLD siRNA

With the recent discovery of a controlled signaling network that regulates necrotic cell death, Hitomi et al. challenged the long held belief that necrotic cell death always occurs in an uncontrolled manner (63). Until then, only apoptosis was regarded as an ordered form of cell death involving tightly regulated, highly controlled and

interconnected signaling pathways. Necrosis, in contrast, was considered to occur in response to nonspecific and unphysiological stress, leading to an unregulated cellular rupture (123).

Though plenty of open questions remain unanswered concerning the precise executing mechanisms of necrosis, several key players have been identified (69). In addition to CYLD, the complex formation of RIP1 and RIP3, also termed necrosome, is considered as a central component in the regulation of necroptosis (63; 100). Interestingly, this study found an increasing formation of the necrosome in neuronal HT-22 cells exposed to glutamate. Consequently, oxytosis in HT-22 cells cannot be regarded as pure apoptosis, but rather a mixed form of cell death, with a prominent contribution of necroptosis.

Repressing CYLD, in turn, prevented cell death and inhibited the formation of the necrosome, indicating a regulatory link between these molecular entities. If this involved a direct interaction of CYLD with the necrosome, however, remains to be established, since we could not detect any physical interaction between CYLD and the RIP1-RIP-3 complex.

In TNF-α induced cell death, two distinct cytosolic complexes have been described secondary to receptor stimulation and assembly of the multiprotein complex 1 (69).

One of these complexes is the previously mentioned pro-necrotic necrosome, which encompasses next to RIP1 and RIP3 also FADD, TRADD and an inactive caspase-8. The second complex consists of FADD, TRADD and an active form of caspase-8, which triggers the activation of downstream caspases, thus promoting apoptotic cell death. This proapoptotic complex II is stabilized by the active caspase-8, which has been shown to cause degradation of both, RIP1 and RIP3 and thereby prevent the formation of the alternative pro-necrotic variant of complex II, the necrosome (99; 124).

Consequently, complex II promotes either caspase mediated apoptosis or RIP mediated necroptosis, depending on the activity of caspase-8.

The formation of the caspase-dependent pro-apoptotic complex and a possible contribution to cell death in HT-22 cells, however, seems very unlikely, as this study and earlier reports clearly ruled out any involvement of caspase-8 in oxytosis. In fact, no protection could be detected in cells that had been treated with the well-accepted pan-caspase inhibitor zVAD-FMK.

This data confirms earlier findings by Landshamer et al. who reported similar observations with zVAD-fmk and the more specific IETD-fmk, which both failed to protect HT-22 cells against oxytosis (78). The same study further demonstrated, that caspase-8 activity was not enhanced after glutamate treatment, thereby supporting the conclusion that caspase-8 is dispensable for oxytosis (78).
The mechanism proposed by this thesis, a caspase independent and RIP1/RIP3 dependent type of cell death is further supported by the finding, that neither RIP1, nor RIP3 were markedly degraded during cell death in HT-22 cells. This were to be expected according to earlier reports on complex II and caspase-8 dependent cell death, if apoptotic signaling predominated (69).
In summary, these findings suggested that the formation of the necrosome in HT-22 cells likely contributed to glutamate-induced cell death in a RIP1 and RIP3 dependent manner, but occurred independently of caspase-8 function. Further, CYLD siRNA was found to prevent RIP1/RIP3 complex formation, thereby promoting survival in HT-22 cells.

5.5. Inhibition of RIP1 and RIP3 promotes protection against neuronal cell death in HT-22 cells

In addition to the aforementioned keyplayers of necroptosis, like CYLD, RIP1 and RIP3, the kinase function of RIP1 has been demonstrated to be of great importance for the formation of the necrosome and the inhibition of cell death (98). It has been suggested, that reciprocal phosphorylation of RIP1 and RIP3 is the determinant of a successful kinase-driven initiation of necroptosis (98).
With the development of necrostatin-1, a compound became available which specifically prevented necroptosis by inhibiting RIP1-kinase (66). Recent reports, however, challenge the specificity of this compound for blocking necroptosis, since e.g. cIAP induced apoptotic cell death was also prevented with necrostatin-1 (125; 126). Nevertheless, necrostatin-1 is still considered an important predictive tool for evaluating the involvement of necroptosis (69).
In the present study this compound was successfully used to prevent cell death in HT-22 cells, thus supporting the idea of a significant role of necroptosis in this model system. In accordance with this notion, repressing RIP1 by siRNA offered a similar degree of protection against glutamate toxicity. These findings thus confirm and

extend an earlier report, according to which necrostatin-1 protects HT-22 cells in an BNIP3-dependent way (Bcl-2/E1B 19kDa-interacting protein 3-like protein) (127).
The decisive role of RIP3 kinase in necroptotic cell death has been well accepted and loss of RIP3 has been found to protect against necroptotic cell death in any model system studied until today (128).
In the system of HT-22 cells, silencing RIP3 by siRNA or inducing its degradation by geldanamycin likewise attenuated oxytosis. These findings, thus, establish a line of evidence for the actual contribution of RIP1 and RIP3 to glutamate dependent cell death in HT-22 cells.
As outlined before, FADD and TRADD have been identified as further components of complex II. The role of these molecular entities for the progression of necrotic cell death, however, remains controversial (65; 129). In a recent report Welz et al. (2011) found in colonic epithelial cells, that FADD deficiency stimulates necrosis, while the presence of FADD within complex II promotes apoptosis, as reported by Kalai et al. (2002) (129; 130). These findings thus render FADD a putative regulative factor within complex II. Intriguingly though, in a different model system of mouse embryonic fibroblasts, FADD has been found as an integral part of the active necrosome (98). In the light of these controversial findings it would be interesting to decipher the role of FADD in the model system of HT-22 cells and oxytosis.

5.6. The ubiquitination of RIP1 may not be detrimental in HT-22 cells

Ubiquitination of RIP1 is considered a central regulatory element within the pathways of TNF dependent necroptosis and apoptosis (125; 131). In this respect, deubiquitination of RIP1 has been highlighted as a prerequisite for the induction of apoptotic cell death.
For necroptotic signaling, however, the role of deubiquitinated RIP1 for the progression of cell death has only been established indirectly or deduced from the findings gained in studies on apoptosis (100).
Research within the field has been significantly stimulated by the discovery of Smac-mimetics, a class of compounds, which mimics the effect of mitochondrial Smac/DIABLO on the inhibitor of apoptosis (IAP) family of proteins, causing their proteasomal degradation (103). cIAPs recently have been recognized as ubiquitin

ligases, causing K63 linked polyubiquitination of their various target proteins, including RIP1 (131). Using SMAC-mimetics, Bertrand et al. reported, that by depleting cIAPs, RIP1 becomes deubiquitinated and thereby loosens its association with the prosurvival transforming growth factor-β-activated kinase 1 (TAK1) (131). As a consequence, upon TNFR1 stimulation the deubiquitinated RIP1 was found to facilitate the assembly of the pro-death complex II (or DISC), encompassing TRADD, Fas associated death protein (FADD) and caspase-8 (131).
Caspase-8 then triggers apoptosis through the caspase-cascade and simultaneously cleaves RIP1 and RIP3 thereby preventing necroptosis.
In conclusion, these findings render RIP1 deubiquitination a major determinant of apoptotic cell death.

Similarly, it was shown that treatment with Smac mimetics, sensitizes L929 cells to necroptotic cell death in response to TNF-α (102). This report, unfortunately, could not correlate the effect of Smac mimetics with the level of RIP1-ubiquitination, as the amount of polyubiquitinated RIP1 fell below the detection level. Most intriguingly, the same report unveiled, that loss of cIAPs sensitizes L929-cells to TNF-dependent necroptosis, but had no effect on all other necroptotic stimuli investigated, including FAD and poly(I:C) (102).
In summary, it may seem plausible from a mechanistic point of view that deubiquitination of RIP1 is a general requirement for necroptosis, but explicit proof is pending (69; 123; 128; 132) and the intriguing reports at hand deeply require further studies.

For the model system of HT-22 cells, the present study likewise tried to address this question and sought to establish the role of ubiquitination of RIP1 for the progression of glutamate dependent cell death. To this end, the highly potent Smac-mimetic, SM-164 was applied to achieve a near total depletion of cIAP1 and cIAP2. Interestingly, the loss of these RIP1 ubiquitinating proteins did not have any adverse effect on cell viability in HT-22 cells. Further, depletion of both cIAPs did not enhance cell death in response to glutamate, a process one may have expected to be facilitated, once the prosurvival ubiquitin residues on RIP1 were removed.
Similar to the report by Vanlangenakker et al. the actual level of ubiquitination of RIP1 could not be assessed, as it fell below the detection level. Consequently, it

remains elusive if RIP1 deubiquitination is necessary for necroptosis and, further, if Smac mimetics affect the ubiquitination level of RIP1 at all.
To further address the potential link between RIP1- ubiquitination and CYLD, the deubiquitinating protein CYLD was overexpressed.
Similar to the effect of Smac mimetics, this approach should also lead to RIP1 deubiquitination. Overexpressing CYLD, however, was not toxic to the cells, and neither enhanced glutamate toxicity.
Overexpression of CYLD may not have enhanced glutamate toxicity, since the endogeneous levels of CYLD were sufficient for a maximal stimulation of necroptosis, which consequently cannot be elevated further by CYLD overexpression.

A possible explanation for the first observation, that cIAP depletion does not facilitate glutamate dependent cell death in HT-22 cells could be that the loss of the ubiquitinating enzymes cIAP1 and cIAP2 is compensated by a yet unidentified E3-ligase. A potential candidate is the linear-ubiquitin assembly complex (LUBAC), a ubiquitin ligase, which adds linear ubiquitin chains to NEMO and RIP1, thereby propagating NF-κB signaling and inhibiting apoptosis (53; 133).
Another explanation for the absent effect of cIAPs could be that cIAP degradation does cause RIP1 deubiquitination, but is not of relevance for the induction nor progression of cell death in this model.
In order to verify this hypothesis, a mutated RIP1 lacking all known endogenous ubiquitination sites could be generated and expressed in HT-22 cells, while wild-type RIP1 is simultaneously repressed by siRNA.
This approach could serve to clarify the impact of RIP1 ubiquitination on glutamate dependent cell death in HT-22 cells.
Currently, however, the exact role of RIP1 ubiquitination still remains to be established, as well as the regulative link between RIP1 and CYLD.

5.7. ROS- Homeostasis and mitochondrial integrity are preserved by inhibiting necroptosis in HT-22 cells

The executing mechanisms of necroptosis remain largely unknown with current data pointing at the involvement of lipidperoxidation and the formation of ROS at the level of mitochondria (104-106). Interestingly, similar mechanisms have been shown in the

past to play a major role in glutamate dependent cell death in HT-22 cells, with lipidperoxide-formation starting already in the initial phase and mitochondrial damage occurring at mid and late stages.

To highlight its importance, mitochondrial disintegration has also been referred to as the “point of no return” in programmed cell death (76; 79). Ultimately, glutamate-induced cell death in HT-22 cells is executed in a caspase independent manner by AIF (78).

This study confirmed these earlier findings, showing both increased lipidperoxidation and mitochondrial damage in response to glutamate. Importantly, necrostatin-1 or CYLD siRNA prevented the increase in lipidperoxidation and rescued mitochondrial morphology. These data suggest, that key-events established so far in glutamate dependent cell death in HT-22 cells also are pivotal downstream events of the necroptotic response in HT-22 cells.

Based on these findings, it can be concluded, that both apoptotic and necroptotic pathways must converge upstream of mitochondria and cell death may ultimately be executed in a conserved manner through mechanisms of ROS formation and mitochondrial demise.

In line with that notion, a further molecular entity shared between both pathways is the NADPH-oxidase. In TNF mediated necrosis, NADPH-oxidase has been recognized as a possible source of ROS in addition to mitochondria (134; 135). In HT-22 cells, NADPH likewise seems to be involved in oxytosis, as NADPH inhibitors significantly attenuated cell death (143).

Necrosis has long been associated with a decline in ATP levels, which also were suggested as a characteristic to differentiate between forms of apoptotic and necrotic cell death (4; 136; 137). In line with this perception, another downstream mechanism of necroptosis has been shown to involve inhibition of the adenine nucleotide translocase (ANT), an integral protein of the inner mitochondrial membrane. Under physiological circumstances ANT exchanges mitochondrial ATP with cytosolic ADP. Thus, inhibition of ANT will reduce intra-mitochondrial ADP levels causing a subsequent depletion of ATP synthesis (108). Interestingly, HT-22 cells have previously been shown to similarly exhibit a decline in ATP levels when undergoing glutamate dependent cell death (143).

A possible link between RIP-proteins and the execution of cell death at the level of mitochondria was provided by reports describing a direct physical interaction of RIP1 and RIP3 with mitochondria (107; 108). The data on the cellular localization of RIP1 and RIP3 obtained in this study, however, could not confirm these earlier reports. Accordingly, both RIP proteins showed a predominant cytosolic distribution with no detectable changes after glutamate challenge. Therefore, the link, between the activation of necroptosis and mitochondrial demise likely occurs at a different stage independent of RIP1-RIP3 translocation to the mitochondria.

5.8. Necroptotic cell death in HT-22 cells follows a novel mechanism independent of TNF-receptor signaling

As discussed in previous chapters several lines of evidence support an involvement of necroptosis in glutamate dependent cell death in HT-22 cells. Despite the shared characteristics of TNF dependent necroptosis and glutamate-induced cell death in HT-22 cells, significant differences are apparent between the stimuli by which cell death is induced.

Induction of necroptosis is usually carried out by activation of death receptors by their respective ligands including FASL, TNF and Trail-ligand. Importantly, death receptors are closely associated with downstream complexes of necroptosis like the necrosome (69). This connectivity results in a great homology of receptor related proteins shared by the necrosome, which not only contains RIP1 and RIP3 but may also contain TRADD and FADD.

In contrast hereto, no glutamate receptor stimulation is involved in glutamate-induced cell death in HT-22 cells, which is initiated through glutathione depletion and the subsequent accumulation of intracellular ROS (73). Recent reports, however, suggested that ROS induced necroptosis involves the secretion and autocrine effects of TNF-α. Consequently, TNF-α had to be considered as the initiating cause of necroptosis also in the present model system of glutamate-induced oxytosis (68; 109).

To address this issue, the current study evaluated the possibility of TNF-α, as the trigger of cell death in HT-22 cells that had been exposed to glutamate. The data obtained here, using TNF-α and a TNF-α sequestering antibody together with

glutamate, suggested that no autocrine stimulation of TNF-α occurs in HT-22 cells. Further, even when administered exogenously, TNF-α did not promote cell death, for which reason the hypothesis of necroptosis due to an autocrine effect of TNF-α was rejected for HT-22 cells.
Thus, it can be concluded that the necrotic response in HT-22 cells is mediated by RIP1 and RIP3, triggered independently of death receptor stimulation by a yet unidentified mechanism.

Interestingly, Hitomi et al. found a putative involvement of certain components of the glutathione redox machinery, namely Gpx4, in necrosis (63).
Recently, depletion of Gpx4 was shown to enhance lipidperoxidation and subsequent caspase-independent but AIF-dependent neuronal cell death (77). Therefore, Gpx4 may not only function as a pivotal upstream effector of cell death in neuronal HT-22 cells, but further initiates necroptosis and thus interconnects both, apoptotic and necroptotic pathways in this model.
Very recently, Tenev et al. identified a cytosolic complex, termed ripoptosome, which similarly to complex 2 triggers both, necroptosis and apoptosis (126). This does not come as a surprise, since the molecular entities recruited to form this complex are very similar to complex 2. The major difference is, however, that the formation of the ripoptosome occurs exclusively in the cytosol, independent of receptor stimulation. To emphasize this difference, the complex has been designated as ripoptosome.

In conclusion, this report supports the notion, that necroptosis can after all be initiated independently of membrane bound death receptors by the formation of a cytosolic complex, as observed in HT-22 cells. The ripoptosome, nevertheless, is most likely not the underlying cause of the RIP1-RIP3 complex formation in HT-22 cells, as the formation is confined to cell death in response to SMAC-mimetic treatment. (126).

5.9. RIP-1, but not CYLD mediates glutamate dependent excitotoxic cell death in primary neurons

As most of the presented findings on the detrimental role of RIP proteins and CYLD are based exclusively on data gained in HT-22 neurons, the experiments were extended to glutamate toxicity in primary cortical neurons.

In this model system, it is well established that the underlying death program is triggered by excitotoxicity and includes mitochondrial damage and AIF release to the nucleus (19).

Using the experimental setup of glutamate-induced cell death in primary cultured neurons, this study could extend previous findings which had shown a neuroprotective effect of necrostatin-1 in a similar model (113).

Considering necrostatin-1 an indicator for the involvement of necroptosis, this finding suggests that also glutamate-induced cell death in primary neurons cannot be regarded as a pure form of apoptotic cell death.

Since RIP1 knockout mice are not viable and siRNA transfection in primary neuronal cells was not efficient, this finding could not be confirmed by gene silencing so far. As pharmacological compounds may exert unspecific effects besides modulating their major target, caution should be warranted when evaluating the role of RIP1 and necroptosis in primary neurons solely on the basis of data obtained from experiments using necrostatin (138).

In sharp contrast to siRNA results in HT-22 cells, cultured primary neurons from $CYLD^{-/-}$ did not show any protection against glutamate-induced excitotoxicity compared to wild-type controls. Whether this was the case because of a different death signaling pathway in primary neurons that renders CYLD function dispensable for the execution of excitotoxicity, remains to be clarified. The finding, that CYLD depletion offered no protection against excitotoxicity even in the presence of caspase inhibitors, however, speaks in favour of this hypothesis.

Caspase inhibitors had been employed to facilitate the detection of a possibly marginal protection in CYLD depleted cells, by repressing apoptosis and shifting the death signaling towards necrotic processes. However, no difference in glutamate toxicity was detected when $CYLD^{-/-}$ neurons were treated with caspase inhibitors compared to wild-type controls, suggesting, that CYLD indeed is not involved in death signaling in this model.

In summary, these data show a convoluted picture of the involvement of necroptosis in primary neurons, with a possible role for RIP1 but not CYLD in excitotoxicity. Future studies are required to resolve these controversial findings. Open questions, that might be addressed include the possible formation of the necrosome in primary cultures and the role of RIP3, for which viable knockout mice have been generated (130).

Additionally, it would be worthwhile investigating, if loss of CYLD protects against cell death in response to oxygen-glucose deprivation, representing an in vitro model of cerebral ischemia with a mechanism independent of NMDA-receptor stimulation.

5.10. Loss of CYLD protects against traumatic brain injury in vivo

In vitro research offers a feasible and economic way to decipher cell death signaling pathways and to determine putative therapeutic approaches in simplified models of neuronal cell death. Whether the findings gained in vitro can be transfered to more physiological conditions in vivo is the ultimate challenge of every study.

Since no inhibitor of CYLD is available until today, the current study used $CYLD^{-/-}$ mice in a mouse model system of traumatic brain injury to explore the potential therapeutic benefit of this approach.

Interestingly, $CYLD^{-/-}$ mice showed significantly decreased secondary infarct volume, brain edema and intracranial pressure 24h after traumatic brain injury, compared to wild-type littermates. This finding highlights the significant protective effect of CYLD depletion in a model of acute brain damage.

As mentioned previously, necrosome formation is an essential indicator of necroptotic cell death. For this reason, future research should also evaluate brain extracts from $CYLD^{-/-}$ mice and wild-type littermates for signs of necrosome formation. Interestingly, Northington et al. found a first hint for an involvement of necroptosis in acute brain damage using an in vivo model of neonatal ischemia. In this model, Northington et al. detected an increase in necrosome formation 3h and 24 h after ischemia, which was significantly attenuated, when mice received necrostatin-1 (139).

Furthermore, Weltz et al. found in a model of chronic intestinal inflammation, that programmed necrosis significantly contributes to cellular demise in colitis of the small bowel, which was dependent on RIP3 and CYLD function.

In the light of these findings it is tempting to speculate that neuroprotection in CYLD$^{-/-}$ mice was mediated by blocking necroptotic cell death, the proof of this hypothesis however, will have to be delivered in future studies, which may also embrace the recently generated RIP3 knockout mice.
The role of necroptosis in vivo is subject of ongoing research with only few reports available on this topic. The findings reported so far, however, fuel the hope that inhibiting necroptosis will evolve as an effective strategy for targeting cell death in a variety of diseases, including traumatic brain injury and possibly cerebral ischemia (130; 140; 141).

5.11. Conclusion and outlook

This thesis identified CYLD as a major player in neuronal cell death in vitro and in vivo. Despite the prominent role of CYLD in regulating NF-κB signaling, it could be excluded that this pathway mediates the neuroprotective effect inherent with CYLD depletion in HT-22 cells.
Instead, inhibition of cell death through silencing CYLD has been linked to the kinases RIP1 and RIP3. These two molecular entities promote cellular death secondary to the formation of a RIP1-RIP3 complex.
In fact, CYLD depletion could prevent complex formation of RIP1-RIP3 and strongly attenuate cell death, indicating, that CYLD acts upstream of RIP1 and RIP3. Since repressing CYLD by siRNA significantly reduced mitochondrial damage, it can be concluded, that CYLD dependent signaling must converge with other pathways of cell death in HT-22 cells upstream of mitochondria. A direct interaction of mitochondria and RIP kinases as the putative downstream effectors of CYLD seems unlikely, as neither protein has been found to translocate to this organelle upon glutamate toxicity.
The pro-apoptotic Bcl-2 and BAX protein, however, could possibly constitute this molecular link between activation of RIP kinases and the downstream events of cell death, since phosphorylation of BAX has been reported to enhance its membrane affinity and toxicity (142). Therefore it would be interesting to investigate if RIP kinases could potentially trigger BAX translocation by inducing its phosphorylation.

The BH3-only protein Bid, another prominent pro-apoptotic protein is also modified by phosphorylation. Contrasting to Bax, however, phosphorylation of Bid at all

phosphorylation sites known today, commonly diminishes the pro-apoptotic potential (142). So, it is tempting to hypothesize, that Bid may carry additional phosphorylation sites still unknown today that promote the pro-apoptotic funcion of this protein.

For this reason a RIP kinase driven activation of Bid seems a possible, though at this point hypothetical link between the established mechanisms of cell death in HT-22 cells and CYLD dependent signaling.

Depletion of Gpx4 has been established as an initiating mechanism of neuronal cell death through enhanced activation of 12/15 LOX, which subsequently triggers downstream effector mechanisms of cell death (77). Interestingly, Gpx4 has also been linked to CYLD/RIP kinase dependent cell death by a systems biology approach, indicating that a decrease in Gpx4 levels may indeed initiate necroptosis (63).

On the basis of the findings obtained in this study, a model is proposed for CYLD mediated cell death signaling, incorporating the established findings and the proposed interactions (Figure 39).

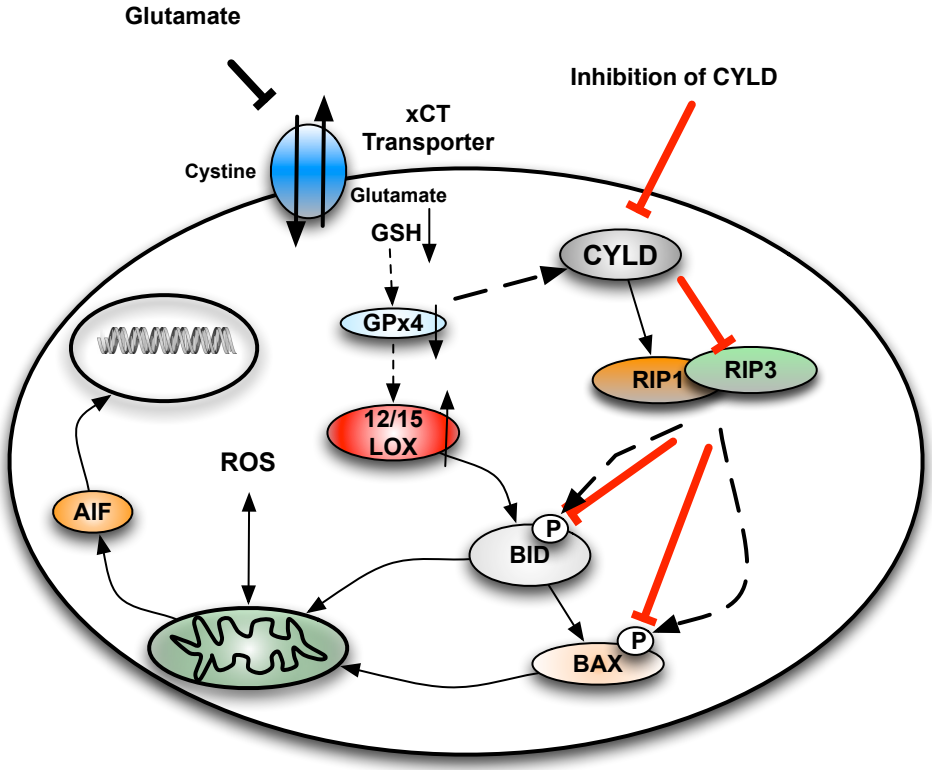

Figure 39: Proposed model of CYLD signaling in oxytosis. Glutamate dependent inhibition of the Xc- transporter causes subsequent glutathione depletion and reduced activity of the glutathione peroxidase-4 (GPx4). A fall in GPx4 triggers 12/15 LOX activation, but may also initiate the CYLD dependent pathway. CYLD activity leads to RIP1-RIP3 complex formation and mitochondrial damage, possibly through a RIP-kinase dependent activation of BAX and Bid. Downstream events involve mitochondrial depolarization, release of apoptosis inducing factor (AIF) and DNA damage.

6. Summary

Neuronal cell death causes progressive loss of brain tissue and function after acute brain injury and in chronic neurodegenerative diseases. Although the pathological features of stroke and brain trauma or Alzheimer's and Parkinson's disease differ greatly, the underlying neuronal damage shares common molecular and cellular mechanisms. Despite extensive research and increasing knowledge on the molecular pathology, no efficient therapy has been born from these efforts until today. As a promising concept to overcome this plight, it has been suggested to enhance endogenous survival signaling pathways like the transcription factor NF-κB and thus obtain neuroprotection.

Increasing neuroprotective NF-κB signaling can be achieved by blocking repressors of NF-κB transcriptional activity such as p53 and CYLD.

Both factors may mediate cell death by mechanisms dependent on and independent of NF-KB signaling. Therefore, the major aim of this study was to explore the roles of p53 and CYLD in neuronal cell death and to connect their detrimental effects with NF-κB activity. This issue was addressed in immortalized mouse hippocampal HT-22 neurons and in primary neuronal cultures exposed to glutamate toxicity. Furthermore, an in vivo model system of traumatic brain injury was employed to compare infarct development after controlled cortical impact in wild-type and $CYLD^{-/-}$ mice.

The present study revealed that both approaches, inhibiting p53 and CYLD successfully preserved mitochondrial integrity and function, and significantly attenuated neuronal cell death. Surprisingly, however, the pronounced neuroprotective effect of the p53-inhibitor pifithrin-α occurred independently of enhanced NF-κB activity in HT-22 cells. In addition, neuroprotection induced by silencing of CYLD was completely independent of NF-κB, despite of the previously established role of CYLD as a negative regulator of NF-κB in keratinocytes.

In line with that notion, the NF-κB subunit expression and NF-κB transcriptional activity were not significantly altered in HT-22 neurons undergoing glutamate dependent cell death.

In conclusion, these data suggested that the NF-κB pathway was neither significantly affected by glutamate dependent cell death, nor did it mediate the neuroprotective response of CYLD and p53 inhibition in this model system of glutamate toxicity.

Interestingly, inhibiting p53 with pifithrin-α maintained mitochondrial morphology and mitochondrial membrane potential in HT-22 cells. This effect occurred independently of p53 dependent transcription.

Investigating the underlying cause of neuroprotection associated with CYLD depletion, it was unveiled that glutamate-induced oxytosis in HT-22 cells occurred through mechanisms of necroptosis. This conclusion is based on the detection of RIP1/RIP3 complexes as a hallmark of necroptotic cell death in HT-22 cells exposed to glutamate. Further, silencing either RIP-kinase provided strong protection of the cells. Repressing CYLD, in turn, prevented the formation of the RIP1/RIP3 necrosome, suggesting that inhibition of necroptosis was the underlying mechanism of neuroprotection after CYLD depletion.
In contrast, CYLD depletion had no effect on cell death in a model of glutamate excitotoxicity in primary cultured neurons, while inhibition of RIP1 kinase by necrostatin-1 significantly enhanced neuronal survival. These data suggest a CYLD independent but RIP1 dependent mechanism of glutamate toxicity in primary neurons, which requires further investigation.
In vivo, however, using a model of traumatic brain injury, CYLD knockout mice showed a significantly reduced infarct size compared to wild-type littermates suggesting a potent neuroprotective effect inherent with CYLD repression.

In summary the data from this thesis highlight a yet unknown role of CYLD in neuronal cell death and unravel CYLD and p53-dependent mechanisms of cell death as a putative therapeutic approach for the treatment of acute and chronic neurodegenerative diseases. Future research, however, is warranted to further elucidate the exact mechanisms leading to CYLD and RIP-kinase activation in neurons and to determine the exact molecular link to mitochondria.

7. Zusammenfassung

Der Untergang von funktionsfähigem Hirngewebe durch neuronalen Zelltod stellt eine zentrale Ursache für die klinische Manifestation von Spätschäden nach Schädel-Hirn Trauma und cerebraler Ischämie dar. Auch die Symptomatik fortgeschrittener chronisch neurodegenerativer Erkrankungen, wie der Alzheimer- und Parkinsonerkrankung ist auf den Verlust neuronaler Funktionalität zurückzuführen. Interessanterweise zeigen die zugrundeliegenden zellulären Mechanismen große Gemeinsamkeiten, so dass neuronaler Zelltod in diesen Erkrankungen ungeachtet ihrer grundsätzlich verschiedenen Ursachen und Ausprägungen in der Regel nach Signalwegen der Apoptose, Nekroptose, oder Autophagie erfolgt.
Trotz intensiver Forschung ist es bis heute jedoch nicht gelungen das gewachsene Verständnis der molekularen Zusammenhänge in die Entwicklung einer effektiven neuroprotektiven Strategie zu überführen.
Ein vielversprechender Ansatz, um diesem Mangel an Therapieoptionen in Zukunft zu begegnen, sieht die Verstärkung endogener Signalwege vor, die das zelluläre Überleben durch Neutralisierung von toxischen Einflüssen sichern.
Ein wichtiger Vertreter dieser neuroprotektiven Signalwege ist der NF-κB Transkriptionsfaktor. Eine Steigerung der Transkriptionsaktivität von NF-κB kann durch Hemmung von p53 und CYLD erzielt werden, zwei wichtigen Proteinen, die das zelluläre Überleben nicht nur durch Ihren Einfluss auf NF-κB, sondern auch durch weitere Mechanismen beeinflussen können.
Vor diesem Hintergrund war es ein zentrales Ziel dieser Arbeit die Bedeutung von p53 und CYLD im neuronalen Zelltod zu untersuchen und ihre Auswirkung auf den neuronalen NF-κB Signalweg zu analysieren.
Um diese Fragestellung zu bearbeiten, wurden im Rahmen dieser Arbeit eine neuronale hippokampale Zelllinie (HT-22 Zellen) wie auch Kulturen von primären kortikalen Neuronen eingesetzt. Darüber hinaus fand ein in vivo Modell zum Schädel-Hirn Trauma Anwendung, um die gewonnenen Erkenntnisse in einem physiologisch etablierten Tiermodel der akuten Hirnschädigung zu verifizieren.

Die Ergebnisse dieser Untersuchungen zeigen, dass Inhibition von p53 und CYLD neuronalen Zelltod verhindern und mitochondriale Funktionalität erhalten kann.

Interessanterweise waren die protektiven Effekte beider Ansätze in HT-22 Zellen unabhängig vom NF-κB Transkriptionsfaktor.
Im Einklang mit diesen Ergebnissen stand die Beobachtung, dass Glutamat-induzierter Zelltod in HT-22 Zellen keine detektierbare Veränderung des NF-κB Transkriptionsweges zeigte. In HT-22 Zellen scheint der NF-κB Transkriptionsfaktor daher eine untergeordnete Rolle zu spielen und ist zudem an der Vermittlung der neuroprotektiven Wirkung von p53 Inhibition und CYLD Depletion nicht beteiligt.
Es konnte weiterhin gezeigt werden, dass der schützende Effekt von Pifithrin-α vermittelter p53 Hemmung anteilig auf transkriptionsunabhängigen Effekten am Mitochondrium beruht.
Der Mechanismus, der dem neuroprotektiven Effekt der CYLD-Depletion zugrunde liegt, konnte ebenfalls identifiziert werden.
Entgegen dem früheren Verständnis haben jüngere Forschungsergebnisse gezeigt, dass Mechanismen des kontrollierten Zelltodes nicht rein apoptotische Vorgänge sein müssen. Im Einklang mit diesen Erkenntnissen konnte die vorliegende Arbeit das Verständnis über kontrollierte nicht-apoptotische Mechanismen des neuronalen Zelltods erweitern und zeigen, dass in HT-22 Neuronen Glutamat induzierter Zelltod anteilig nach Signalwegen der Nekroptose erfolgt.
Die Formierung des Nekrosoms, eines Komplexes aus den beiden RIP-Kinasen RIP1 und RIP3, gilt gemeinhin als zentraler Induktions- und zugleich Exekutionsmechanismus der Nekroptose. Die Bildung dieses Komplexes konnte erstmalig für neuronale Zellen im Glutamat-abhängigem Zelltod nachgewiesen werden. Mit Blick auf den neuroprotektiven Effekt der CYLD Depletion konnte ferner gezeigt werden, dass der Verlust von CYLD die Bildung des Nekrosoms zu unterdrücken vermag.
Die herausragende Bedeutung der beiden RIP Kinasen im Glutamat-abhängigen Zelltod in HT-22 Zellen konnte unter Anwendung von siRNA vermittelter selektiver Depletion von RIP1 und RIP3 nachgewiesen werden. Der Verlust von jeweils einer der beiden RIP-Kinasen sowie die Inhibition der Kinase-Funktion von RIP1 durch Necrostatin1 reduzierten signifikant die Glutamat-induzierte Toxizität und den Verlust mitochondrialer Funktionalität.

Im exzitotoxischem Zelltod in primären kortikalen Neuronen konnte die vorliegende Arbeit keinen protektiven Effekt durch CYLD Depletion zeigen. Die Hemmung der

RIP-1 Kinase durch Necrostatin1 hingegen ermöglichte in Analogie zum Model der HT-22 Zellen eine deutliche Reduktion des neuronalen Zelltodes.
Diese Daten deuten auf einen CYLD unabhängigen, aber RIP1 anhängigen Mechanismus hin, der Gegenstand künftiger Forschungsbemühungen sein wird.
Im Tiermodel zum Schädel Hirn-Trauma konnte die vorliegende Arbeit das protektive Potential der kontrollierten Hemmung von CYLD jedoch bestätigen und zeigen, dass CYLD defiziente Mäuse ein deutlich reduziertes Infarkt-Volumen und Hirnödem nach Schädel-Hirn Trauma aufweisen.

Zusammenfassend konnte in dieser Arbeit erstmalig dargestellt werden, dass neuronaler Zelltod in vitro und in vivo durch Depletion von CYLD hemmbar ist. Weiterhin konnte im Rahmen dieser Arbeit gezeigt werden, dass der neuroprotektive Effekt einer Hemmung von p53 anteilig auf mitochondrialen Prozessen beruht. Weitere Forschungsbemühungen sind jedoch erforderlich, um den genauen Mechanismus zu identifizieren, der zu einer Aktivierung der CYLD und RIP-abhängigen Signalwege führt und die Effekte von p53 am Mitochondrium auf molekularer Basis erklärt.

8. Abbreviations

µ	Micro
µM	Micrometer
AD	Alzheimer's Disease
ADP	Adenosindiphosphate
AIF	Apoptosis inducing factor
AMPA	2-amino-3-(3-hydroxy-5-methylisoxazol-4-yl)proprionate
ANOVA	Analysis of variance
ANT	Adenine nucleotide translocase
APAF-1	Apoptosis protease-activating factor-1
Aqua demin.	Demineralized water
ATM	Ataxia telangiectasia mutated
ATP	Adenosinetriphosphate
ATR	ATM-related protein
BC	before Christ
BCA	Bicinchoninic acid
Bcl-2	B-cell lymphoma-2
BH	Bcl-2 homology
BNIP-3	Bcl-2/E1B 19kDa-interacting protein 3-like protein
BODIPY	4,4-difluoro-5-(4- phenyl-1,3-butadienyl) - 4-bora-3a,4a-diaza-s-indacene-3-undecanoic acid
bp	base pair
CAD	Caspase-activated deoxyribunuclease
cIAP1	Cellular inhibitor of apoptosis protein-1
CBP	CREB binding protein
CCCP	Carbonyl cyanide 3-Chlorophenylhydrazone
CCI	Controlled cortical impact

CO_2	Carbon dioxide
COX	Cyclooxigenase
CREB	Cyclic AMP response element binding protein
CYLD	Cylindromatosis
CYPA	Cyclophilin A
Cytc	Cytochrome c
DAPI	4‘, 6-diamidino-2-phenylindole dihydrochloride
DISC	Death-inducing signaling complex
DMEM	Dulbecco's Modified Eagle Medium
DMSO	Dimethylsulfoxide
DNA	Desoxyribonucleic acid
dNTP	Desoxyribonucleosidtriphosphate
DPI	Diphenyleneiodonium chloride
Drp-1	Dynamin-related protein 1
ds	double stranded
DTT	DL-Dithiothreitol
DUB	Deubiquitinating
EBSS	Earl’s balanced salt solution
EDTA	Ethylenediaminetetraacetic acid
e.g.	for example (exempli gratia)
EGTA	Ethylene glycol-bis(2-aminoethylether)-*N,N,N′,N′*-tetraacetic acid
ER	Endoplasmatic reticulum
FACS	Fluorescence-activated cell sorting
FADD	Fas-associated death domain
FasL	Fas-ligand
FCS	Fetal calf serum
FITC	Fluorescein isothiocyanat
fw	forward

GAPDH	Glyceraldehyde-3-phosphate dehydrogenase
Gbr2	Growth-factor-receptor-bound-protein 2
GFP	Green fluorescent protein
GLUD1	Glutamate dehydogenase 1
GLUT	Glutamate
GO	Glucose oxidase
GpX 4	Glutathione peroxidase 4
GSH	Glutathione
h	hour
HBSS	Hank's balanced salt solution
HCl	Hydrochloric acid
HEPES	4-(2-Hydroxyethyl)piperazine-1-ethanesulfonic acid
H_2O_2	Hydrogen peroxide
HRP	Horseradish peroxidase
HSP	Heat shock protein
IAP	Inhibitor of apoptosis
ICAD	Inhibitor of caspase-activated deoxyribonuclease
ICC	Immunocytochemistry
IGF	Insulin-like growth factor
IκB-α	Inhibitory κB-α
IKKα	Inhibitory κB-α kinase
IKKβ	Inhibitory κB-β kinase
JC-1	5,5',6,6'-tetrachloro-1,1',3,3'-tetraethyl-benzimidazolylcarbocyanine iodide
JNK	c-Jun N-terminal kinase
kDa	Kilo Dalton
LOX	Lipoxygenase
LUBAC	Linear-ubiquitin assembly complex
MEM	Minimum essential medium

mM	Millimolar
MnSOD	Manganese superoxide dismutase
MOMP	Mitochondrial outer membrane permeabilization
MPTP	1-methyl-4-phenyl-1,2,3,5-tetrahydropyridine
MTT	3-(4,5-Dimethylthiazol-2-yl)-2,5-diphenyltetrazolium bromide
NADPH(oxidase)/NOX	Nicotinamide adenine dinucleotide phosphate
NaOH	Sodium hydroxide
NEC1	Necrostatin-1
NF-κB	Nuclear factor-κB
nm	Nanometre
NMDA	N-methyl-D-aspartic acid
OGD	Oxygen glucose deprivation
Omi/HtrA2	High temperature requirement protein A2
PARP	Poly(ADP-ribose) polymerase
PBS	Phosphate buffered solution
PCR	Poly chain reaction
PD	Parkinson’s Disease
PEI	Polyethylenimine
PFA	Para formaldehyde
PFT	Pifithrin-α
pH	Potentia hydrogenii
PI	Propidium iodide
PUMA	p53 up-regulated modulator of apoptosis
PVDF	Polyvinylidenfluorid
RHD	Rel homology domain
RIP1	Receptor interacting protein 1
RIP3	Receptor interacting protein 3
ROS	Reactive oxygen species

rpm	Rounds per minute
rv	reverse
S.D.	Standard deviation
SDS	Sodium dodecyl sulfate
siRNA	small interfering ribonucleic acid
Smac/DIABLO	Second mitochondria - derived activator of caspase/direct IAP binding protein with low pI
ss	single stranded
TAK1	Transforming growth factor-β activated kinase 1
TBE	Tris/Borate/EDTA
tBid	Truncated Bid
TBS	Tris-buffered solution
TBST	Tris-buffered solution with Tween 20
TE	Trypsin-EDTA
TEMED	Tetramethylenethylendiamin
(Cu/Mn/Zn)-SOD	Copper/Manganese/zinc)- superoxide dismutase
TNF-α	Tumor necrosis factor α
TNFR1	Tumor necrosis factor receptor 1
TPA	12-O-tetradecanoylphorbol-13 acetate
TRADD	Tumor necrosis factor receptor type 1-associated DEATH domain protein
TRAF2/5	TNF receptor-associated factor 2/5
TRAIL	Tumor necrosis factor-related apoptosis-inducing ligand
UV	ultraviolet
Vi	Infarct volume
Water demin.	Demineralised water
wt	Wild type
XIAP	X-chromosomal linked inhibitors of apoptosis

9. References

1. Gustavsson A, Svensson M, Jacobi F, Allgulander C, Alonso J, Beghi E, et al. Cost of disorders of the brain in Europe 2010. Eur Neuropsychopharmacol. 2011;21(10):718–779.

2. Kakar V, Nagaria J, John Kirkpatrick P. The current status of decompressive craniectomy. Br J Neurosurg. 2009;23(2):147–157.

3. Maas AIR, Roozenbeek B, Manley GT. Clinical trials in traumatic brain injury: Past experience and current developments. Neurotherapeutics. 2010;7(1):115–126.

4. Kroemer G, Galluzzi L, Vandenabeele P, Abrams J, Alnemri ES, Baehrecke EH, et al. Classification of cell death: recommendations of the Nomenclature Committee on Cell Death 2009. Cell Death Differ. 2009;16(1):3–11.

5. Gorman AM. Neuronal cell death in neurodegenerative diseases: recurring themes around protein handling. Journal of Cellular and Molecular Medicine. 2008;12(6A):2263–2280.

6. Yuan J, (null), Degterev A. Diversity in the mechanisms of neuronal cell death. Neuron. 2003;40(2):401–413.

7. Kerr JF, Wyllie AH, Currie AR. Apoptosis: a basic biological phenomenon with wide-ranging implications in tissue kinetics. Br J Cancer. 1972;26(4):239–257.

8. Vaux DL, Korsmeyer SJ. Cell death in development. Cell. 1999;96(2):245–254.

9. Oppenheim RW. Cell death during development of the nervous system. Annu. Rev. Neurosci. 1991;14453–501.

10. Mattson MP, Duan W, Pedersen WA, Culmsee C. Neurodegenerative disorders and ischemic brain diseases. Apoptosis. 2001;6(1-2):69–81.

11. Ola MS, Nawaz M, Ahsan H. Role of Bcl-2 family proteins and caspases in the regulation of apoptosis. Mol Cell Biochem. 2011;351(1-2):41–58.

12. Taylor RC, Cullen SP, Martin SJ. Apoptosis: controlled demolition at the cellular level. Nat Rev Mol Cell Biol. 2008;9(3):231–241.

13. Golstein P, Kroemer G. A multiplicity of cell death pathways. Symposium on Apoptotic and Non-Apoptotic Cell Death Pathways. EMBO Rep. 2007;8(9):829.

14. Shore GC, Nguyen M. Bcl-2 Proteins and Apoptosis: Choose Your Partner. Cell. 2008;135(6):1004–1006.

15. Culmsee C, Plesnila N. Targeting Bid to prevent programmed cell death in neurons. Biochem Soc Trans. 2006;34(Pt 6):1334–1340.

16. Jabbour AM, Heraud JE, Daunt CP, Kaufmann T, Sandow J, O'Reilly LA, et al. Puma indirectly activates Bax to cause apoptosis in the absence of Bid or Bim. Cell Death Differ. 2009;16(4):555–563.

17. van Delft MF, Wei AH, Mason KD, Vandenberg CJ, Chen L, Czabotar PE, et al. The BH3 mimetic ABT-737 targets selective Bcl-2 proteins and efficiently induces apoptosis via Bak/Bax if Mcl-1 is neutralized. Cancer Cell. 2006;10(5):389–399.

18. Vogler M, Vogler M, Dinsdale D, Dinsdale D, Dyer MJS, Dyer MJS, et al. Bcl-2 inhibitors: small molecules with a big impact on cancer therapy. Cell Death Differ. 2008;16(3):360.

19. Culmsee C, Zhu C, Landshamer S, Becattini B, Wagner E, Pellechia M, et al. Apoptosis-inducing factor triggered by poly(ADP-ribose) polymerase and bid mediates neuronal cell death after oxygen-glucose deprivation and focal cerebral ischemia. J Neurosci. 2005;2510262–10272.

20. Plesnila N, Zhu C, Culmsee C, Gröger M, Moskowitz MA, Blomgren K. Nuclear translocation of apoptosis-inducing factor after focal cerebral ischemia. J Cereb Blood Flow Metab. 2004;24(4):458–466.

21. Boujrad H, Gubkina O, Robert N, Krantic S, Susin SA. AIF-mediated programmed necrosis: a highly regulated way to die. Cell Cycle. 2007;6(21):2612–2619.

22. Mehta SL, Manhas N, Raghubir R. Molecular targets in cerebral ischemia for developing novel therapeutics. Brain Research Reviews. 2007;54(1):34–66.

23. Joza N, Susin SA, Daugas E, Stanford WL, Cho SK, Li CY, et al. Essential role of the mitochondrial apoptosis-inducing factor in programmed cell death. Nature. 2001;410(6828):549–554.

24. Galluzzi L, Joza N, Tasdemir E, Maiuri MC, Hengartner M, Abrams JM, et al. No death without life: vital functions of apoptotic effectors. Cell Death Differ. 2008;15(7):1113–1123.

25. Hangen E, De Zio D, Bordi M, Zhu C, Dessen P, Caffin F, et al. A brain-specific isoform of mitochondrial apoptosis-inducing factor: AIF2. Cell Death Differ. 2010;17(7):1155–1166.

26. Vousden KH, Prives C. Blinded by the Light: The Growing Complexity of p53. Cell. 2009;137(3):413–431.

27. Yu J, Zhang L. The transcriptional targets of p53 in apoptosis control. Biochemical and Biophysical Research Communications. 2005;331(3):851–858.

28. Culmsee C, Mattson MP. p53 in neuronal apoptosis. Biochemical and Biophysical Research Communications. 2005;331(3):761–777.

29. Vousden KH, Lane DP. p53 in health and disease. Nat Rev Mol Cell Biol. 2007;8(4):275–283.

30. Gobbel GT, Chan PH. Neuronal death is an active, caspase‐dependent process after moderate but not severe DNA damage. J Neurochem. 2001;76(2):520–531.

31. Martin F Lavin. Ataxia-telangiectasia: from a rare disorder to a paradigm for cell signalling and cancer. Nat Rev Mol Cell Biol. 2008;9(10):759.

32. Wadgaonkar R, Phelps KM, Haque Z, Williams AJ, Silverman ES, Collins T. CREB-binding protein is a nuclear integrator of nuclear factor-kappaB and p53 signaling. J Biol Chem. 1999;274(4):1879–1882.

33. Mattson M, Culmsee C, Yu Z, Camandola S. Roles of nuclear factor kappa B in neuronal survival and plasticity. J Neurochem. 2000;74(2):443–456.

34. Ravi R, Mookerjee B, van Hensbergen Y, Bedi GC, Giordano A, El-Deiry WS, et al. p53-mediated repression of nuclear factor-kappaB RelA via the transcriptional integrator p300. Cancer Research. 1998;58(20):4531–4536.

35. Webster GA, Perkins ND. Transcriptional Cross Talk between NF- B and p53. Mol Cell Biol. 1999;19(5):3485.

36. Culmsee C, Siewe J, Junker V, Retiounskaia M, Schwarz S, Camandola S, et al. Reciprocal inhibition of p53 and nuclear factor-kappaB transcriptional activities determines cell survival or death in neurons. J Neurosci. 2003;23(24):8586–8595.

37. Plesnila N, Baumgarten von L, Retiounskaia M, Engel D, Ardeshiri A, Zimmermann R, et al. Delayed neuronal death after brain trauma involves p53-dependent inhibition of NF-kappaB transcriptional activity. Cell Death Differ. 2007;14(8):1529–1541.

38. Mattson M. NF-kappa B in the survival and plasticity of neurons. Neurochem Res. 2005;30883–893.

39. Basseres D, Baldwin A. Nuclear factor-κB and inhibitor of κB kinase pathways in oncogenic initiation and progression. Oncogene. 2006;25(51):6817–6830.

40. Duckworth E, Butler T, Collier L, Collier S, Pennypacker K. NF-κB protects neurons from ischemic injury after middle cerebral artery occlusion in mice. Brain Res. 2006;1088(1):167–175.

41. Schneider A, Martin-Villalba A, Weih F, Vogel J, Wirth T, Schwaninger M. NF-kappaB is activated and promotes cell death in focal cerebral ischemia. Nat Med. 1999;5(5):554–559.

42. Herrmann O, Baumann B, De Lorenzi R, Muhammad S, Zhang W, Kleesiek J, et al. IKK mediates ischemia-induced neuronal death. Nat Med. 2005;11(12):1322–1329.

43. Ridder DA, Schwaninger M. NF-kappaB signaling in cerebral ischemia. Neuroscience. 2009;158(3):995–1006.

44. Camandola S, Mattson MP. NF-kappa B as a therapeutic target in

neurodegenerative diseases. Expert Opin. Ther. Targets. 2007;11(2):123–132.

45. Gilmore TD. Introduction to NF-κB: players, pathways, perspectives. Oncogene. 2006;25(51):6680–6684.

46. Palmer S, Chen YH. Bcl-3, a multifaceted modulator of NF-kappaB-mediated gene transcription. Immunol. Res. 2008;42(1-3):210–218.

47. Bonizzi G, Karin M. The two NF-kappaB activation pathways and their role in innate and adaptive immunity. Trends in Immunology. 2004;25(6):280–288.

48. Pizzi M, Sarnico I, Boroni F, Benarese M, Steimberg N, Mazzoleni G, et al. NF-κB factor c-Rel mediates neuroprotection elicited by mGlu5 receptor agonists against amyloid β-peptide toxicity. Cell Death Differ. 2005;12(7):761–772.

49. Guerrini L, Blasi F, Denis-Donini S. Synaptic activation of NF-kappa B by glutamate in cerebellar granule neurons in vitro. Proc Natl Acad Sci USA. 1995;92(20):9077.

50. Perkins ND. Integrating cell-signalling pathways with NF-kappaB and IKK function. Nat Rev Mol Cell Biol. 2007;8(1):49–62.

51. Sun S. CYLD: a tumor suppressor deubiquitinase regulating NF-κB activation and diverse biological processes. Cell Death Differ. 2009;17(1):25–34.

52. Bertrand MJM, Lippens S, Staes A, Gilbert B, Roelandt R, De Medts J, et al. cIAP1/2 are direct E3 ligases conjugating diverse types of ubiquitin chains to receptor interacting proteins kinases 1 to 4 (RIP1-4). PLoS ONE. 2011;6(9):e22356.

53. Haas TL, Emmerich CH, Gerlach B, Schmukle AC, Cordier SM, Rieser E, et al. Recruitment of the linear ubiquitin chain assembly complex stabilizes the TNF-R1 signaling complex and is required for TNF-mediated gene induction. Molecular Cell. 2009;36(5):831–844.

54. Habelhah H, Takahashi S, Cho S-G, Kadoya T, Watanabe T, Ronai Z. Ubiquitination and translocation of TRAF2 is required for activation of JNK but not of p38 or NF-κB. EMBO J. 2004;23(2):322–332.

55. Ea C-K, Deng L, Xia Z-P, Pineda G, Chen ZJ. Activation of IKK by TNFalpha requires site-specific ubiquitination of RIP1 and polyubiquitin binding by NEMO. Molecular Cell. 2006;22(2):245–257.

56. Li H, Kobayashi M, Blonska M, You Y, Lin X. Ubiquitination of RIP is required for tumor necrosis factor alpha-induced NF-kappaB activation. J Biol Chem. 2006;281(19):13636–13643.

57. Shembade N, Ma A, Harhaj EW. Inhibition of NF-kappaB signaling by A20 through disruption of ubiquitin enzyme complexes. Science. 2010;327(5969):1135–1139.

58. Bignell GR, Warren W, Seal S, Takahashi M, Rapley E, Barfoot R, et al. Identification of the familial cylindromatosis tumour-suppressor gene. Nat. Genet. 2000;25(2):160–165.

59. Courtois G, Gilmore TD. Mutations in the NF-κB signaling pathway: implications for human disease. Oncogene. 2006;25(51):6831–6843.

60. Komander D, Lord CJ, Scheel H, Swift S, Hofmann K, Ashworth A, et al. The structure of the CYLD USP domain explains its specificity for Lys63-linked polyubiquitin and reveals a B box module. Molecular Cell. 2008;29(4):451–464.

61. Zhang J, Stirling B, Temmerman ST, Ma CA, Fuss IJ, Derry JMJ, et al. Impaired regulation of NF-kappaB and increased susceptibility to colitis-associated tumorigenesis in CYLD-deficient mice. J Clin Invest. 2006;116(11):3042–3049.

62. Sun S-C. Deubiquitylation and regulation of the immune response. Nature Reviews Immunology. 2008;8(7):501–511.

63. Hitomi J, Christofferson DE, Ng A, Yao J, Degterev A, Xavier RJ, et al. Identification of a molecular signaling network that regulates a cellular necrotic cell death pathway. Cell. 2008;135(7):1311–1323.

64. Chan FK-M, Shisler J, Bixby JG, Felices M, Zheng L, Appel M, et al. A role for tumor necrosis factor receptor-2 and receptor-interacting protein in programmed necrosis and antiviral responses. J Biol Chem. 2003;278(51):51613–51621.

65. Holler N, Zaru R, Micheau O, Thome M, Attinger A, Valitutti S, et al. Fas triggers an alternative, caspase-8-independent cell death pathway using the kinase RIP as effector molecule. Nat Immunol. 2000;1(6):489–495.

66. Degterev A, Hitomi J, Germscheid M, Ch'en IL, Korkina O, Teng X, et al. Identification of RIP1 kinase as a specific cellular target of necrostatins. Nat Chem Biol. 2008;4(5):313–321.

67. Degterev A, Huang Z, Boyce M, Li Y, Jagtap P, Mizushima N, et al. Chemical inhibitor of nonapoptotic cell death with therapeutic potential for ischemic brain injury. Nat Chem Biol. 2005;1(2):112–119.

68. Vandenabeele P, Declercq W, Van Herreweghe F, Vanden Berghe T. The role of the kinases RIP1 and RIP3 in TNF-induced necrosis. Sci Signal. 2010;3(115):re4.

69. Vandenabeele P, Galluzzi L, Vanden Berghe T, Kroemer G. Molecular mechanisms of necroptosis: an ordered cellular explosion. Nat Rev Mol Cell Biol. 2010;11(10):700–714.

70. Culmsee C, Krieglstein J. Ischaemic brain damage after stroke: new insights into efficient therapeutic strategies. International Symposium on Neurodegeneration and Neuroprotection. EMBO Rep. 2007;8(2):129–133.

71. Lin MT, Beal MF. Mitochondrial dysfunction and oxidative stress in neurodegenerative diseases. Nature. 2006;443(7113):787–795.

72. Culmsee C, Landshamer S. Molecular insights into mechanisms of the cell death program: role in the progression of neurodegenerative disorders. Curr Alzheimer Res. 2006;3(4):269–283.

73. Murphy T, Myamoto M, Sastre A, Schnaar RL, Coyle JT. Glutamate toxicity in a neuronal cell line involves inhibition of cystine transport leading to oxidative stress. Neuron. 1989;2(6):1547–1558.

74. Sagara Y, Dargusch R, Chambers D, Davis J, Schubert D, Maher P. Cellular mechanisms of resistance to chronic oxidative stress. Free Radical Biology and Medicine. 1998;24(9):1375–1389.

75. Tan S, Schubert D, Maher P. Oxytosis: a novel form of programmed cell death. Current topics in medicinal chemistry. 2001;1(6):497–506.

76. Tobaben S, Grohm J, Seiler A, Conrad M, Plesnila N, Culmsee C. Bid-mediated mitochondrial damage is a key mechanism in glutamate-induced oxidative stress and AIF-dependent cell death in immortalized HT-22 hippocampal neurons. Cell Death Differ. 2010;18(2):282–292.

77. Seiler A, Schneider M, Förster H, Roth S, Wirth EK, Culmsee C, et al. Glutathione peroxidase 4 senses and translates oxidative stress into 12/15-lipoxygenase dependent- and AIF-mediated cell death. Cell Metab. 2008;8(3):237–248.

78. Landshamer S, Hoehn M, Barth N, Duvezin-Caubet S, Schwake G, Tobaben S, et al. Bid-induced release of AIF from mitochondria causes immediate neuronal cell death. Cell Death Differ. 2008;15(10):1553–1563.

79. Grohm J, Plesnila N, Culmsee C. Bid mediates fission, membrane permeabilization and peri-nuclear accumulation of mitochondria as a prerequisite for oxidative neuronal cell death. Brain, Behavior, and Immunity. 2010;24(5):831–838.

80. Morimoto BH, Koshland DE. Excitatory amino acid uptake and N-methyl-D-aspartate-mediated secretion in a neural cell line. Proc Natl Acad Sci USA. 1990;87(9):3518–3521.

81. Liu Y, Peterson D, Kimura H, Schubert D. Mechanism of cellular 3-(4,5-dimethylthiazol-2-yl)-2,5-diphenyltetrazolium bromide (MTT) reduction. J Neurochem. 1997;69(2):581–593.

82. Diemert S, Dolga AM, Tobaben S, Grohm J, Pfeifer S, Oexler E, et al. Impedance measurement for real time detection of neuronal cell death. Journal of Neuroscience Methods. 2012;203(1):69–77.

83. de Wet JR, Wood KV, DeLuca M, Helinski DR, Subramani S. Firefly luciferase gene: structure and expression in mammalian cells. Mol Cell Biol. 1987;7(2):725–737.

84. Tan S, Sagara Y, Liu Y, Maher P, Schubert D. The regulation of reactive oxygen species production during programmed cell death. The Journal of Cell Biology. 1998;141(6):1423–1432.

85. Zhu X, Yu Q-S, Cutler RG, Culmsee CW, Holloway HW, Lahiri DK, et al. Novel p53 inactivators with neuroprotective action: syntheses and pharmacological evaluation of 2-imino-2,3,4,5,6,7-hexahydrobenzothiazole and 2-imino-2,3,4,5,6,7-hexahydrobenzoxazole derivatives. J. Med. Chem. 2002;45(23):5090–5097.

86. Culmsee C, Zhu X, Yu QS, Chan SL, Camandola S, Guo Z, et al. A synthetic inhibitor of p53 protects neurons against death induced by ischemic and excitotoxic insults, and amyloid beta-peptide. J Neurochem. 2001;77(1):220–228.

87. Knott AB, Bossy-Wetzel E. Impairing the mitochondrial fission and fusion balance: a new mechanism of neurodegeneration. Ann. N. Y. Acad. Sci. 2008;1147283–292.

88. Wang X, Su B, Lee H-G, Li X, Perry G, Smith MA, et al. Impaired balance of mitochondrial fission and fusion in Alzheimer's disease. J Neurosci. 2009;29(28):9090–9103.

89. Martin LJ. Mitochondrial and Cell Death Mechanisms in Neurodegenerative Diseases. Pharmaceuticals (Basel). 2010;3(4):839–915.

90. Manero F. The Small Organic Compound HA14-1 Prevents Bcl-2 Interaction with Bax to Sensitize Malignant Glioma Cells to Induction of Cell Death. Cancer Research. 2006;66(5):2757–2764.

91. Kovalenko A, Chable-Bessia C, Cantarella G, Israël A, Wallach D, Courtois G. The tumour suppressor CYLD negatively regulates NF-kappaB signalling by deubiquitination. Nature. 2003;424(6950):801–805.

92. Bhakar A, Tannis L, Zeindler C, Russo M, Jobin C, Park D, et al. Constitutive nuclear factor-kappa B activity is required for central neuron survival. J Neurosci. 2002;22(19):8466–8475.

93. Kaltschmidt B, Kaltschmidt C. NF-kappaB in the nervous system. Cold Spring Harb Perspect Biol. 2009;1(3):a001271.

94. Courtois G. Tumor suppressor CYLD: negative regulation of NF-kappa B signaling and more. Cell Mol Life Sci. 2008;65(7-8):1123–1132.

95. Brummelkamp TR, Nijman SMB, Dirac AMG, Bernards R. Loss of the cylindromatosis tumour suppressor inhibits apoptosis by activating NF-κB. Nature. 2003;424(6950):797–801.

96. Simonson SJS, Wu Z-H, Miyamoto S. CYLD: a DUB with many talents. Developmental Cell. 2007;13(5):601–603.

97. Massoumi R, Chmielarska K, Hennecke K, Pfeifer A, Fässler R. Cyld Inhibits Tumor Cell Proliferation by Blocking Bcl-3-Dependent NF-κB Signaling. Cell.

2006;125(4):665–677.

98. Cho Y, Challa S, Moquin D, Genga R, Ray TD, Guildford M, et al. Phosphorylation-Driven Assembly of the RIP1-RIP3 Complex Regulates Programmed Necrosis and Virus-Induced Inflammation. Cell. 2009;137(6):1112–1123.

99. He S, Wang L, Miao L, Wang T, Du F, Zhao L, et al. Receptor Interacting Protein Kinase-3 Determines Cellular Necrotic Response to TNF-α. Cell. 2009;137(6):1100–1111.

100. Moquin D, Chan FK-M. The molecular regulation of programmed necrotic cell injury. Trends Biochem Sci. 2010;35(8):434–441.

101. Christofferson DE, Yuan J. Necroptosis as an alternative form of programmed cell death. Curr Opin Cell Biol. 2010;22(2):263–268.

102. Vanlangenakker N, Vanden Berghe T, Bogaert P, Laukens B, Zobel K, Deshayes K, et al. cIAP1 and TAK1 protect cells from TNF-induced necrosis by preventing RIP1/RIP3-dependent reactive oxygen species production. Cell Death Differ. 2011;18(4):656–665.

103. Lu J, Bai L, Sun H, Nikolovska-Coleska Z, Mceachern D, Qiu S, et al. SM-164: A Novel, Bivalent Smac Mimetic That Induces Apoptosis and Tumor Regression by Concurrent Removal of the Blockade of cIAP-1/2 and XIAP. Cancer Research. 2008;68(22):9384–9393.

104. Schulze-Osthoff K, Bakker AC, Vanhaesebroeck B, Beyaert R, Jacob WA, Fiers W. Cytotoxic activity of tumor necrosis factor is mediated by early damage of mitochondrial functions. Evidence for the involvement of mitochondrial radical generation. J Biol Chem. 1992;267(8):5317–5323.

105. Morgan MJ, Kim Y-S, Liu Z-G. TNFalpha and reactive oxygen species in necrotic cell death. Cell Res. 2008;18(3):343–349.

106. Festjens N, Kalai M, Smet J, Meeus A, Van Coster R, Saelens X, et al. Butylated hydroxyanisole is more than a reactive oxygen species scavenger. Cell Death Differ. 2006;13(1):166–169.

107. Kasof G, Prosser J, Liu D, Lorenzi M, Gomes B. The RIP-like kinase, RIP3, induces apoptosis and NF-kappa B nuclear translocation and localizes to mitochondria. Febs Lett. 2000;473(3):285–291.

108. Temkin V, Huang Q, Liu H, Osada H, Pope RM. Inhibition of ADP/ATP exchange in receptor-interacting protein-mediated necrosis. Mol Cell Biol. 2006;26(6):2215–2225.

109. Wu Y-T, Tan H-L, Huang Q, Sun X-J, Zhu X, Shen H-M. zVAD-induced necroptosis in L929 cells depends on autocrine production of TNFα mediated by the PKC-MAPKs-AP-1 pathway. Cell Death Differ. 2011;18(1):26–37.

110. Arundine M, Tymianski M. Molecular mechanisms of glutamate-dependent neurodegeneration in ischemia and traumatic brain injury. Cell Mol Life Sci.

2004;61(6):657–668.

111. Lau A, Tymianski M. Glutamate receptors, neurotoxicity and neurodegeneration. Pflugers Arch - Eur J Physiol. 2010;460(2):525–542.

112. Bonfoco E, Krainc D, Ankarcrona M, Nicotera P, Lipton SA. Apoptosis and necrosis: two distinct events induced, respectively, by mild and intense insults with N-methyl-D-aspartate or nitric oxide/superoxide in cortical cell cultures. Proc Natl Acad Sci USA. 1995;92(16):7162–7166.

113. Li Y, Yang X, Ma C, Qiao J, Zhang C. Necroptosis contributes to the NMDA-induced excitotoxicity in rat's cultured cortical neurons. Neurosci Lett. 2008;447(2-3):120–123.

114. Joers A, Jaks V, Kase J, Maimets T. p53-dependent transcription can exhibit both on/off and graded response after genotoxic stress. Oncogene. 2004;236175–6185.

115. Tergaonkar V, Perkins ND. p53 and NF-kappaB crosstalk: IKKalpha tips the balance. Molecular Cell. 2007;26(2):158–159.

116. Kaltschmidt C, Kaltschmidt B. Stimulation of ionotropic glutamate receptors activates transcription factor NF-kappa B in primary neurons. 1995.

117. Diemert S, Grohm J, Hartmannsgruber R, Culmsee C; Inhibition of p53 preserves mitochondrial morphology and function and prevents glutamate-induced cell death in neurons. Abstracts of the 50th Annual Meeting of the Deutsche Gesellschaft für Experimentelle und Klinische Pharmakologie und Toxikologie. Mainz, Germany. March 10-12, 2009. Naunyn-Schmiedeberg's archives of pharmacology.

118. Endo H, Kamada H, Nito C, Nishi T, Chan PH. Mitochondrial translocation of p53 mediates release of cytochrome c and hippocampal CA1 neuronal death after transient global cerebral ischemia in rats. J Neurosci. 2006;26(30):7974–7983.

119. Nijboer CH, Heijnen CJ, van der Kooij MA, Zijlstra J, van Velthoven CTJ, Culmsee C, et al. Targeting the p53 pathway to protect the neonatal ischemic brain. Ann. Neurol. 2011;70(2):255–264.

120. Pizzi M, Sarnico I, Lanzillotta A, Battistin L, Spano PF. Post-ischemic brain damage: NF-κB dimer heterogeneity as a molecular determinant of neuron vulnerability. FEBS Journal. 2009;276(1):27–35.

121. Schulze-Bergkamen. Down-regulation of CYLD as a trigger for NF-κB activation and a mechanism of apoptotic resistance in hepatocellular carcinoma cells. Int J Oncol. 2010;38(1):

122. Byun JY, Yune TY, Lee JY, Yeo SG, Park MS. Expression of CYLD and NF-kappaB in human cholesteatoma epithelium. Mediators Inflamm. 2010;2010796315.

123. Galluzzi L, Kroemer G. Necroptosis: a specialized pathway of programmed

necrosis. Cell. 2008;135(7):1161–1163.

124. Feng S, Yang Y, Mei Y, Ma L, Zhu D-E, Hoti N, et al. Cleavage of RIP3 inactivates its caspase-independent apoptosis pathway by removal of kinase domain. Cell. Signal. 2007;19(10):2056–2067.

125. Wang L, Du F, Wang X. TNF-α Induces Two Distinct Caspase-8 Activation Pathways. Cell. 2008;133(4):693–703.

126. Tenev T, Bianchi K, Darding M, Broemer M, Langlais C, Wallberg F, et al. The Ripoptosome, a Signaling Platform that Assembles in Response to Genotoxic Stress and Loss of IAPs. Molecular Cell. 2011;43(3):432–448.

127. Xu X, Chua CC, Kong J, Kostrzewa RM, Kumaraguru U, Hamdy RC, et al. Necrostatin-1 protects against glutamate-induced glutathione depletion and caspase-independent cell death in HT-22 cells. J Neurochem. 2007;103(5):2004–2014.

128. Wu W, Liu P, Li J. Necroptosis: An emerging form of programmed cell death. Crit. Rev. Oncol. Hematol. 2012;82(3):249–258.

129. Kalai M, Van Loo G, Vanden Berghe T, Meeus A, Burm W, Saelens X, et al. Tipping the balance between necrosis and apoptosis in human and murine cells treated with interferon and dsRNA. Cell Death Differ. 2002;9(9):981–994.

130. Welz P-S, Wullaert A, Vlantis K, Kondylis V, Fernández-Majada V, Ermolaeva M, et al. FADD prevents RIP3-mediated epithelial cell necrosis and chronic intestinal inflammation. Nature. 2011;477(7364):330–334.

131. Bertrand MJM, Milutinovic S, Dickson KM, Ho WC, Boudreault A, Durkin J, et al. cIAP1 and cIAP2 Facilitate Cancer Cell Survival by Functioning as E3 Ligases that Promote RIP1 Ubiquitination. Molecular Cell. 2008;30(6):689–700.

132. Vanden Berghe T, Vanlangenakker N, Parthoens E, Deckers W, Devos M, Festjens N, et al. Necroptosis, necrosis and secondary necrosis converge on similar cellular disintegration features. Cell Death Differ. 2009;17(6):922–930.

133. Gerlach B, Cordier SM, Schmukle AC, Emmerich CH, Rieser E, Haas TL, et al. Linear ubiquitination prevents inflammation and regulates immune signalling. Nature. 2011;471(7340):591–596.

134. Kim Y-S, Morgan MJ, Choksi S, Liu Z-G. TNF-Induced Activation of the Nox1 NADPH Oxidase and Its Role in the Induction of Necrotic Cell Death. Molecular Cell. 2007;26(5):675–687.

135. Yazdanpanah B, Wiegmann K, Tchikov V, Krut O, Pongratz C, Schramm M, et al. Riboflavin kinase couples TNF receptor 1 to NADPH oxidase. Nature. 2009;460(7259):1159–1163.

136. Bradbury D, Simmons T, Slater K, Crouch S. Measurement of the ADP: ATP ratio in human leukaemic cell lines can be used as an indicator of cell

viability, necrosis and apoptosis. Journal of immunological methods. 2000;240(1):79–92.

137. Eguchi Y, Shimizu S, Tsujimoto Y. Intracellular ATP levels determine cell death fate by apoptosis or necrosis. Cancer Research. 1997;57(10):1835–1840.

138. Tamura Y,Chiba T, Tanioka T, Shimizu N.
NO donor induces Nec-1-inhibitable, but RIP1-independent, necrotic cell death in pancreatic β-cells. 2011;585(19):3058–3064.

139. Northington FJ, Chavez-Valdez R, Graham EM, Razdan S, Gauda EB, Martin LJ. Necrostatin decreases oxidative damage, inflammation, and injury after neonatal HI. Journal of Cerebral Blood Flow & Metabolism. 2011;31(1):178–189.

140. Northington FJ, Chavez-Valdez R, Graham EM, Razdan S, Gauda EB, Martin LJ. Necrostatin decreases oxidative damage, inflammation, and injury after neonatal HI. J Cereb Blood Flow Metab. 2010;31:178-189

141. Smith CCT, Davidson SM, Lim SY, Simpkin JC, Hothersall JS, Yellon DM. Necrostatin: a potentially novel cardioprotective agent? Cardiovasc Drugs Ther. 2007;21(4):227–233.

142. Billen LP, Shamas-Din A, Andrews DW. Bid: a Bax-like BH3 protein. Oncogene. 2008;27 Suppl 1S93–104.

143. Tobaben. The role of 12/15-lipoxygenases in ROS- mediated neuronal cell death “, dissertation 2011

144. Grohm, “Molecular regulation of mitochondrial dynamics by dynamin-related protein 1 (Drp1) and Bid in model systems of neuronal cell death“, dissertation 2011

10. Publications

10.1. Original papers

S Diemert, J Grohm, S Tobaben, A Dolga, C Culmsee; Real-Time Detection of Neuronal Cell Death by Impedance-Based Analysis using the xCELLigence System. Application Note, Issue 06, Roche Diagnostics GmbH, Roche Applied Science, Penzberg, Germany, 2010

S Diemert, A Dolga, S Tobaben, J Grohm, S Pfeifer, E Oexler, C Culmsee; Impedance measurement for real time detection of neuronal cell death. Neuroscience methods, 2012 Jan 15;203(1):69-77.

S Diemert, S Krieg, S W Kim, N Plesnila, C Culmsee; Neuroprotection through CYLD depletion in-vitro and in-vivo. Apoptosis (under revision)

10.2. Oral Presentations and Poster presentations

S Diemert, J Grohm, R Hartmannsgruber, C Culmsee; Inhibition of p53 preserves mitochondrial morphology and function and prevents glutamate-induced cell death in neurons, 50. Jahrestagung der Deutschen Gesellschaft für Experimentelle und Klinische Pharmakologie und Toxikologie Mainz, 10.3.2009-12.3.2009

S Diemert, S Krieg, S W Kim, N Plesnila, C Culmsee; Loss of CYLD protects neurons in vitro and in vivo, Jahrestagung der deutschen pharmazeutischen Gesellschaft, Jena, 28.9.2009-1.10.2009

S Diemert, J Grohm, S Tobaben, A Dolga, C Culmsee; Real time detection of neuronal cell death by the xCELLigence system, Jahrestagung der deutschen pharmazeutischen Gesellschaft, Jena, 28.9.2009-1.10.2009

S Diemert, S Krieg, S W Kim, N Plesnila, C Culmsee; Neuroprotection through targeted deletion of CYLD, Society for Neuroscience, Chicago, USA 17.10.2009-21.10.2009

S Diemert, J Grohm, S Tobaben, C Culmsee; Online-measurement of neuronal cell death, 51. Jahrestagung der Deutschen Gesellschaft für Experimentelle und Klinische Pharmakologie und Toxikologie Mainz, 23.3.2010-25.3.2010

S Diemert, Krieg, S W Kim, N Plesnila, C Culmsee; Implications of CYLD in neuronal cell death, 18th Euroconference on Apoptosis, Ghent, Belgium, 1.09.2010-4.09.2010

S Diemert, S Tobaben, J Grohm, R Hartmannsgruber, N Plesnila, C Culmsee; Inhibition of p53 preserves mitochondrial morphology and function and protects against glutamate-induced cell death, 6th International Symposium on Neuroprotection and Neurorepair, Rostock 01.10.2010-14.10.2010

S Diemert, Krieg, S W Kim, N Plesnila, C Culmsee; Repressing CYLD promotes neuroprotection against glutamate dependent cell death in vitro and cerebral ischemia in vivo, 19th Euroconference on Apoptosis, Stockholm, Sweden, 14.09.2011-17.09.201

11. Acknowledgements

First of all I would like to thank my supervisor Prof. Dr. Carsten Culmsee for giving me the opportunity to work as a PhD student in his lab. Due to his enduring support and constant advice paired with the freedom to follow up on personal hypotheses I could master the hardships of my PhD thesis while enjoying to work in his lab. Thank you very much for this! Further, i would like to express my gratitude for the chance to attend the numerous national and international conferences, gaining further insight into the current status of research in the field of interest and meanwhile absorbing the great socio-cultural circumstances.

I would also like to thank my colleagues Amalia, Julia and Svenja for the great time we have had working together, setting up the lab in the beginning and spending our evenings and holidays together, unforgetable bear action included. Thanks also to Julia for the introduction to bacterial cultivation and plasmid preparation and to Amalia for supporting me in the struggle with the xCELLigence paper.

Further, I would like to thank Steffi, Sina, Christina and Eva for the great atmosphere, encouraging kites, a relentless source of sweets, and the kind downhill and Wetzlar shuttle service. Thanks!

Further thanks to Renate and Sandra, as well as to Katharina who not only introduced me, the newly arrived greenhorn to cell culture in the beginning of my PhD time, but also offered a helping hand and top-advice, whenever needed! Mirroring the great atmosphere in the lab, we also enjoyed great evenings and unforgettable shows starring e.g. Marburg´s most peculiar waitress.

Thanks also to my dear swedish “amazon” Anderson for repeatedly treating us to his exceptional cooking skills, helpful assistance on primer design and great trips and parties. I would also like to thank the great discoverer and geographer Valentine Espert for on time delivery of the newest scientific literature, late night discussions in shabby Altstadt-pubs and much more. And yes, I will carry you to the next hilltop – the promise will be kept.

Thank you Emma for backing me up on organizational challenges, homepage editing, proof reading of manuscripts and the whole bunch of issues that remained unsolved before dropping by at your office. Thanks! I would also like to thank Svenja for her constant emotional support, helpful assistance with editing and exam preparations and proof reading. I would also like to thank all my “Wahlpflichtfach-

students” for their enthusiastic and dedicated work.
I also want to thank the friends of mine with whom I spent a great time outside of the lab, which nevertheless helped me to overcome any hardship experienced within. Finally, I thank my parents and sister for their profound support which helped me to conclude my thesis.

12. Curriculum vitae

Personal details

Date of birth: 03.03.1983

Place of birth: Hamburg

Education

02/2008 – today	P.h.D thesis at the deparment of Pharmacology and Clinical Pharmacy, Philipps University of Marburg; supervisor: Prof. Dr. Carsten Culmsee
12/2007	License as a pharmacist
05/2007-10/2007	Internship at Pelikan-Apotheke, Hamburg
11/2006-04/2007	Internship at Bayer Healthcare, Leverkusen
10/2002-10/2006	Study of Pharmacy, Philipps University of Marburg
08/1993-06/2002	Secondary school, Erzbischöfliches Suitbertus Gymnasium, Kaiserswerth, Düsseldorf
08/1989-07/1993	Gemeinschaftsgrundschule Kaiserswerth, Düsseldorf